CAPITAL UNIVERSITY OF SCIENCE AND TECHNOLOGY, ISLAMABAD

Numerical Simulations of Squeezing Flow Problems in a Channel

by

Maleeha Atlas

A thesis submitted in partial fulfillment for the degree of Doctor of Philosophy

in the

Faculty of Computing
Department of Mathematics

2021

Numerical Simulations of Squeezing Flow Problems in a Channel

By

Maleeha Atlas

(DMT143002)

Dr. M. Irfan Hameed, Professor

University of South Carolina Upstate, USA

(Foreign Evaluator 1)

Dr. Engin Gedil, Assistant Professor

Karabük University, Turkey

(Foreign Evaluator 2)

Dr. Shafqat Hussain

(Thesis Supervisor)

Dr. Muhammad Sagheer

(Head, Department of Mathematics)

Dr. Muhammad Abdul Qadir

(Dean, Faculty of Computing)

DEPARTMENT OF MATHEMATICS

CAPITAL UNIVERSITY OF SCIENCE AND TECHNOLOGY

ISLAMABAD

2021

To my family and teachers.

CAPITAL UNIVERSITY OF SCIENCE & TECHNOLOGY
ISLAMABAD

Expressway, Kahuta Road, Zone-V, Islamabad
Phone:+92-51-111-555-666 Fax: +92-51-4486705
Email: info@cust.edu.pk Website: https://www.cust.edu.pk

CERTIFICATE OF APPROVAL

This is to certify that the research work presented in the thesis, entitled "**Numerical Simulations of Squeezing Flow Problems in a Channel**" was conducted under the supervision of **Dr. Shafqat Hussain**. No part of this thesis has been submitted anywhere else for any other degree. This thesis is submitted to the **Department of Mathematics, Capital University of Science and Technology** in partial fulfillment of the requirements for the degree of Doctor in Philosophy in the field of **Mathematics**. The open defence of the thesis was conducted on **January 07, 2021**.

Student Name : Maleeha Atlas (DMT143002)

The Examining Committee unanimously agrees to award PhD degree in the mentioned field.

Examination Committee :

(a) External Examiner 1: Dr. Shams ul Islam,
Associate Professor
COMSATS University, Islamabad

(b) External Examiner 2: Dr. Rashid Mahmood,
Associate Professor
Air University, Islamabad

(c) Internal Examiner : Dr. Abdul Rehman Kashif
Associate Professor
CUST, Islamabad

Supervisor Name : Dr. Shafqat Hussain
Associate Professor
CUST, Islamabad

Name of HoD : Dr. Muhammad Sagheer
Professor
CUST, Islamabad

Name of Dean : Dr. Muhammad Abdul Qadir
Professor
CUST, Islamabad

AUTHOR'S DECLARATION

I, **Maleeha Atlas (Registration No. DMT-143002)**, hereby state that my PhD thesis entitled, '**Numerical Simulations of Squeezing Flow Problems in a Channel**' is my own work and has not been submitted previously by me for taking any degree from Capital University of Science and Technology, Islamabad or anywhere else in the country/ world.

At any time, if my statement is found to be incorrect even after my graduation, the University has the right to withdraw my PhD Degree.

(Maleeha Atlas)

Dated: 7 January, 2021

Registration No : DMT-143002

PLAGIARISM UNDERTAKING

I solemnly declare that research work presented in the thesis titled "**Numerical Simulations of Squeezing Flow Problems in a Channel**" is solely my research work with no significant contribution from any other person. Small contribution/ help wherever taken has been duly acknowledged and that complete thesis has been written by me.

I understand the zero tolerance policy of the HEC and Capital University of Science and Technology towards plagiarism. Therefore, I as an author of the above titled thesis declare that no portion of my thesis has been plagiarized and any material used as reference is properly referred/ cited.

I undertake that if I am found guilty of any formal plagiarism in the above titled thesis even after award of PhD Degree, the University reserves the right to withdraw/ revoke my PhD degree and that HEC and the University have the right to publish my name on the HEC/ University Website on which names of students are placed who submitted plagiarized thesis.

(Maleeha Atlas)

Dated: 7 January, 2021

Registration No : DMT-143002

List of Publications

It is certified that following publication(s) have been made out of the research work that has been carried out for this thesis:-

1. **M. Atlas**, S.Hussain, M. Sagheer , "Entropy generation and unsteady Casson fluid flow squeezing between two parallel plates subject to Cattaneo-Christov heat and mass flux" *The European Physical Journal Plus*, vol. 134, pp. 33, 2019.

2. **M. Atlas**, S.Hussain, M. Sagheer , "Entropy generation and squeezing flow past a Riga plate with Cattaneo-Christov heat flux" *Bulletin of the Polish Academy of Sciences: Technical Sciences*, vol. 66, No. 3, 2018.

3. **M. Atlas**, S.Hussain, M. Sagheer , "Squeezing Flow of Upper Convected Maxwell Nanofluid Subject to Entropy Generation and Cattaneo-Christove Double Diffusion" *Journal of Nanofluids*, vol. 8, pp. 420-429, 2018.

(Maleeha Atlas)
Registration No: DMT143002

Acknowledgement

First and foremost I would like to pay my cordial gratitude to the Almighty **Allah**, who created us as a human being with the great boon of intellect. I would like to pay my humble gratitude to the Allah Almighty, for blessing us with the Holy Prophet **Hazrat Muhammad (Sallallahu Alaihay Wa'alihi wasalam)** for whom the whole universe is being created. He (Sallallahu Alaihay Wa'alihi wasalam) removed the ignorance from the society and brought us out of darkness. Thanks again to that Mono-realistic power for granting me with a strength and courage whereby I dedicately completed my PhD thesis with positive and significant result.

I express my profound gratitude to my supervisor **Dr. Shafqat Hussain**, who very compassionately provided to me an enabling environment and patronge to complete my thesis. Thanks to his unending co-operation and guidance.

I particulary thank to the head of the department of Mathematics and all the faculty members of the department of Mathematics, especally **Dr. Muhammad Sagheer** who very efficiently taught us that and their advices enabled me to improve my study.

I want to extend my heartfelt thanks to my colleagues **Ms Shahana Rizvi** and **Ms Sobia Jamal** for constant support, love and wonderful company.

It will be injustice if I forget my beloved parents. Thanks to my father **Khalid Mehmood**, my great mother **Yasmeen Manuchaher**, due to which I am able to be at this position in my life today. Furthermore, I would also like to acknowledge my **husband** for abiding my ignorance with patience during critical stages of my Ph.D. Words would never say how much I grateful to him. I am thankful to my sisters. May Almighty Allah shower his blessings and prosperity on all those who assisted me during the completion of this thesis. Collectively, I am greatful to my sisters for their ever encouragement and overall support. May Almighty Allah shower his blessings and prosperity on all those who assisted me during the completion of this thesis.

Abstract

This thesis is devoted to the study of squeezing fluid flow between two parallel plates. The results are obtained regarding the flow behavior of Newtonian, Maxwell, Casson and micropolar fluid flow. Instead of Fourier's and Fick's laws, heat and mass transfer mechanisms are discussed by using the Cattaneo-Christov heat and mass fluxes. The impact of entropy generation has been considered. For the enhancement of thermophysical properties of such fluids, the concept of nanofluid is utilized. No slip and stratification effects at the boundary are taken into account. Further, the effect of chemical reaction and thermal radiation are also considered. The physical flow models are governed in the form of prtial differential equations. The governing partial differential equations of the fluid flow are converted into ordinary differential equations by using the similarity transformation. The ordinary differential equations are solved numerically. Shooting method with fourth order Runga Kutta integration scheme is used to calculate the numerical results. For the validation of the results obtained by the shooting method, a MATLAB built in function bvp4c is also employed. A comparison of presently computed and already publish results is made. The quantities of physical significance, for example skin friction, Nusselt number and sherwood number are computed numerically and presented through tables. The effect of physical parameters on velocity, temperature and concentration have been investigated through graphs.

Contents

Author's Declaration v

Plagiarism Undertaking vi

List of Publications vii

Acknowledgement viii

Abstract ix

List of Figures xiii

List of Tables xvi

Abbreviations xvii

Symbols xviii

1 Introduction 1
- 1.1 Introduction . . . 1
  - 1.1.1 Nanofluid . . . 2
  - 1.1.2 Cattaneo-Christov Model . . . 4
  - 1.1.3 Non-Newtonian Fluid . . . 6
  - 1.1.4 Micropolar Fluid . . . 7
  - 1.1.5 Stratification . . . 8
  - 1.1.6 Entropy Generation . . . 9
- 1.2 Thesis Contributions . . . 10
- 1.3 Thesis Outline . . . 11

2 Basic Governing Laws and Solution Methodology 13
- 2.1 Fundamental Laws . . . 13
  - 2.1.1 Law of Conservation of Mass . . . 13
  - 2.1.2 Law of Conservation of Momentum . . . 14
  - 2.1.3 Energy Equation (Conservation Law of Energy) . . . 15
  - 2.1.4 Mass Transfer with Chemical Reaction . . . 15

2.2 Heat Flux Models . . . 16
2.2.1 Fourier's Law . . . 16
2.2.2 Cattaneo-Christov Heat Flux [32, 88] . . . 17
2.3 Classification of Fluids . . . 17
2.3.1 Newtonian Fluid . . . 18
2.3.2 Non-Newtonian Fluid . . . 19
2.3.2.1 Upper Convected Maxwell Fluid . . . 19
2.3.3 Casson Fluid [91] . . . 21
2.4 Principle of Entropy Generation [92] . . . 21
2.5 Solution Methodology . . . 22
2.5.1 Shooting Method [93] . . . 22
2.5.2 Example [94] . . . 24

3 Entropy Generation and Unsteady Casson Fluid Flow Squeezing between Two Parallel Plates Subject to Cattaneo-Christov Heat and Mass Flux 27
3.1 Introduction . . . 27
3.2 Problem Formulation . . . 28
3.2.1 The Problem Configuration . . . 28
3.2.2 Governing Equations . . . 29
3.2.3 Dimensionless Equations . . . 30
3.2.4 Physical Quantities . . . 31
3.2.5 Entropy Generation Analysis . . . 32
3.3 Solution Methodology . . . 33
3.3.1 Code Validation . . . 34
3.4 Results and Discussions . . . 34
3.4.1 Outcome of Various Parameters on Velocity and Temperature 36
3.4.2 Influence of Various Parameters on Concentration . . . 40
3.4.3 Impact of Different Parameters on Entropy Generation . . . 41
3.4.4 Effect of Various Parameters on Nusselt Number . . . 45
3.5 Conclusion . . . 47

4 Entropy Generation and Squeezing Flow Past a Riga Plate With Cattaneo-Christov Heat Flux 49
4.1 Introduction . . . 49
4.2 Problem Formulation . . . 50
4.2.1 The Problem Configuration . . . 50
4.2.2 Governing Equations . . . 51
4.2.3 Dimensionless Equations . . . 52
4.2.4 Physical Quantities . . . 53
4.2.5 Entropy Generation Analysis . . . 53
4.3 Solution Methodology . . . 54
4.3.1 Code Validation . . . 55
4.4 Results and Discussions . . . 56
4.4.1 Outcome of Different Parameters on Velocity and Temperature 56

4.4.2 Significance of Various Parameters on Concentration 60
4.4.3 Consequences of Different Parameters on Entropy Generation 62
4.5 Conclusion 65

5 Squeezing Flow of Upper Convected Maxwell Nanofluid Subject to Entropy Generation and Cattaneo-Christove Double Diffusion 67
5.1 Introduction 67
5.2 Problem Formulation 68
5.2.1 Problem Configuration 68
5.2.2 The Governing Equations 69
5.2.3 Dimensionless Governing Equations 70
5.2.4 Physical Quantities of Interest 71
5.2.5 Entropy Generation Analysis 72
5.3 Solution Methodology 72
5.4 Results and Discussions 74
5.4.1 Outcome of Velocity and Temperature for Different Values . 75
5.4.2 Effect of Various Parameters on Concentration 79
5.4.3 Consequence of Different Parameters on Entropy Generation 81
5.5 Conclusion 83

6 Squeezing Flow of Micropolar Nanofluid between Two Parallel Plates 85
6.1 Introduction 85
6.2 Problem Formulation 86
6.2.1 The Physical Configuration 86
6.2.2 The Governing Equations 86
6.2.3 The Dimensionless Governing Equations 88
6.2.4 Physical Quantities of Interest 88
6.2.5 Entropy Generation Analysis 89
6.3 Solution Methodology 90
6.4 Results and Discussion 92
6.4.1 Influence of Various Parameters on Velocity and Temperatures 93
6.4.2 Outcome of Concentration for Numerous Parameters 97
6.4.3 Impact of Various Parameters on Microrotation Profile . . . 100
6.4.4 Outcome of Concentration for Varied Parameters 101
6.5 Concluding remarks 104

7 Conclusion and The Future Work 106
7.1 Concluding Remarks 107
7.1.1 Future Outlook 108

A The bvp4c Function 122

List of Figures

3.1 Schematic illustration of the squeezing flow. 29
3.2 Impact of positive Sq on f'. 36
3.3 Impact of negative Sq on f'. 37
3.4 Impact of γ on f'. 37
3.5 Impact of Rd on θ. 38
3.6 Impact of Pr on θ. 38
3.7 Impact of Bi_1 on θ. 39
3.8 Impact of β_e on θ. 39
3.9 Impact of Sq on θ. 39
3.10 Impact of Sc on ϕ. 40
3.11 Impact of Bi_2 on ϕ. 40
3.12 Impact of β_c on ϕ. 41
3.13 Impact of Kr on ϕ. 41
3.14 Impact of Pr on ϕ. 42
3.15 Impact of Sq on NG. 42
3.16 Impact of β_r on NG. 43
3.17 Impact of Re on NG. 43
3.18 Impact of γ on NG. 43
3.19 Impact of Rd on Be. 44
3.20 Impact of γ on Be. 44
3.21 Impact of β_r on Be. 44
3.22 Impact of Ω on Be. 45
3.23 Impact of Sq on Nu. 46
3.24 Impact of Pr on Nu. 46
3.25 Impact of β_e on Nu. 46
3.26 Impact of Rd on Nu. 47
3.27 Impact of Bi_1 on Nu. 47

4.1 Diagram of flow model. 50
4.2 Influence of positive Sq on f'. 57
4.3 Influence of negative Sq on f'. 57
4.4 Influence of Z on f'. 58
4.5 Influence of Rd on θ. 58
4.6 Influence of Pr on θ. 59
4.7 Influence of Bi_1 on θ. 59

4.8 Influence of Sq on θ. 59
4.9 Influence of β_e on θ. 60
4.10 Influence of Sc on ϕ. 61
4.11 Influence of Bi_2 on ϕ. 61
4.12 Influence of β_e on ϕ. 61
4.13 Influence of Kr on ϕ. 62
4.14 Influence of Pr on ϕ. 62
4.15 Influence of Sq on NG. 63
4.16 Influence of β_r on NG. 63
4.17 Influence of Re on NG. 64
4.18 Influence of Bi_1 on N_G. 64
4.19 Influence of Sq on Be. 64
4.20 Influence of β_r on Be. 65
4.21 Influence of Bi_1 on Be. 65

5.1 Schematic illustration of the squeezing flow. 68
5.2 Impact of positive Sq on f'. 76
5.3 Impact of negative Sq on f'. 76
5.4 Impact of De on f'. 77
5.5 Impact of β_e on θ. 77
5.6 Impact of Nb on θ. 77
5.7 Impact of Nt on θ. 78
5.8 Impact of Pr on θ. 78
5.9 Impact of S_1 on θ. 79
5.10 Impact of β_c on ϕ. 79
5.11 Impact of Nb on ϕ. 80
5.12 Impact of Nt on ϕ. 80
5.13 Impact of Pr on ϕ. 80
5.14 Impact of S_2 on ϕ. 81
5.15 Impact of Sc on ϕ. 81
5.16 Impact of Br on N_G. 82
5.17 Impact of S_1 on N_G. 82
5.18 Impact of Sq on N_G. 83
5.19 Impact of Re on N_G. 83

6.1 Schematic illustration of squeezing flow. 86
6.2 Influence of Sq on $f'(\eta)$. 93
6.3 Influence of K on $f'(\eta)$. 94
6.4 Influence of Sq on $\theta(\eta)$. 94
6.5 Influence of K on $\theta(\eta)$. 95
6.6 Influence of Pr on $\theta(\eta)$. 95
6.7 Influence of Ec on $\theta(\eta)$. 95
6.8 Influence of Nb on $f\theta(\eta)$. 96
6.9 Influence of Nt on $\theta(\eta)$. 96
6.10 Influence of Rd on $\theta(\eta)$. 97

6.11 Influence of Sq on $\phi(\eta)$. 97
6.12 Influence of Pr on $\phi(\eta)$. 98
6.13 Influence of Rd on $\phi(\eta)$. 98
6.14 Influence of Nt on $\phi(\eta)$. 98
6.15 Influence of Nb on $\phi(\eta)$. 99
6.16 Influence of K on $\phi(\eta)$. 99
6.17 Influence of Ec on $\phi(\eta)$. 100
6.18 Influence of Sc on $\phi(\eta)$. 100
6.19 Influence of K on $\phi(\eta)$. 101
6.20 Influence of n on $g(\eta)$. 101
6.21 Influence of N_1 on $g(\eta)$. 102
6.22 Influence of Sq on $g(\eta)$. 102
6.23 Influence of β_r on NG. 103
6.24 Influence of Re on NG. 103
6.25 Influence of Sq on NG. 103
6.26 Influence of K on NG. 104
6.27 Influence of n on NG. 104

List of Tables

3.1 The Comparison of Nusselt number when $S = 0.5$, $\phi = 0.0$ and $\delta = 0.1$. 34
3.2 Values of skin friction and Sherwood number, when $Pr = 1$, $\beta_e = 0.1$, $\beta_c = 0.1$, $Bi_1 = Bi_2 = 0.2$. 35

4.1 Comparison of skin friction cofficient $C_f Re_x^{1/2}$. 55
4.2 Numerical values of $Sh_x Re_x^{-1/2}$ when $\beta_e = 0.1, B = 10.0$, $Bi_1 = 0.2 = Bi_2$, $Z = 1.5$, $Sq = 0.2$, $Pr = 1.5$. 56

5.1 Comparison of the skin friction cofficient $C_f Re_x^{1/2}$. 74
5.2 Numerical values of $Sh_x Re_x^{-1/2}$ when $\beta_e = \beta_c = 0.1, De = 0.0, S_1 = 0.1, Sc = 1.1, S_2 = 0.1, Pr = 2.0$. 75

6.1 Comparison of the Nusselt number in the absence of the micropolar fluid with those of [107] and [20] by taking $Nb = 0.1$, $Nt = 0.2$, Pr, $Sq = 0.5$, and $Ec = 0.01$ and in the absence of micropolar fluid. . . 91
6.2 Nusselt number Nu and Sherwood number Sh. 92

Abbreviations

CFD	Computational fluid dynamics
DTM	Differential transform method
FDM	Finite difference method
FFI	Fluid friction irreversibility
HTI	Heat transfer irreversibility
KKL	Ko-Kleinstreuer-Li
MTI	Mass transfer irreversibility
ODEs	Ordinary differential equations
PDEs	Partial differential equations

Symbols

$(U,\ V)$	Velocity components
C	Concentration of fluid
T	Temperature of fluid
$h(t)$	Distance between two plates.
U_w	Stretching velocity of the lower plate
a	Stretching rate
γ_1	Characteristic parameter
$\mathbf{q_1}$	Heat flux
$\mathbf{J_1}$	Mass flux
δ_{E_1}	Relaxation time of heat flux
δ_{C_1}	Relaxation time of mass flux
P	Pressure
γ	Casson fluid parameter
ρ	Density of fluid
c_p	Specific heat
α	Thermal diffusivity
$\hat{\delta}_e$	Stefan-Boltzmann constant
$\hat{\beta}_R$	Absorption coefficient
k_1	Thermal conductivity
D_B	Molecular diffusivity
$\hat{q}_r$	Radiative heat flux
Sq	Squeezing parameter
Kr	Chemical reaction

Pr	Prandtl number
Rd	Radiation parameter
β_e	Relaxation time of heat transfer
Sc	Schmidt number
Bi_1	Biot number for temperature
K_1	Reaction rate
Bi_2	Biot number for concentration
C_f	Skin friction
Sh_x	Sherwood number
Nu	Nusselt number
β_c	Relaxation time of mass transfer
η	Dimensionless variable
Re	Reynolds number
δ_{E_1}	Heat flux relaxation time
δ_{C_1}	Mass flux relaxation time
λ_E	Thermal relaxation time
λ_C	Concentration relaxation time
B_r	Brinkman number
χ	Constant parameter
Ω	Dimensionless temperature difference
B	Dimensionless constants
j_0	Applied current density
M_0	Magnetization
b	Width of magnets and electrodes
Z	Modified Hartman number
π	Component of deformation
λ_1	Constant parameter
D_T	Thermophoretic diffusion cofficient
Nb	Brownian motion parameter
Nt	Thermophoresis parameter
S_1	Thermal stratification

S_2	Solutal stratification
N	Microrotation velocity
k_f	Material parameter
j	Micro inertia density
De	Deborah number
N_1	Coupling constant parameter
n	Boundary parameter
γ_n	Microrotation viscosity
K	Micropolar parameter

Chapter 1

Introduction

1.1 Introduction

Squeezing flows are referred as the flows between two parallel plates or the flows in which two boundaries approach each other. The squeezing flow received attention in nineteenth century because of its comprehensive employment in science and engineering. The particular utilization of squeezing flow is in injection molding, biology, polymer and agricultural industries [1]. Squeezing flows are also applicable in the extraction of crude oil from the rocks. Lubrication system can be designed with the assistance of squeezing flow. Stefan [2] formulated the first mathematical model of squeezing flow under the lubrication system. Later on, for elliptic plate, Reynolds [3] studied the same problem. Archibald [4] studied the Stefan problem for angular plates. It was concluded that the film thickness decreases in a specified time. Wang [5] considered the viscous squeezing fluid flow. Asymptotic solution is achieved for smaller and greater squeezing parameter and is found that the resistance is opposite to the direction of motion. Bhattacharyya and Pal [6] conducted an investigation on the squeezing flow between two parallel disks. From the study, it was observed that with an increment in the magnetic field and angular velocity, the torque on the lower disc increases. Verma [7] studied the numerical solution of the unsteady squeezing fluid flow. The study is performed with all values of the

Reynolds number permissible in lubrication problems. The squeezing and extrusion of a fluid flow having invariant temperature was observed by Duwairi *et al.* [8]. It was concluded that with an increase in the extrusion parameter the velocity and heat transfer rate increases. Engmann *et al.* [9] presented the squeeze flow theory and applications to rheometry. The investigation illustrated the impact of different boundary conditions and how these interact with different types of materials. Squeezing fluid flow problem for the case of viscous and incompressible fluid using the perturbation method was concluded by Ghori *et al.* [10]. The obtained results exhibit that the homotopy perturbation method is efficient and easy to implement. Saif *et al.* [11] studied the heat and mass transfers in the unsteady squeezing flow, using a perturbation iteration algorithm. It was found that an increase in Pr and Ec lead to an increase in the temperature. Variable magnetic field effect on the squeezing flow was observed by Khan *et al.* [12]. The parametric continuation method has been adopted to get the solutions. The results exhibit that as the magnetic and squeezing parameter grow, the fluid temperature increases.

1.1.1 Nanofluid

The homogeneous mixture of nanoparticles and a conventional fluid is known as the nanofluid [13]. The nano-sized particles encompass metals, non-metals, oxides, carbides, etc. Nanoparticles have higher thermal conductivity than the base fluid. The heat transfer in the base fluids can be enhanced by magnification of the thermal conductivity. Nanofluids have various applications including paper and printing, paints and coating, power generation, drugs, cancer therapy and food products [14]. Buongiorno [15] proposed a model based on two mechanisms, namely, the Brownian motion and thermophoresis for the convective transport in nanofluids. The solution of entropy generation and MHD flow of nanofluid over a rotating circular permeable plate was explored by Rashidi *et al.* [16]. It was shown that the temperature boundary layer enhance with an increases in the nanoparticles volume fraction. The unsteady squeezing flow of five different kinds

of nanofluids was analyzed by Sheikholeslami *et al.* [17]. The adomian decomposition method has been utilized to acquire the results. The results showed that with increasing volume fraction of nanoparticles, temperature is elevated. Similarly, Domairry and Hatami [18] presented the impact of Copper water nanofluid on the flow between two parallel plates by adopting the DTM and Pade approximation. The study reported that for the increasing squeezing parameter and Eckert number, the Nusselt number also increases. Singh *et al.* [19] evaluated the squeezing flow with the impact of magnetic field and slip velocity by using the shooting technique. The results indicated that the heat and mass transfers rate are inversely proportional to the volume fraction of nanoparticles. Atlas *et al.* [20] explored the squeezing flow of nanofluid. This study concluded that the temperature decreases and concentration enhances for passive control of nanoparticles. Sheikholeslami *et al.* [21] attained the solution of unsteady nanofluid flow by using DTM. It was noticed that the Nusselt number rises as the Hartmann number increases. Buongiorno's mathematical model was studied by Kafayati [22], who also considered the effects of mixed convection of non-Newtonian nanofluid. The results were acquired with the help of finite difference Lattice Boltzmann scheme. It was also noticed that rise in the Brownian motion and thermophoretic parameter increases the mass transfer and decreases the heat transfer. Five different shapes of nanoparticles, on unsteady flow between two sheets is examined by Ahmad *et al.* [23]. NDsolve technique has been utilized to obtain the solution. It is proved, by inspection, that temperature depends directly on nanoparticles volume fraction. Hosseinzadeh *et al.* [24] reviewed the hydrothermal analysis on squeezing nanofluid flow. The homotopy perturbation and collocation methods were applied to achieve the results. They also concluded that the temperature enhances with the rise in Brownian motion parameter. Ullah *et al.* [25] studied the magneto nanofluid flow. They found that the Brownian motion and thermophoresis have direct link with the temperature. Unsteady squeezing nanofluid flow with the characteristics of melting heat transfer is determined by Farooq *et al.* [26]. Homotopy analysis technique was used to compute the results, which show that

temperature and concentration values escalate as Brownian motion parameter increases. Ahmed and Rashed [27] used the Buongiorno mathematical model to investigate the magnetohydrodynamic free convection of nanofluid and solution was obtained by using the FDM. The obtained results exhibit an increase in heat transfer and the wavy contraction ratio. Derakhshan *et al.* [28] discovered the influence of thermophoresis and Brownian motion in the abovementioned model and applied the Akbari-Ganji's method to obtain the solutions. In these results, enhancement in the Nusselt number was seen for greater Brownian motion and thermophoresis parameter. The method of variation of parameters was applied for analyzing the unsteady squeezing flow of water based nanofluid. The results from this study revealed that temperature profile shows enhancement as buoyancy parameter rises. Krishna and Chamka [29] performed the study of MHD nanofluid flow in a porous medium under the Hall effect, adopting the Galerkin optimal homotopy asymptotic method. The graphs show that as the values of Brownian motion and thermophoresis grow, the temperature and concentration increase.

1.1.2 Cattaneo-Christov Model

Heat transfer occurrence is the natural phenomena in which heat transfer from one object to another or in same object due to temperature difference. It has many applications in engineering, for example, nuclear reactors, energy production, fuel cells and micro electronics [30]. From the past two decades, to study the mechanism of heat transfer, Fourier's law [31] for heat conduction has been applied. This law represents the instant reaction of an initial disturbance with the system under consideration. Cattaneo [32] added the relaxation time to modify the Fourier's law. In Cattaneo model, temperature field yielded hyperbolic energy equation. Furthermore, Christov [33] refined this model, by adjoining the Oldroyld upper convected derivatives instead of material derivative. Ali and Sandeep [34] applied the Runge-Kutta Fehlberg integration method on the above mentioned model for MHD radiative ferrofluid flow. The study stated that in comparison to the flow over a cone and plate, heat transfer was found greater in case of a wedge.

Numerical solution of MHD Maxwell fluid flow, for the same model, is considered by Shah *et al.* [35]. Also, this study extrapolated that temperature field increases for increasing radiation parameter and Eckert number. Sui *et al.* [36] presented heat and mass flux model of Cattaneo-Christov for a stretchable sheet under the combined effect of upper convected Maxwell nanofluid. The study concluded that for the increasing temperature relaxation parameter, the temperature profile decreases. Hayat *et al.* [37] discussed the Cattaneo-Christov double diffusion for three dimensional nanofluid flow on a linear stretching sheet. It was depicted that as the thermal and concentration relaxation parameter enhanced, temperature and concentration were decreased. Muhammad *et al.* [38] developed mathematical model for squeezed nanofluid flow with double diffusion. The results showed that both the concentration and temperature gradients were decreased as the thermal and solutal relaxation parameters increased. Dogonchi and Ganji [39] used the Daun-Rach approach to explore the MHD nanofluid flow. The outcome exhibits a low temperature distribution in case of Cattaneo-Christov model instead of Fourier's law. Akmal *et al.* [40] applied Keller box method to study the Cattaneo-Christov model for squeezing flow of nanofluid. The observations showed that at lower plate, entropy is greater as compared to the upper plate. The squeezing nanofluid for unsteady flow is analyzed by Dogonchi *et al.* [41]. They applied Duan-Rach approach to achieve results, which demonstrated a direct relation of Nusselt number to the shrinking parameter while an inverse relation for the stretching parameter. The combined effect of Cattaneo-Christov and homogeneous and heterogenous reaction on unsteady squeezing flow were examined by Dianchen *et al.* [42]. They reported that for squeezing parameter skin friction and Nusselt number show opposite behavior. Zubair *et al.* [43] discussed the Cattaneo-Christov model in squeezing nanofluid flow. This investigation reveled that temperature gradient was increased for increasing squeezing parameter and Eckert number. The influence of Carreau fluid subject to the squeezing flow was inquired by Ramadevi *et al.* [44]. The results showed that an increase in the thermal relaxation parameter resulted in decay of temperature and concentration profiles. Shankar *et al.* [45] worked on the features of flow between parallel plates

in case of an unsteady Casson fluid. The results obtained from the study exhibit that the temperature and concentration distribution are less for double diffusivity as compared to classical Fourier's law.

1.1.3 Non-Newtonian Fluid

Some of the fluids related to the engineering and industrial applications can not be examined through the traditional Navier-Stokes equations. These fluids include paint, polymer, solutions, oils, coating of clay etc [46]. To discuss all the important constituent of the non-Newtonian fluids, a single relation is not adequate. Non-Newtonian fluid is described by different models and studied in literature. Several models like Casson, Maxwell, Jeffrey, Oldroyd, Sisko etc, have been recommended. Maxwell model is the most trivial example of the rate type fluid in which the essential attributes of the relaxation time are described. Maxwell model excludes the effect of shear depending viscosity and, thus, is helpful in focusing the impact of fluid elasticity on the properties of boundary layer. The flow of Maxwell nanofluid in the coaxial cylinder with shear stress was presented by Jamil and Fetecua [47]. Awais *et al.* [48] calculated that the presence of stretching sheet implies the unsteady flow of Maxwell fluid in three dimensions. It was seen that the impact of the Deborah number reduces the velocity. Ibrahim [49], numerically analyzed the nanoparticles with convective heating on a stretchable sheet, when upper convected Maxwell fluid is present. Their results show that as the Deborah number escalates, profiles for skin friction and rates of heat and mass transfer increase. Reddy *et al.* [50] obtained the numerical solution for the above mentioned flow with convective boundary conditions. The momentum boundary layer declines as magnetic parameter increases. The effect of Maxwell nanofluid flow using Buongiorno's model is deliberated by Farooq *et al.* [51]. Homotopy analysis method was applied to acquire the results. It is worthwhile to note that for greater material parameter, the cross flow variation of velocity is observed. Kumar *et al.* [52] deliberated the features of magnetohydrodynamic UCM in a channel. The Runge-Kutta method of fourth order was applied to obtain the solution. The

results exhibit that the temperature increases as the thermal and solutal dispersion enhance. Rashid *et al.* [53] applied the homotopy analysis method to find the solution for the Maxwell fluid along with the activation energy and thermal radiation. It was concluded that for higher Deborah number results in decreasing velocity.

One of the prominent mathematical model which expresses the rheological fluid flow properties is the Casson fluid. The formulation of this fluid is provided in [54, 55]. Shashikumar *et al.* [56] explored the influence of radiative heat flux on unsteady Casson fluid flow. They acquired results by Runge-Kutta-Fehlberg method. Kumar *et al.* [57] applied the MATLAB builtin function bvp4c for the study of proposed fluid flow for the unsteady case. The observation indicated that for increasing squeezing parameter the temperature field declines. Patel [58] presented a heat generation and Hall current on MHD Casson fluid flow. It was seen that the heat generation and Hall current have a tendency to improve the motion. Saif *et al.* [59] explored the MHD fluid flow of Casson fluid and found that the velocity profile enhances as the squeeze number grows. Ahmadpour *et al.* [60] acquired the numerical solution for convective heat transfer of Casson fluid flow between squeezing disks. It was noticed that for higher heat generation, temperature is enhanced.

1.1.4 Micropolar Fluid

Micropolar fluids are the fluids containing the rotating micro constituents. Micropolar fluids contain a suspension of the rigid particles. Animal blood and liquid crystals are the typical examples of micropolar fluids. Polymer solutions, lubricant fluids, colloidal expansions and complex biological structures are also the applications of micropolar fluids [61]. At first, Eringen [62] formulated the theory of micropolar fluid, introducing a new constitutive equation for the fluids with microstructures. The flow of micropolar fluid with suction and injection by using Van Dyke perturbation technique is studied by Ramachandran *et al.* [63]. It was concluded that a rise in injection parameter results in increase in the velocity. Kelson

and Farrel [64] analyzed the boundary layer flow of a micropolar fluid in a porous sheet. Ashraf *et al.* [65] conducted the numerical study for two dimensional flow of micropolar fluid and observed that microrotation profile changes from asymmetric shape to symmetric shape as the permeability parameter increases. Joneidi *et al.* [66] inquired into the micropolar fluid in a porous channel and concluded that for increasing dimensionless parameter $N1$, the microrotation profile rises. Gibanov *et al.* [67] observed the laminar steady convectional flow of micropolar fluid in a trapezoidal cavity. It was confirmed that as the vortex viscosity enhances the heat transfer decreases. Bilal *et al.* [68] presented the micropolar fluid flow under the Hall and ion-slip effects. The results indicated that the coupling parameter has decreasing impact on microrotation profile. The MHD micropolar nanofluid flow in a channel was explored by Alizadeh *et al.* [69]. Applying Duan–Rach Approach (DRA), the nonlinear ordinary differential equations were solved. As the values of micropolar parameter grow the temperature was enhanced.

1.1.5 Stratification

In heat and mass transfer, stratification has considerable recognition and has been investigated by many researchers. The variation in temperature and concentration gradients and presence of different fluids with different densities, cause the stratification. The application of stratification in engineering includes heat rejection into the environment such as ocean, rivers etc. Rashad *et al.* [70] looked into the natural convection flow through a vertical cylinder with stratified nanofluid. The study reported an enhancement in heat and mass transfer rates for an increasing buoyancy ratio parameter. Ibrahim and Makinde [71] studied this flow in an upright plate with double stratification. Also, the study reported that Nusselt and Sherwood number decay with the augmentation of the stratification parameter. Srinivasacharya and Surrender [72] presented the mixed convection flow over a vertical plate, having porous and double stratification. It is highlighted that as the stratification parameter increases, the temperature declines.

1.1.6 Entropy Generation

When heat is transferred, the fluid looses its energy due to the resulting scattering process and frictional forces. For improving the performance of heat transfer entropy is a substantial property. It is described as an estimate of chaos of the system. Entropy production is zero for reversible processes. Only in an irreversible process, the entropy generation is observed. Examples of irreversible processes include diffusion, chemical reaction, liquid flow and fluid viscosity. Air separators, reactors, chillers, fuel cells and solar panels are the examples of entropy generation. In recent years, second law of thermodynamics is utilized to analyze this irreversibility phenomenon. Recently, many researchers used the second law of thermodynamics for thermal engineering systems. At first, Bejan [73] deliberated the entropy generation minimization. Sheikholeslami and Ganji [74] discussed how the entropy generation affects in presence of magnetic field. Applying the Lattic-Boltzmann method, a numerical solution was obtained. Butt and Ali [75] inspected the entropy generation of a viscous fluid in a revolving channel and applied Runge-Kutta-Fehlberg method for obtaining the solution. Abolbashari *et al.* [76] illustrated the entropy generation for the non-Newtonian fluid flow due to a stretching sheet. It was anticipated that for greater values of Biot and Reynolds numbers, entropy generation enhances. Srinivasacharya and Bindu [77] examined the influence of entropy generation due to micropolar fluid through an inclined channel and found that the entropy generation increases for an increasing Brinkman number. Hussain *et al.* [78] analyzed the entropy generation and mixed convection in a partially heated square cavity by applying finite element procedure. It was highlighted that enhancement in Reynolds number indicates an increase in entropy generation and Bejan number. Zeeshan *et al.* [79] discussed the entropy generation for the various shaped nanoparticles on mixed convection flow over a rotating disk. Their study reported that by using the nanoparticles the irreversibility process reduced. Radiative flow and entropy generation was strengthen by Khan *et al.* [80]. By applying the shooting method, the numerical solution was obtained. The results exhibit that the entropy generation and Bejan number behave opposite to Prandtl number. Ojjela *et al.* [81] analyzed the

MHD and entropy generation on squeezing Casson fluid by utilizing the shooting method. The results concluded that entropy decreases when suction parameter increases. Khan *et al.* [82] found the solution of entropy generation for flow of Carreau nanofluid, by employing the homotopy analysis method. It was deliberated that greater Brinkman number reults in higher entropy generation rate. Siavashi *et al.* [83] found the numerical solution of natural convection and entropy generation inside a cavity. It was shown that enhancement in number of fins results in decay of entropy generation. Dawar *et al.* [84] studied MHD Carbon nanofluid flow with the entropy generation and results are obtained by Homotopy analysis method. The result discloses that the entropy generation escalates when Prandtl and Eckert numbers increase.

Considering aforementioned literature survey, it is substantial to observe that the unsteady squeezing flow between parallel plates have a great interest in several engineering and biomedical. It is observed from the available literature that the squeezing behavior of non-Newtonian fluid is paid less attention. The author has made an attempt to analyze the squeezing fluid flow for the non-Newtonian fluid models. Some non-Newtonin fluid models such as Maxwell and Casson are adopted. Stratification and convective boundary conditions are taken into account. Instead of Fourier's and Fick's laws of heat and mass transfer, Cattaneo-Christov heat and mass fluxes are considered. To enhances the thermal conductivity of the fluid the model for nanofluid is adopted.

1.2 Thesis Contributions

In this thesis, numerical simulation of unsteady fluid flow between two parallel plates has been preformed. The solutions are obtained by employing the the shooting method. Initially, we consider the influence of entropy generation and Casson fluid on the unsteady squeezing flow. Then the impact of entropy generation and

Cattaneo-Christov heat flux past through a Riga plate was examined. Furthermore, upper convected Maxwell and Cattaneo-Christov double diffusion has been analyzed. At the end, micropolar nanofluid is discussed. The tables for Nusselt number, skin friction and Sherwood number are presented against different values of the governing parameters. The behaviour of different governing parameters are exhibited through the graphs for velocity, temperature and concentration. Furthermore, the behaviour of the entropy generation and Bejan number have been investigated under the impact of different physical parameters.

1.3 Thesis Outline

This thesis is further subdivided in the following way.

The basic definitions, governing laws for fluid flows, continuity equation, momentum equation, concentration equation, Fourier's law, Cattaneo Christov heat and mass flux are discussed in **Chapter 2**. For upper convected Maxwell fluid, tensor analysis is carried out. The shooting method is discussed in detail, with the help of an example.

The unsteady Casson fluid flow and Cattaneo-Christov heat and mass flux with the convective boundary conditions have been discussed in **Chapter 3**. The governing PDEs are formulated into ODEs by similarity transformation. The formulated boundary value problem is solved by applying the shooting technique. This work is published in "The European Physical Journal Plus", Vol. 134, No. 1, Pages 33-43, 2019.

Unsteady squeezing flow past a Riga plate with entropy generation and Cattaneo Christov heat flux is considered in **Chapter 4**. Similarity transformations are used to change the system of partial differential equations into ordinary one. Then we

applied the shooting technique to solve the system. This work has been published in "Bulletin of the Polish Academy of Sciences, Technical sciences", Vol. 66, No. 3, 2018.

Squeezing flow of upper convected Maxwell nanofluid is investigated in **Chapter 5**. Cattaneo-Christov double diffusion is employed. Entropy generation is also discussed. The partial differential equations are converted into ordinary system of equations to obtain the numerical solution. This work is published in "Journal of Nanofluids", Vol. 8, No. 2, Pages, 420-429, 2019.

The unsteady squeezing micropolar nanofluid flow between two parallel plates with the Buongiorno's model is studied in **Chapter 6**. The laws of fluid motions are in the form of PDEs. These PDEs are converted into ODEs by similarity transformation. The solution of the ODEs is obtained through the shooting method.

The conclusion along with a discussion for the future work is presented in **Chapter 7**.

Chapter 2

Basic Governing Laws and Solution Methodology

The basic laws governing the mathematical models are discussed in this chapter. Heat flux models along with the non-Newtonian fluid models are presented. Solution methodology is briefly discussed. The shooting method has been explained through an example.

2.1 Fundamental Laws

2.1.1 Law of Conservation of Mass

The expression for law of conservation of mass according to [85] is as follows: "For any fluid, conservation of mass is expressed by the scalar equation,

$$\frac{\partial \rho}{\partial t} + \nabla . (\rho \mathbf{V}) = 0, \tag{2.1}$$

where ρ is the density and $\mathbf{V}$ is the velocity of the fluid. Hence a velocity profile represents an admissible (real) flow, if and only if it satisfies the continuity

equation. For incompressible fluids, Eq. (2.1) reduces to

$$\nabla.\mathbf{V} = 0, \tag{2.2}$$

In Cartesian coordinates

$$\frac{\partial u}{\partial x} + \frac{\partial v}{\partial y} + \frac{\partial w}{\partial z} = 0. \tag{2.3}$$

Here, u, v and w are the velocity components along x, y and z direction respectively."

2.1.2 Law of Conservation of Momentum

Momentum equation is stated as [85] "For any fluid, the momentum equation is,

$$\rho\frac{D\mathbf{V}}{Dt} = \nabla.\tau + \rho\mathbf{b}, \tag{2.4}$$

The Cauchy stress tensor for an incompressible flow is $\tau = -p\mathbf{I} + \mathbf{S}$ in which p is the pressure, $\mathbf{I}$ is the identity tensor, $\mathbf{S}$ is the extra stress tensor, $\mathbf{b}$ is the body force and $\frac{D}{Dt}$ is the material time derivative. The Cauchy stress tensor and the velocity field are

$$\begin{bmatrix} \sigma_{xx} & \tau_{xy} & \tau_{xz} \\ \tau_{yx} & \sigma_{yy} & \tau_{yz} \\ \tau_{zx} & x_{zy} & \sigma_{zz} \end{bmatrix},$$

$$\mathbf{V} = [u(x,y,z,t)\ , v(x,y,z,t),\ w(x,y,z,t)]\,,$$

where σ_{xx}, σ_{yy} and σ_{zz} are the normal stresses, τ_{xy}, τ_{xz}, τ_{yx}, τ_{yz}, τ_{zx} τ_{zy} are shear stresses and u, v, w are the velocity components along the x, y and z direction respectively. Eq. (2.4) in component form yields

$$\rho\left(\frac{\partial u}{\partial t} + u\frac{\partial u}{\partial x} + v\frac{\partial u}{\partial y} + w\frac{\partial u}{\partial z}\right) = \frac{\partial(\sigma_{xx})}{\partial x} + \frac{\partial(\tau_{xy})}{\partial y} + \frac{\partial(\tau_{xz})}{\partial z} + \rho b_x, \tag{2.5}$$

$$\rho\left(\frac{\partial v}{\partial t}+u\frac{\partial v}{\partial x}+v\frac{\partial v}{\partial y}+w\frac{\partial v}{\partial z}\right)=\frac{\partial(\tau_{yx})}{\partial x}+\frac{\partial(\sigma_{yy})}{\partial y}+\frac{\partial(\tau_{yz})}{\partial z}+\rho b_y, \tag{2.6}$$

$$\rho\left(\frac{\partial w}{\partial t}+u\frac{\partial w}{\partial x}+v\frac{\partial w}{\partial y}+w\frac{\partial w}{\partial z}\right)=\frac{\partial(\tau_{zx})}{\partial x}+\frac{\partial(\tau_{zy})}{\partial y}+\frac{\partial(\sigma_{zz})}{\partial z}+\rho b_z, \tag{2.7}$$

where, b_x, b_y and b_z show the components of body force along the x, y and z-axes, respectively. The above equations for two dimensional flow become

$$\rho\left(\frac{\partial u}{\partial t}+u\frac{\partial u}{\partial x}+v\frac{\partial u}{\partial y}\right)=\frac{\partial(\sigma_{xx})}{\partial x}+\frac{\partial(\tau_{xy})}{\partial y}+\rho b_x, \tag{2.8}$$

$$\rho\left(\frac{\partial v}{\partial t}+u\frac{\partial v}{\partial x}+v\frac{\partial v}{\partial y}\right)=\frac{\partial(\tau_{yx})}{\partial x}+\frac{\partial(\sigma_{yy})}{\partial y}+\rho b_y.\text{"} \tag{2.9}$$

2.1.3 Energy Equation (Conservation Law of Energy)

Conservation of thermal energy is expressed by [85]:

$$\text{"}\rho\left[\frac{\partial \mathbf{U}}{\partial t}+\mathbf{V}.\nabla\mathbf{U}\right]=[\tau:\nabla\mathbf{V}+p\nabla.\mathbf{V}]+\nabla(k_1\nabla T)\pm\dot{H}_r, \tag{2.10}$$

where $\mathbf{U}$ is the internal energy, $\dot{H}_r$ is the heat of reaction and : is the double dot product. According to the internal energy, $d\mathbf{U}=C_v dT$, Eq. (2.10) becomes,

$$\rho C_v\left[\frac{\partial T}{\partial t}+\mathbf{V}.\nabla T\right]=[\tau:\nabla\mathbf{V}+p\nabla.\mathbf{V}]+\nabla(k_1\nabla T)\pm\dot{H}_r, \tag{2.11}$$

For heat conduction in solids, when $\mathbf{V}=0$, $\nabla\mathbf{V}=0$, and $C_v=C$, the resulting equation is

$$\rho C\frac{\partial T}{\partial t}=\nabla(k_1\nabla T)\pm\dot{H}_r.$$

For phase change, the latent heat rate per unit volume must be added as a source term to the energy equation."

2.1.4 Mass Transfer with Chemical Reaction

According to [86], "the general equation of mass transfer when accompanied by a chemical reaction is an unsteady state mass transport equation, that incorporates

not only diffusion but also the convective mass transport and chemical reaction contribution. In the two dimensional form, the equation for mass transfer can be written as follows:

$$\frac{\partial C}{\partial t} + u\frac{\partial C}{\partial x} + v\frac{\partial C}{\partial y} = D\left(\frac{\partial^2 C}{\partial x^2} + \frac{\partial^2 C}{\partial y^2}\right) + R_i, \tag{2.12}$$

where

$$u\frac{\partial C}{\partial x} + v\frac{\partial C}{\partial y}, \tag{2.13}$$

is the convective transport contribution and $D\left(\frac{\partial^2 C}{\partial x^2} + \frac{\partial^2 C}{\partial y^2}\right)$ is the molecular contribution, R_i is the chemical reaction contribution, and D is the diffusion coefficient of the liquid."

2.2 Heat Flux Models

2.2.1 Fourier's Law

According to [87], "Governing rate equation for conduction is given by Fourier's law. This is an empirical law based on the experimental observation of Biot, but formulated by the French mathematician and physicist, Fourier in 1822. It states that the rate of heat flow by conduction in a given direction is proportional to the area normal to the direction of the heat flow and to the gradient of temperature in the direction. Mathematically,

$$q_{1_x} = -k_1 A\frac{dT}{dx}. \tag{2.14}$$

here q_{1_x} is the rate of heat transfer in the x-direction, A is the area normal to the direction of heat flow, $\frac{dT}{dx}$ is the temperature gradient in the x-direction."

2.2.2 Cattaneo-Christov Heat Flux [32, 88]

"To resolve the paradox associated with Fourier's law. Cattaneo proposed the model in 1948 known as Maxwell-Cattaneo (MC) model. Cattaneo inserted relaxation time in Fourier's relation which characterizes the time necessitated for heat conduction to establish in a volume element when temperature gradient is imposed across it. Mathematical expression is:

$$\mathbf{q_1} + \lambda_1 \frac{\partial \mathbf{q_1}}{\partial t} = -k_1 \nabla T, \tag{2.15}$$

where λ_1 is the thermal relaxation time, $\mathbf{q_1}$ is the heat flux and k_1 is the thermal conductivity.

In 2009 Christov done incredible modification in Cattaneo-Maxwell model. He replaced the ordinary derivative with upper convected derivatives. After this modification of MC model, the main advantage is that one can eliminate $\mathbf{q_1}$ in order to obtain one equation of temperature. Cattaneo-Christov heat flux theory for fluids is defined as

$$\mathbf{q_1} + \delta_{E_1} \left[\frac{\partial \mathbf{q_1}}{\partial t} + \mathbf{V}.\nabla \mathbf{q_1} - \mathbf{q_1}.\nabla \mathbf{V} \right] = -k_1 \nabla T." \tag{2.16}$$

2.3 Classification of Fluids

According to the [89] "An important parameter that characterizes the behavior of fluids is viscosity because it relates the local stresses in a moving fluid to the rate of deformation of the fluid element. When a fluid is sheared, it begins to move at a rate of deformation inversely proportional to viscosity.

To better understand the concept of shear viscosity we assume the model consists of two solid parallel plates are set on the top of each other with a liquid film of thickness Y between them. The lower plate is at rest and the upper plate can be set in motion by a force $\mathbf{F}$ resulting in velocity $\mathbf{V}$. The movement of the upper plate first sets the immediately adjacent layer of liquid molecules into motion, this

layer transmits the action to the subsequent layers underneath it because of the intermolecular forces between the liquid molecules.

The applied force act on an area, A, of the liquid surface, inducing a shear stress $\left(\frac{\mathbf{F}}{A}\right)$. The displacement of liquid at the top plate, Δx, relative to the thickness of the film is called shear strain $\frac{\Delta x}{L}$, and the shear strain per unit time is called the shear rate $\frac{\mathbf{U}}{Y}$. If the distance Y is not too large or the velocity $\mathbf{V}$ is too high, the velocity gradient will be a straight line. For large class of fluid,

$$\mathbf{F} \sim \frac{A\mathbf{V}}{Y},$$

From above $\frac{\mathbf{V}}{Y}$ can be replaced by the velocity gradient $\frac{d\mathbf{V}}{dy}$. If a constant of proportionality is introduced, the shearing stress between any two thin sheets of fluid may be expressed by:

$$\tau = \frac{\mathbf{F}}{A} = \mu\frac{\mathbf{V}}{Y} = \mu\frac{d\mathbf{V}}{dy}, \tag{2.17}$$

In transposed from it serves to define the proportionality constant

$$\mu = \frac{\tau}{\frac{d\mathbf{V}}{dy}}. \tag{2.18}$$

which is called the dynamic coefficient of the viscosity. The dimension of dynamic viscosity is force per unit area divided by velocity gradient or shear rate. In the metric system, the dimension of dynamic viscosity is Pa.s. In general, fluids are classified into two main types, namely, Newtonian and non-Newtonian fluids. These two types of fluids cover most of the applications of industry, engineering, and biomedical sciences.

2.3.1 Newtonian Fluid

A fluid for which the constant of proportionality (the viscosity) does not change with rate of deformation is said to be a Newtonian fluid and represented by a

straight line. The slope of this line is determine by the viscosity. Examples of Newtonian fluids include water, air, glycerol, oils, alcohol, etc.

2.3.2 Non-Newtonian Fluid

There is a certain class of fluids, called non-Newtonian fluids, in which the viscosity varies with the shear rate. Typical representation of non-Newtonian fluids are liquids which are formed either partially or wholly of polymers or two phase materials. Examples of non-Newtonian fluids include salt solutions, molten polymers, ketchup, custard, starch suspensions, honey, paints, blood, and synovial fluid, etc. There are various types of non-Newtonian fluid. Pseudoplastic fluids are those fluids for which viscosity decreases by increasing the shear rate and hence are often referred to as shear thinning fluids. These fluids are found in many real fluids such as polymer melts and solutions. When the viscosity increases with shear rate the fluid are referred to as dilatant or shear thickening fluids. Some fluids do not flow unless the stress applied exceeds a certain value referred to as the yield stress. These fluid are termed fluids with yield stress or viscoplastic fluids. There are numerous non-Newtonian fluid models that have been developed and studied in the literature. However, two of the commonly used and related to our thesis is the Maxwell and Casson fluid models."

2.3.2.1 Upper Convected Maxwell Fluid

"It is a simple subclass of the rate type fluids which elaborates the features of linear viscoelastic fluids having only the relaxation time [90]. The extra stress tensor $\mathbf{S}$ for a Maxwell fluid and the Cauchy stress tensor τ are given by

$$\left(1 + \lambda_1 \frac{D}{Dt}\right) \mathbf{S} = \mu A_1, \tag{2.19}$$

$$\tau = -p\mathbf{I} + \mathbf{S}, \tag{2.20}$$

in which λ_1 is the relaxation time, $\frac{D}{Dt}$ the covariant differentiation, μ denotes the dynamic viscosity and A_1 the first Rivlin-Erickson tensor. The first Rivlin-Erickson tensor and contravariant convected derivative $\frac{D}{Dt}$ are respectively defined as

$$A_1 = \nabla \mathbf{V} + (\nabla \mathbf{V})^*, \tag{2.21}$$

$$\frac{D\mathbf{S}}{Dt} = \frac{d\mathbf{S}}{dt} - \mathbf{SL} - \mathbf{SL}^*, \tag{2.22}$$

The equations which governs the incompressible flow are

$$\nabla.\mathbf{V} = 0, \tag{2.23}$$

$$\rho \frac{d\mathbf{V}}{dt} = -\nabla p + \nabla.\mathbf{S}, \tag{2.24}$$

where ρ is the density, $\mathbf{V}$ is the velocity. We have to eliminate the extra stress tensor $\mathbf{S}$ from Eq. (2.19) and Eq. (2.24). From Eq. (2.24) one can write

$$\rho \left(1 + \lambda_1 \frac{d\mathbf{V}}{dt}\right) \frac{D\mathbf{V}}{Dt} = -\left(1 + \lambda_1 \frac{D}{Dt}\right) \nabla p + \left(1 + \lambda_1 \frac{D}{Dt}\right) (\nabla.\mathbf{S}), \tag{2.25}$$

$$\rho \left(1 + \lambda_1 \frac{D}{Dt}\right) \frac{D\mathbf{V}}{Dt} = -\left(1 + \lambda_1 \frac{D}{Dt}\right) \nabla p + \nabla.\left(1 + \lambda_1 \frac{D}{Dt}\right) \mathbf{S}, \tag{2.26}$$

$$\rho \left(1 + \lambda_1 \frac{D}{Dt}\right) \frac{D\mathbf{V}}{Dt} = -\left(1 + \lambda_1 \frac{D}{Dt}\right) \nabla p + \mu \nabla.A_1, \tag{2.27}$$

Component form of the two dimensional steady flow of Maxwell fluid can be represented by the following expression:

$$u\frac{\partial u}{\partial x}+v\frac{\partial u}{\partial y}+\lambda_1\left(u^2\frac{\partial^2 u}{\partial x^2}+v^2\frac{\partial^2 u}{\partial y^2}+2uv\frac{\partial^2 u}{\partial x\partial y}\right)=\nu\left(\frac{\partial^2 u}{\partial x^2}+\frac{\partial^2 u}{\partial y^2}\right), \tag{2.28}$$

$$u\frac{\partial v}{\partial x}+v\frac{\partial v}{\partial y}+\lambda_1\left(u^2\frac{\partial^2 v}{\partial x^2}+v^2\frac{\partial^2 v}{\partial y^2}+2uv\frac{\partial^2 v}{\partial x\partial y}\right)=\nu\left(\frac{\partial^2 v}{\partial x^2}+\frac{\partial^2 v}{\partial y^2}\right)." \tag{2.29}$$

2.3.3 Casson Fluid [91]

"Among enormous mathematical models of blood rheology proposed in the past, the Casson fluid has been widely used as the non-Newtonian fluid model to represent the suspension of RBCs in the core region of blood flow in small vessels since the Casson fluid model can predict satisfactorily the flow behavior of a non-Newtonian fluid with yield stress using only a single model parameter. The Casson fluid model could be the best description of blood when flows through narrow arteries at low shear rate and it can be applied to human blood over a wide range of hematocrits and shear rates. The mathematical expression of the Casson fluid model is as follows:

$$\sqrt{\tau_{ij}}=\begin{cases}0 & \text{for} \quad \tau\le\tau_0,\\ \sqrt{\tau_0}+\sqrt{\mu}\sqrt{\dot{\gamma}_{ij}} & \text{for} \quad \tau>\tau_0,\end{cases} \tag{2.30}$$

where τ_{ij} is the deviatoric stress tensor, τ_0 is the yield stress, μ is the dynamic viscosity of the Casson fluid and $\dot{\gamma}_{ij}$ is the shear rate."

2.4 Principle of Entropy Generation [92]

"The concepts of entropy generation and irreversibility, derived from the second law of thermodynamics, were introduced by the German physicist Rudolf Clausius

in 1856. According to the second law of thermodynamics, the entropy of a closed system always increases with the time. It is constant in the case when a process is reversible or in equilibrium. The enhancement in the entropy elucidates the irresponsibility of the natural processes.

Entropy is the thermodynamic characteristics just like pressure and temperature. The change in a closed system subject to entropy is expressed by the ratio $\frac{\mathbf{q}_1}{T}$, where $\mathbf{q}_1$ is net heat transfer and T is temperature. Entropy increases as T decreases or $\mathbf{q}_1$ increases. In a reversible process, a small increase in the entropy dS of a system is defined as a ratio of the small transfer of heat $\delta\mathbf{q}_1$ to a closed system divided by the common temperature T of the system and the surroundings which supply the heat, i.e.,

$$dS = \frac{\delta\mathbf{q}_1}{T}, \tag{2.31}$$

Eq. (2.31) is valid for an ideal, closed and reversible process. For an actually possible small process in an isolated system, the second law requires that the above equation changes to an inequality given by

$$dS > \frac{\delta\mathbf{q}_1}{T}". \tag{2.32}$$

2.5 Solution Methodology

2.5.1 Shooting Method [93]

"In a shooting method, the missing initial condition at the initial point of the interval is assumed, and the differential equation is then integrated numerically as an initial value problem. The accuracy of the assumed missing initial condition is then checked by comparing the calculated value of the dependent variable at the terminal point with its given value here. If a difference exist, another value of the missing initial condition must be assumed and the process is repeated. This process is continued until the agreement between the calculated and the given condition

at the terminal point is within the specified degree of accuracy. One naturally inquires whether or not there is a systematic way of finding each succeeding value of the missing initial point. Consider the second order differential equation

$$\frac{d^2y}{dx^2} = f\left(x,\ y,\ \frac{dy}{dx}\right), \tag{2.33}$$

subject to the boundary conditions

$$y\left(0\right) = 0, \qquad y\left(L\right) = A. \tag{2.34}$$

First, Eq. (2.33) is written in terms of a system of two first order differential equations. By denoting y by y_1 and y_1' by y_2.

$$\left.\begin{aligned} y_1' &= y_2, & y_1\left(0\right) &= 0, \\ y_2' &= f\left(x,\ y_1,\ y_2\right) & y_1\left(L\right) &= A. \end{aligned}\right\} \tag{2.35}$$

We denote the missing initial condition $y_2\left(0\right)$ by s, to have

$$\left.\begin{aligned} y_1' &= y_2, & y_1\left(0\right) &= 0, \\ y_2' &= f\left(x,\ y_1,\ y_2\right) & y_2\left(0\right) &= s. \end{aligned}\right\} \tag{2.36}$$

Now the problem is to find s such that the solution of Eq. (2.35) satisfies the boundary condition $y\left(L\right) = A$. In other words, if the solutions of the initial value problem are denoted by $y_1\left(x, s\right)$ and $y_2\left(x, s\right)$, one searches for the value of s such that

$$y_1\left(L, s\right) - A = \phi\left(s\right) = 0. \tag{2.37}$$

For Newton's method, the iteration formula for s is given by

$$s^{n+1} = s^n - \frac{\phi\left(s^n\right)}{d\phi\left(s^n\right)/ds}, \tag{2.38}$$

$$s^{n+1} = s^n - \frac{y_1(L, s^n) - A}{\partial y_1(L, s^n)/\partial s}. \tag{2.39}$$

To find the derivative of y_1 with respect to s, Eqs. (2.35), (2.33), and (2.36) are differentiated with respect to s, and we get

$$\frac{dy_1}{ds} = y_3, \qquad \frac{dy_2}{ds} = y_4. \tag{2.40}$$

This process results in the following initial value problem.

$$\left.\begin{aligned} y_3' &= y_4, & y_3(0) &= 0, \\ y_4' &= \frac{\partial f}{\partial y_1} y_3 + \frac{\partial f}{\partial y_2} y_4, & y_4(0) &= 1. \end{aligned}\right\} \tag{2.41}$$

Now solving the Eq. (2.41), the value of y_3 at L can be computed. This value is actually the derivative of y_1 with respect to s computed at L. Setting the vale of $y_3(L, s)$ in Eq. (2.39), the modified value of s can be achieved. This new value of s is used to solve the Eq. (2.36) and the process is repeated until the value of s is within a described degree of accuracy."

2.5.2 Example [94]

"Let us consider the boundary value problem having order four.

$$y^{iv} - 2yy'' = 0, \qquad 0 \le x \le 1, \tag{2.42}$$

with the boundary conditions

$$y(0) = 1, \quad y'(0) = 0, \quad y(1) = 0, \quad y'(1) = 0. \tag{2.43}$$

To convert Eq. (2.42), into a system of first order equations, the following notations have been introduced

$$y = y_1, \quad y' = y_2, \quad y'' = y_3, \quad y''' = y_4. \tag{2.44}$$

The given boundary value problem is then converted to the following form

$$\left.\begin{aligned} y_1' &= y_2, & y_1(0) &= 0, \\ y_2' &= y_3, & y_2(0) &= 0, \\ y_3' &= y_4, & y_1(1) &= 0, \\ y_4' &= 2y_1y_3, & y_2(1) &= 0. \end{aligned}\right\} \tag{2.45}$$

Denote the missing initial conditions $y_3(0)$ and $y_4(0)$ by Γ and Λ respectively, to have the following initial value problem

$$\left.\begin{aligned} y_1' &= y_2, & y_1(0) &= 0, \\ y_2' &= y_3, & y_2(0) &= 0, \\ y_3' &= y_4, & y_1(1) &= \Gamma, \\ y_4' &= 2y_1y_3, & y_2(1) &= \Lambda. \end{aligned}\right\} \tag{2.46}$$

Now, solving the above initial value problem by using the RK-4 method over the interval $[0,1]$. The solution obtained by the RK-4 method is then analyzed for y_1 and y_1'. If these solutions meet the boundary condition given in Eq. (2.42), then the problem is solved. However, usually this does not happen in the first go. So, we have to refine the initial guesses iteratively. For this purpose we use the Newtons method to solve the following system of nonlinear algebraic equations.

$$\left.\begin{aligned} y_1(x,\Gamma,\Lambda) &= 0, \\ y_2(x,\Gamma,\Lambda) &= 0. \end{aligned}\right\} \tag{2.47}$$

The iterative scheme for the Newton's method for the system of non-linear equations (2.46), is given by

$$\begin{bmatrix} \Gamma_{n+1} \\ \Lambda_{n+1} \end{bmatrix} = \begin{bmatrix} \Gamma_n \\ \Lambda_n \end{bmatrix} - \begin{bmatrix} \frac{\partial}{\partial\Gamma} y_1(1,\Gamma_n,\Lambda_n) & \frac{\partial}{\partial\Lambda} y_1(1,\Gamma_n,\Lambda_n) \\ \frac{\partial}{\partial\Gamma} y_2(1,\Gamma_n,\Lambda_n) & \frac{\partial}{\partial\Lambda} y_2(1,\Gamma_n,\Lambda_n) \end{bmatrix}^{-1} \begin{bmatrix} y_1(1,\Gamma_n,\Lambda_n) \\ y_2(1,\Gamma_n,\Lambda_n) \end{bmatrix}. \tag{2.48}$$

For simplification, use the following notations,

$$\left.\begin{array}{ll} \dfrac{\partial y_1}{\partial \Gamma} = y_5, & \dfrac{\partial y_2}{\partial \Gamma} = y_6, \\ \dfrac{\partial y_3}{\partial \Gamma} = y_7, & \dfrac{\partial y_4}{\partial \Gamma} = y_8, \\ \dfrac{\partial y_1}{\partial \Lambda} = y_9, & \dfrac{\partial y_2}{\partial \Lambda} = y_{10}, \\ \dfrac{\partial y_3}{\partial \Lambda} = y_{11}, & \dfrac{\partial y_4}{\partial \Lambda} = y_{12}. \end{array}\right\} \tag{2.49}$$

To find the Jacobin matrix, differentiating the system of Eqs. (2.46) first with respect to Γ and then with respect to Λ and using the new notations, we get

$$\left.\begin{array}{ll} y_5' = y_6, & y_5(0) = 0, \\ y_6' = y_7, & y_6(0) = 0, \\ y_7' = y_8, & y_7(0) = 1, \\ y_8' = 2\left(y_1 y_7 + y_3 y_5\right), & y_8(0) = 0, \\ y_9' = y_{10}, & y_9(0) = 0, \\ y_{10}' = y_{11}, & y_{10}(0) = 0, \\ y_{11}' = y_{12}, & y_{11}(0) = 1, \\ y_{12}' = 2\left(y_1 y_{11} + y_3 y_9\right), & y_{12}(0) = 1. \end{array}\right\}. \tag{2.50}$$

Solve the above system of equations (2.50) by the RK-4 method and put the computed values of y_5, y_9, y_6 and y_{10} in (2.48). This gives the modified initial guesses. This procedure is repeated until we achieve the solutions with required accuracy".

Chapter 3

Entropy Generation and Unsteady Casson Fluid Flow Squeezing between Two Parallel Plates Subject to Cattaneo-Christov Heat and Mass Flux

3.1 Introduction

In this chapter, unsteady two-dimensional Casson fluid flow that influences entropy generation on the squeezing flow is numerically investigated. Instead of Fourier's and Fick's laws, Cattaneo-Christov model for heat and mass flux is adopted. Conservation laws for mass, momentum, energy and concentration describe attributes of fluid flow. The nonlinear PDEs are non-dimensionalized to the ODEs by using a suitable similarity transformation. Shooting method is employed to get the numerically solutions of system of ODEs. A built-in MATLAB function bvp4c has

been utilized to validate the results. The numerical values of mass transfer rate and the skin friction coefficient are analyzed by collecting them in tabular form. The profiles for temperature, velocity and concentration are plotted against the influential parameters used in the study. A comparison for the present and already published results has been shown in the form of tables.

3.2 Problem Formulation

3.2.1 The Problem Configuration

This portion includes the mathematical model of unsteady, two-dimensional, viscous, incompressible, Casson fluid flow between two parallel plates (see Figure 3.1). The plate at lower surface is located at $y = 0$, having stretchable velocity $U_w = \frac{ax}{1-\gamma_1 t}$. Furthermore, the upper plate is situated at $y = h\,(t) = \sqrt{\frac{\nu(1-\gamma_1 t)}{a}}$, squeezing with the velocity $v_h = \frac{dh}{dt}$. Heat and mass flux through Cattaneo-Christov model [33] have been considered. Heat flux $\mathbf{q_1}$ and mass flux $\mathbf{J_1}$ [95] are described by

$$\mathbf{q_1} + \delta_{E_1}\left[\frac{\partial \mathbf{q_1}}{\partial t} + \mathbf{V}.\nabla \mathbf{q_1} + (\nabla.\mathbf{V})\,\mathbf{q_1} - \mathbf{q_1}.\nabla \mathbf{V}\right] = -k_1 \nabla T, \tag{3.1}$$

$$\mathbf{J_1} + \delta_{C_1}\left[\frac{\partial \mathbf{J_1}}{\partial t} + \mathbf{V}.\nabla \mathbf{J_1} + (\nabla.\mathbf{V})\,\mathbf{J_1} - \mathbf{J_1}.\nabla \mathbf{V}\right] = -D_B \nabla C. \tag{3.2}$$

In Eqs. (3.1) and (3.2) when δ_{E_1}=δ_{C_1}=0, classical Fourier's and Ficks's laws are presented. Using $\nabla.\mathbf{V} = 0$ in the above equations, the Eqs. (3.1) and (3.2) are converted into the following forms

$$\mathbf{q_1} + \delta_{E_1}\left[\frac{\partial \mathbf{q_1}}{\partial t} + \mathbf{V}.\nabla \mathbf{q_1} - \mathbf{q_1}.\nabla \mathbf{V}\right] = -k_1 \nabla T, \tag{3.3}$$

$$\mathbf{J_1} + \delta_{C_1}\left[\frac{\partial \mathbf{J_1}}{\partial t} + \mathbf{V}.\nabla \mathbf{J_1} - \mathbf{J_1}.\nabla \mathbf{V}\right] = -D_B \nabla T. \tag{3.4}$$

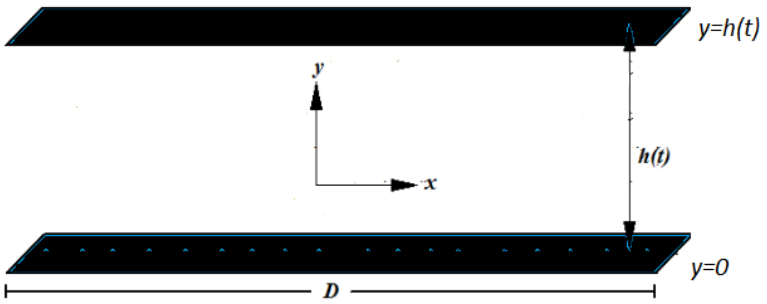

Figure 3.1: Schematic illustration of the squeezing flow.

3.2.2 Governing Equations

The governing equations of continuity, momentum, energy and concentration are given as follows [21]

$$u_x + v_y = 0, \tag{3.5}$$

$$u_t + uu_x + vu_y = \frac{1}{\rho}P_x + \nu\left(1 + \frac{1}{\gamma}\right)(u_{xx} + u_{yy}), \tag{3.6}$$

$$v_t + uv_x + vv_y = \frac{1}{\rho}P_y + \nu\left(1 + \frac{1}{\gamma}\right)(v_{xx} + v_{yy}), \tag{3.7}$$

$$T_t + UT_x + VT_y + \lambda_{E_1}\Omega_{E_1} = \alpha T_{xx} + T_{yy} - \frac{1}{(\rho c_p)}\hat{q}_{ry}, \tag{3.8}$$

$$C_t + UC_x + VC_y + \lambda_{C_1}\Omega_{C_1} = D_B(C_{xx} + C_{yy}) - K_1(C - C_f). \tag{3.9}$$

In Eqs. (3.8)-(3.9) Ω_{E_1} and Ω_{C_1}, are formulated as

$$\begin{aligned}\Omega_{E_1} = {} & T_{tt} + uu_xT_x + vv_yT_y + U^2T_{xx} + v^2T_{yy} + u_tT_x + 2uvT_{xy} \\ & + 2uT_{xt} + uv_xT_y + v_tT_y + vU_yT_x + 2VvT_{yt}.\end{aligned} \tag{3.10}$$

$$\begin{aligned}\Omega_{E_1} = {} & C_{tt} + uu_xC_x + vv_yC_y + u^2C_{xx} + v^2C_{yy} + u_tC_x + 2uvC_{xy} \\ & + 2uC_{xt} + uv_xC_y + v_tC_y + vU_yC_x + 2VC_{yt}.\end{aligned} \tag{3.11}$$

The corresponding boundary conditions for the governing PDEs are given as:

$$\left.\begin{aligned} &u\left(x,y,t\right)=\frac{ax}{1-\gamma_1 t}, \quad v\left(x,y,t\right)=0,\\ &-k_1T_y=h_2(T_h-T), \quad -D_BC_y=h_3(C_h-C), \quad \text{at} \quad y=0,\\ &u\left(x,y,t\right)=0, \quad v\left(x,y,t\right)=v_h=h_t, T=T_f, \quad C=C_f \quad \text{at} \quad y=h\left(t\right). \end{aligned}\right\} \tag{3.12}$$

The thermal radiation heat flux [96] is stated according to the Rosseland approximation,

$$\hat{q}_r=\frac{-4\hat{\delta}_e}{3\hat{\beta}_R}\,T_y^4, \tag{3.13}$$

where $\hat{\delta}_e$ represents Stefan-Boltzmann constant and $\hat{\beta}_R$ represents as absorption coefficient. Taylor's series is applied to expand T^4 about temperature T_h. Omitting higher terms, one obtains

$$T^4=4TT_h^3-3T_h^4. \tag{3.14}$$

3.2.3 Dimensionless Equations

Following transformations [56] have been introduced to convert Eqs. (3.5)-(3.9) into the nondimensional form:

$$\left.\begin{aligned} &\Psi=\sqrt{\frac{a\nu}{1-\gamma_1 t}}\;xf\left(\eta\right), \quad \theta(\eta)=\frac{T-T_f}{T_h-T_f}, \quad u=\Psi_y=U_wf'(\eta)\\ &v=-\Psi_x=-\sqrt{\frac{a\nu}{1-\gamma_1 t}}f\left(\eta\right), \quad \eta=\frac{y}{h(t)}, \quad \phi(\eta)=\frac{C-C_f}{C_h-C_f}. \end{aligned}\right\} \tag{3.15}$$

Equivalently, Eq. (3.5) is fulfilled and the other Eqs. (3.6)-(3.9) acquire the form

$$\left(1+\frac{1}{\gamma}\right)f''''+ff'''-f'f''-\frac{Sq}{2}\left(3f''+\eta f'''\right)=0, \tag{3.16}$$

$$\left.\begin{aligned} &\left(1+Rd\right)\theta''+Pr(f\theta'-\frac{\eta}{2}Sq\;\theta')-Pr\beta_e(ff'\theta'+f^2\theta''-\eta Sq\;f\theta'')\\ &-\frac{Pr}{4}\eta\beta_eSq^2(3\theta'+\eta^2\theta'')+\frac{Pr}{2}\beta\beta_e(\eta f'\theta'+3f\theta')=0, \end{aligned}\right\} \tag{3.17}$$

$$\left.\begin{aligned}&\phi'' + Pr\ Sc\left(f\phi' - \frac{Sq}{2}\eta\phi' - Kr\phi\right) - Pr\ Sc\beta_c\left(ff'\phi' + f^2\phi'' - Sq\eta f\phi''\right)\\&-\frac{\eta}{4}Sc\ Pr\beta_c Sq^2\left(3\phi' + \eta\phi''\right) + \frac{Pr}{2}Sc\beta_c\ Sq\left(3f\phi' + f'\phi'\eta\right) = 0.\end{aligned}\right\} \tag{3.18}$$

By using the similarity transformation Eq. (3.15), the boundary conditions Eq. (3.12) are as follows:

$$\left.\begin{aligned}&f(0) = 0,\ \ \theta'(0) = Bi_1\left(1 - \theta(0)\right),\\&f'(0) = 1,\ \ \phi'(0) = Bi_2\left(1 - \phi(0)\right),\\&f(1) = \frac{Sq}{2},\ \ f'(1) = 1,\ \ \theta(1) = 0,\ \ \phi(1) = 0.\end{aligned}\right\} \tag{3.19}$$

Different dimensionless parameters occurring in Eqs. (3.16)-(3.19), are expressed as

$$\begin{aligned}&Sq = \frac{\gamma_1}{a},\quad Rd = \frac{16T_h^3\hat{\sigma}_e}{3\hat{\beta}_R k_1},\quad Pr = \frac{\nu}{\alpha},\quad Kr = \frac{K_1(1-\gamma_1 t)}{a},\\&Sc = \frac{\alpha}{D_B},\quad Bi_1 = \frac{-h_2}{k_1}\sqrt{\frac{\nu(1-\gamma_1 t)}{a}},\quad Bi_2 = \frac{-h_3}{k_1}\sqrt{\frac{\nu(1-\gamma_1 t)}{a}},\\&\beta_e = \frac{a\lambda_{E_1}}{1-\gamma_1 t},\quad \beta_c = \frac{a\lambda_{C_1}}{1-\gamma_1 t}.\end{aligned}$$

3.2.4 Physical Quantities

The important quantities of interest, heat and mass transfer rate, the skin friction coefficient, are constructed as:

$$C_f = \frac{\tau_w}{\rho U_w^2},\quad Sh_x = \frac{xq_m}{D(C_h - C_f)},\quad Nu_x = \frac{xq_w}{k_1(T_h - T_f)},$$

where τ_w represents the skin friction, q_m denotes concentration flux and q_w denotes the heat flux. The above mentioned quantities are stated as

$$\tau_w = \mu\left(u_y\right)_{y=h(t)},\quad q_m = -D\left(C_y\right)_{y=h(t)},\quad q_w = -\left(k_1 + \frac{16T_h^3\hat{\sigma}_e}{3\hat{\beta}_R}\right)\left(T_y\right)_{y=h(t)}.$$

By employing appropriate similarity transformation, the dimensionless forms of the skin friction, heat and mass transfer rates are:

$$C_f Re_x^{1/2} = f''(1),\ Sh_x Re_x^{-1/2} = -\phi'(1),\ NuRe_x^{-1/2} = -(1+Rd)\theta'(1).$$

The local Reynolds number is interpreted as $Re_x = \dfrac{xU_w}{\nu}$.

3.2.5 Entropy Generation Analysis

According to [76], the entropy generation is defined as

$$S'''_{gen} = \frac{k_1}{T_h^2}\left[(T_y)^2 + \frac{16T_h^3\hat{\sigma}_e}{3\hat{\beta}_R k_1}(T_y)^2\right] + \left(1+\frac{1}{\gamma}\right)\frac{\mu}{T_h}(u_y)^2 + \left[\frac{RD}{C_h}(C_y)^2 + \frac{RD}{T_h}(T_y C_y)\right]. \tag{3.20}$$

From above, the first term indicates heat transfer (also known as heat transfer irreversibility HTI), second term describes fluid friction (also known that fluid friction irreversibility FFI) and the third term is due to mass transfer (also known as the mass transfer irreversibility MTI). The characteristic entropy generation is described as

$$S'''_0 = \frac{k_1 (T_f - T_h)^2}{h^2 T_h^2}. \tag{3.21}$$

The non dimensional form of the entropy generation is obtained after using the similarity transformation

$$\begin{aligned} NG = {} & Re\,(1+Rd)\,\theta'^2(\eta) + \left(1+\frac{1}{\gamma}\right)\frac{ReB_r}{\Omega} f''^2(\eta) + Re\lambda_1\left(\frac{\chi}{\Omega}\right)^2 \phi'^2(\eta) \\ & + Re\lambda_1\left(\frac{\chi}{\Omega}\right)\theta'(\eta)\,\phi'(\eta), \end{aligned} \tag{3.22}$$

where

$$Re = \frac{\mu h^2}{\nu}, Br = \frac{\mu {U_w}^2}{k_1 (T_f - T_h)}, \Omega = \frac{(T_f - T_h)}{T_h}, \chi = \frac{(C_f - C_h)}{C_h}, \lambda_1 = \frac{RDC_h}{k_1}.$$

Another dimensionless parameter, Bejan number [97] is considered. It gives the ratio of heat and mass transfer irreversibility to the total entropy generation

$$Be = \frac{HTI + MTI}{NG}.$$

3.3 Solution Methodology

To solve the Eqs. (3.16)-(3.18) along with the boundary conditions (3.19), a numerical scheme named as shooting method [93] is used. We denote $f \to \Gamma_1$, $\Gamma_1' \to \Gamma_2$, $\Gamma_2' \to \Gamma_3$, $\Gamma_3' \to \Gamma_4$, $\theta \to \Gamma_5$, $\theta' \to \Gamma_6$, $\phi \to \Gamma_7$ and $\phi' \to \Gamma_8$. The boundary value problem (3.16)-(3.19) is converted to the following initial value problem.

$$\begin{aligned}
\Gamma_1' &= \Gamma_2, \\
\Gamma_2' &= \Gamma_3, \\
\Gamma_3' &= \Gamma_4, \\
\Gamma_4' &= \frac{\gamma\left[\Gamma_2\Gamma_3 - \Gamma_1\Gamma_4 + \frac{Sq}{2}\left(3\Gamma_3 + \eta\Gamma_4\right)\right]}{1+\gamma}, \\
\Gamma_5' &= \Gamma_6, \\
\Gamma_6' &= \frac{pr\left[\begin{array}{c}\left(\frac{Sq}{2}\eta\Gamma_6 - \Gamma_1\Gamma_6\right) \\ +\beta_e\left(\frac{3}{4}Sq^2\eta\Gamma_6 + \Gamma_1\Gamma_2\Gamma_6 - \frac{Sq}{2}\eta\Gamma_2\Gamma_6 - \frac{3}{2}Sq\Gamma_1\Gamma_6\right)\end{array}\right]}{1 + Rd - \frac{1}{4}Pr\beta_e Sq^2\eta^2 - Pr\Gamma_1^2\beta_e + PrSq\beta_e\eta\Gamma_1}, \\
\Gamma_7' &= \Gamma_8, \\
\Gamma_8' &= \frac{PrS_c\left[\begin{array}{c}\left(-\Gamma_1\Gamma_8 + \frac{Sq}{2}\eta\Gamma_8 + Kr\Gamma_7\right) \\ +\beta_c\left(\frac{3}{4}\eta Sq^2\Gamma_8 + \Gamma_1\Gamma_2\Gamma_8 - \frac{Sq}{2}\eta\Gamma_2\Gamma_8 - \frac{3}{2}Sq\Gamma_1\Gamma_8\right)\end{array}\right]}{1 - \frac{1}{4}Pr\ Sc\ \beta_c\ Sq^2\eta^2 - Pr\ Sc\ \Gamma_1^2\beta_c + Pr\ Sc\ \eta\ Sq\ \beta_c\ \Gamma_1}.
\end{aligned}$$

subject to the initial conditions

$$\left.\begin{aligned}
&\Gamma_1(0) = 0,\ \ \Gamma_2(0) = 1,\ \ \Gamma_3(0) = \xi_0,\ \ \Gamma_4(0) = \xi_1,\ \ \Gamma_5(0) = \xi_2, \\
&\Gamma_6(0) = -Bi_1\left(1 - \Gamma_5(0)\right),\ \ \Gamma_7(0) = \xi_3,\ \ \Gamma_8(0) = -Bi_2\left(1 - \Gamma_7(0)\right).
\end{aligned}\right\}$$

The system of initial value problem is solved by adopting the RK4 method after the missing initial conditions are chosen. To refine the above missing conditions ξ_0, ξ_1, ξ_2 and ξ_3, we employ the Newton's method. The procedure is repeated as long as we meet the specified convergence criteria. The numerical results are achieved with $\varepsilon = 10^{-6}$.

$$\max\left\{\left|\Gamma_1(1) - \frac{Sq}{2}\right|, \left|\Gamma_2(1)\right|, \left|\Gamma_5(1)\right|, \left|\Gamma_7(1)\right|\right\} < \varepsilon$$

3.3.1 Code Validation

		Pourmehran*et al.* [98]	Present results	
Pr	Ec	$-\theta'(1)$	bvp4c	Shooting
1	1	3.026324	3.02632992	3.02632355
0.5		1.522368	1.52236785	1.52236746
2		5.980530	5.98053038	5.98053038
5		14.439413	14.43941311	14.43941313
	1.2	3.631595	3.63159591	3.63158856
	2	6.052647	6.05265985	6.05264709
	5	15.131617	15.13161775	15.13161774

Table 3.1: The Comparison of Nusselt number when $S = 0.5$, $\phi = 0.0$ and $\delta = 0.1$.

To validate the MATLAB code for the shooting method, the numerical results have also been computed by the MATLAB built-in function bvp4c. For further reliability of our results, we have also reproduced the Nusselt number reported by Pourmehran *et al.* [98]. The present computed results in Table 3.1 reveals a good agreement with those of [98].

3.4 Results and Discussions

Numerical solution of mathematical model (3.16)-(3.19) is demonstrated in this section for different emerging parameters. We first present the numerical results for some parameters of interest in the form of tables followed by the discussion on

the graphical behavior of certain profiles.

					Shooting method		bvp4c	
Sq	Sc	Rd	Kr	γ	$-f''(1)$	$-\phi'(1)$	$-f''(1)$	$-\phi'(1)$
0.5	0.5	0.2	0.2	0.8	4.657236	0.151922	4.657236	0.151922
1.0					3.173596	0.151922	3.173596	0.151922
1.2					2.560514	0.151943	2.560514	0.151943
1.5					1.620368	0.151975	1.620368	0.151975
	1				4.657236	0.138337	4.657236	0.138337
	1.5				4.657236	0.125959	4.657236	0.125959
	2				4.657236	0.114647	4.657236	0.114647
		0.5			4.657236	0.151873	4.657236	0.151873
		1			4.657236	0.151873	4.657236	0.151873
		1.5			4.657236	0.151873	4.657236	0.151873
			0.3		4.657236	0.145029	4.657236	0.145029
			0.5		4.657236	0.132209	4.657236	0.132209
			1.0		4.657236	0.104712	4.657236	0.104712
				0.7	4.637727	0.151873	4.637727	0.151873
				0.5	4.598584	0.151873	4.598584	0.151873
				0.3	4.559275	0.151872	4.559275	0.151872

Table 3.2: Values of skin friction and Sherwood number, when $Pr = 1$, $\beta_e = 0.1$, $\beta_c = 0.1$, $Bi_1 = Bi_2 = 0.2$.

The impact of squeezing parameter Sq, Schmidt number Sc, Radiation parameter Rd, chemical reaction Kr and Casson parameter γ on the skin friction and mass transfer rate is displayed in Table 3.2. It demonstrates that as squeezing parameter Sq enhances, the skin friction grows and Sherwood number decreases. As the values of squeezing parameter increase, fluid at the boundary near the upper wall gets accelerated, thus a decreasing behavior in the skin friction coefficient is observed. With the augmentation of squeezing parameter, the rate of mass transfer reduces. This exhibits that the concentration of nanofluid particles increases

as the fluid is squeezed. Sherwood number shows a decline behavior as Sc rises. Higher Schmidt number leads to higher dynamic viscosity. This dynamic viscosity has a negative influence on the mass transfer rate of nanofluid as Sherwood number decreases. Table 3.2 demonstrated that Sherwood number is reduced at higher rate of chemical reaction. This is consistent with physical explanation that during the greater chemical reaction more mass is consumed. Table 3.2 exhibits that as Casson fluid parameter γ increases, the values of skin friction decrease. The physical explanation to this attitude is that for developing values of Casson parameter, viscosity of fluid increases which in return halts the flow, thus less friction is generated at the surface.

3.4.1 Outcome of Various Parameters on Velocity and Temperature

Figures 3.2-3.9, demonstrate the influence of different parameters on velocity and temperature. In Figure 3.2 the velocity profile demonstrates the influence of squeezing parameter $Sq > 0$. As squeezing parameter escalates, the top plate shifts more quickly towards the bottom plate, which consequently enhances the velocity profile. Figure 3.3 displays the variation in squeezing parameter $Sq < 0$

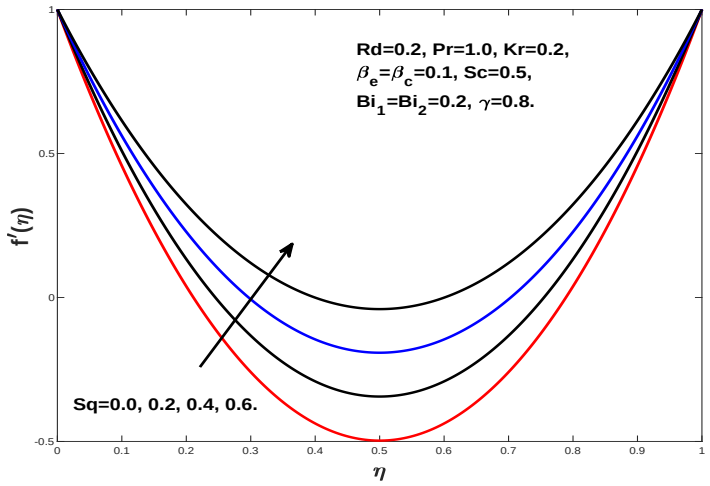

Figure 3.2: Impact of positive Sq on f'.

on velocity profile. The figure demonstrates that as the values of Sq grow, the

top plate moves away from the bottom one. This motion of plate leaves a gap which is filled due to upward fluid movement, resulting in decline in velocity. Fig-

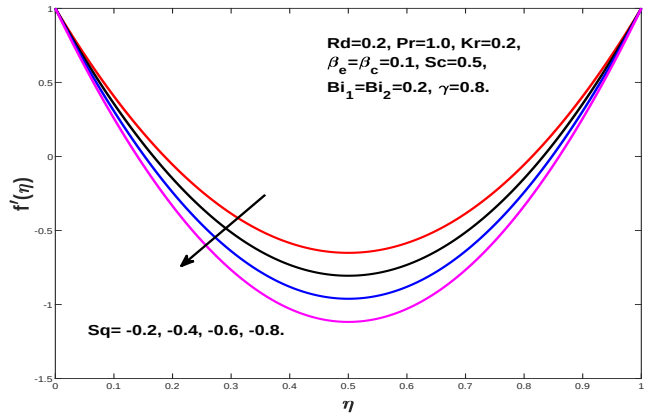

Figure 3.3: Impact of negative Sq on f'.

ure 3.4 depicts the impact of Casson fluid parameter γ on velocity. As γ grows, velocity graph shows the decreasing behavior in the interval $0 \leq \eta \leq 0.3$, whereas the velocity in interval $0.3 \leq \eta \leq 0.7$ escalates. The impact of thermal radiation

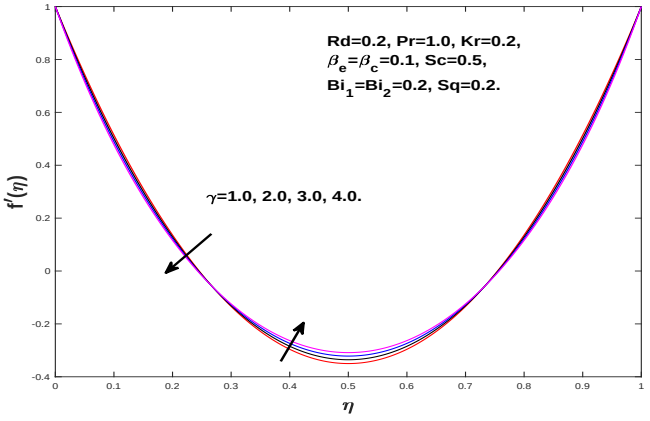

Figure 3.4: Impact of γ on f'.

parameter Rd on temperature is discussed in Figure 3.5, which demonstrates that as Rd increases, an escalation in temperature occurs. Figure 3.6 exhibits the influence of Prandtl number Pr on the temperature profile, higher prandtl number causes a decline in temperature profile. For higher Prandtl number, convection is dominated in transferring energy from the channel. As a result, temperature declines. Figure 3.7 demonstrates the impact of Biot number Bi_1 on the temperature.

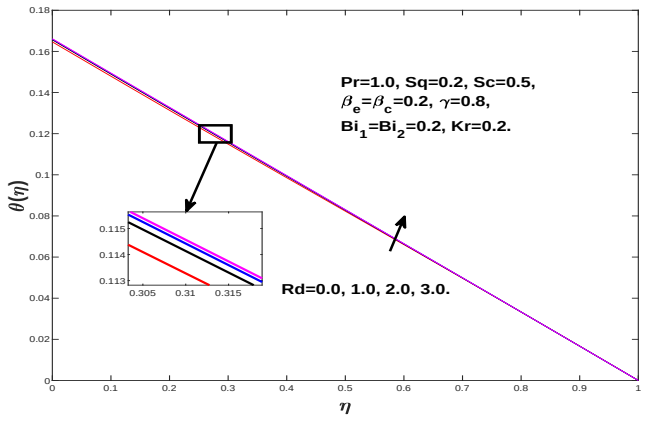

Figure 3.5: Impact of Rd on θ.

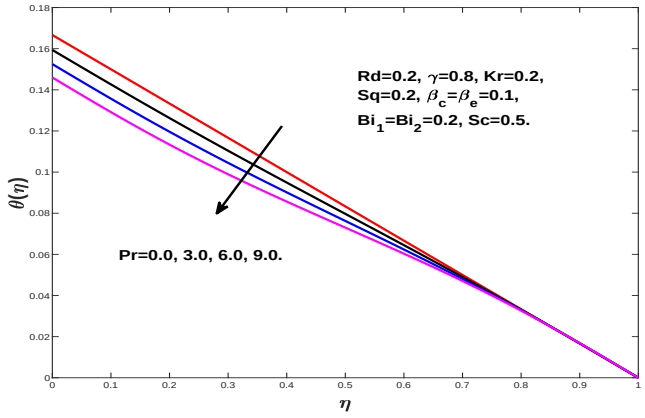

Figure 3.6: Impact of Pr on θ.

An increment in temperature is observed as Biot number escalates. Physically for growing Biot number, there is a depletion in thermal resistance. Due to an increase in convection, surface temperature rises. In Figure 3.8 the impact of temperature relaxation parameter β_e on temperature is displayed, this figure exhibits that as thermal relaxation parameter enhances, temperature exceeds. Physically, this happens because as this parameter β_e increases, fluid particles transfer heat to the neighboring particles, which results an enhancement in temperature. Figure 3.9 exhibits the influence of squeezing parameter Sq on the temperature profile. The squeezing of the fluid escalates the flow temperature which the graph clearly shows.

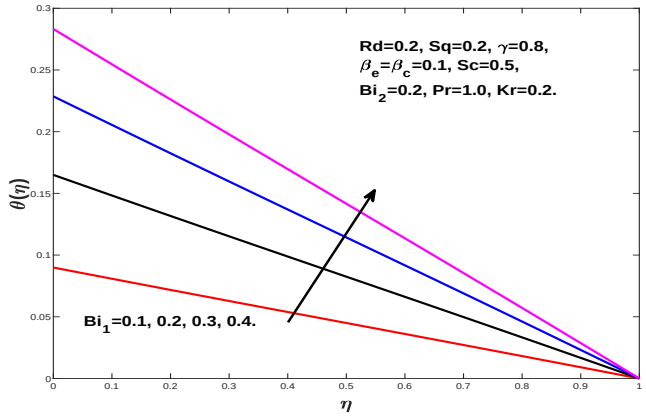

Figure 3.7: Impact of Bi_1 on θ.

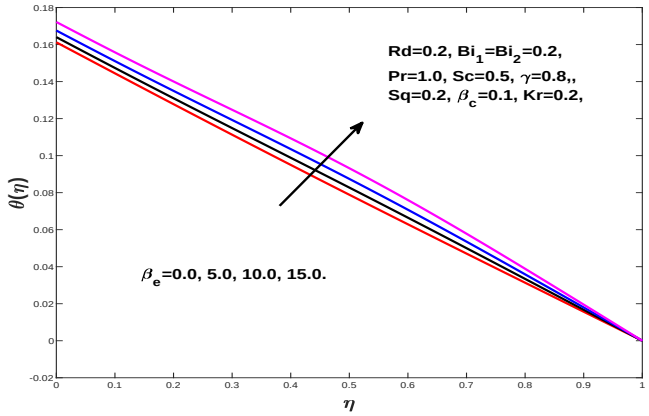

Figure 3.8: Impact of β_e on θ.

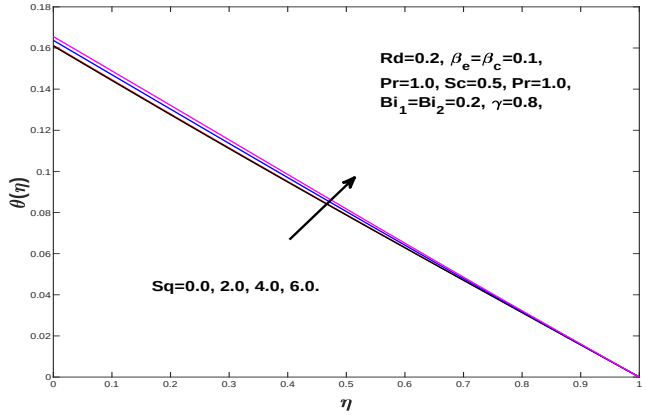

Figure 3.9: Impact of Sq on θ.

3.4.2 Influence of Various Parameters on Concentration

Figure 3.10-3.14 exhibits the impact of different parameters on concentration. The consequence of Schmidt number Sc on concentration is displayed in Fig. 3.10. Concentration profile decays with rising Schmidt number. Increase in Schmidt number

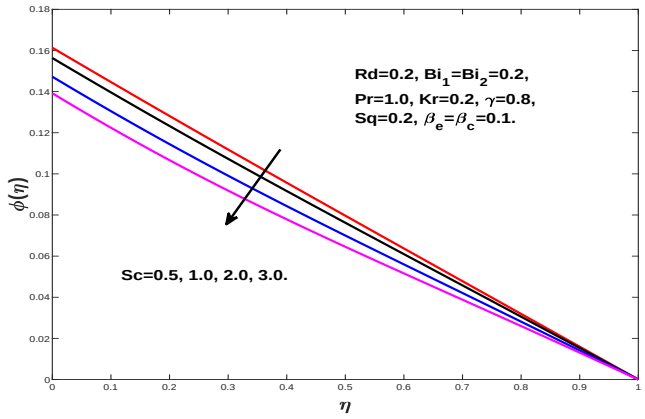

Figure 3.10: Impact of Sc on ϕ.

causes less mass diffusivity. Due to this, concentration profile decays. Figure 3.11 gives a view of the change in concentration with respect to Biot number Bi_2. It is witnessed that greater Biot number causes an increase in the concentration. Physically, greater Biot number recommends a deeper penetration of concentration. In

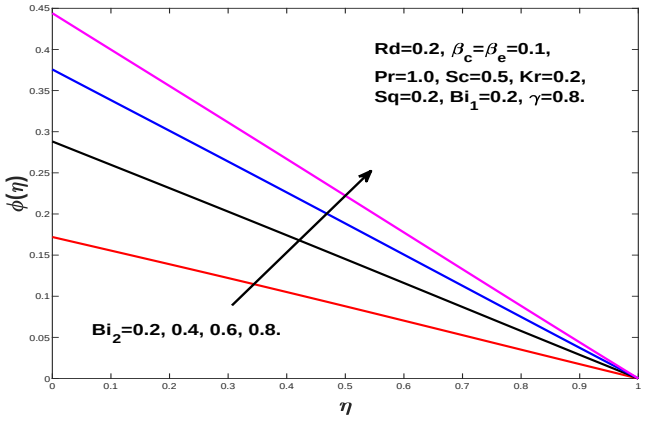

Figure 3.11: Impact of Bi_2 on ϕ.

Figure 3.12 concentration profile is plotted against the relaxation parameter β_c. A decrease in concentration is observed for higher β_c. The effect of chemical reaction Kr on the concentration is plotted through Figure 3.13. It is visualized from

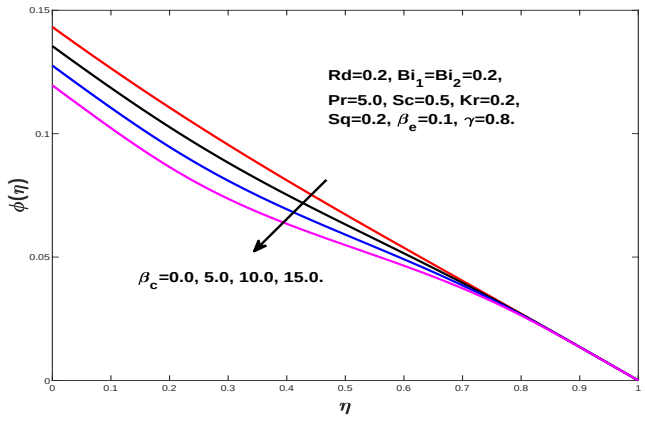

Figure 3.12: Impact of β_c on ϕ.

figure that with increment in values of chemical reaction, the molecular diffusivity reduces, which results in decrease of concentration profile. In Figure 3.14 concen-

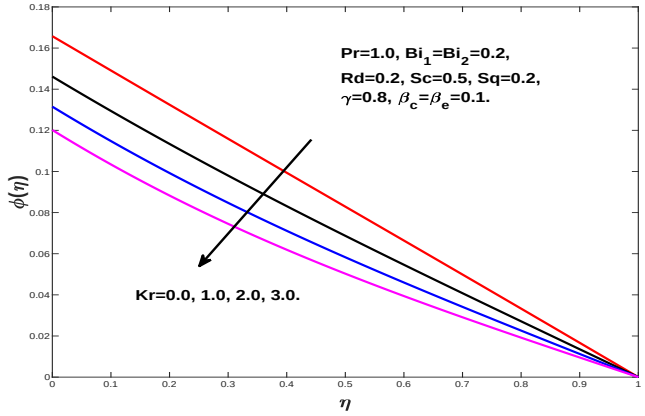

Figure 3.13: Impact of Kr on ϕ.

tration profile declines as the Prandtl number Pr exceeds.

3.4.3 Impact of Different Parameters on Entropy Generation

In Figures. 3.15-3.22 impact of different parameters on the entropy generation and Bejan number for $Re = 0.1$, $\Omega = 1.0$, $\chi = 0.2$, $\lambda_1 = 0.2$ and $\beta_r = 1.0$ is displayed. Figure 3.15 exhibits the impression of the squeezing parameter Sq on NG. The

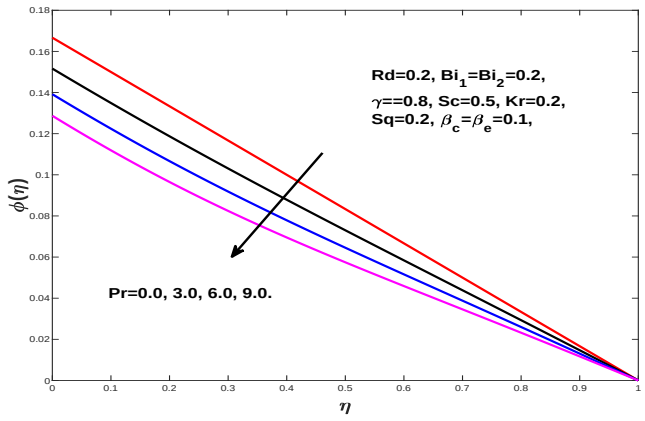

Figure 3.14: Impact of Pr on ϕ.

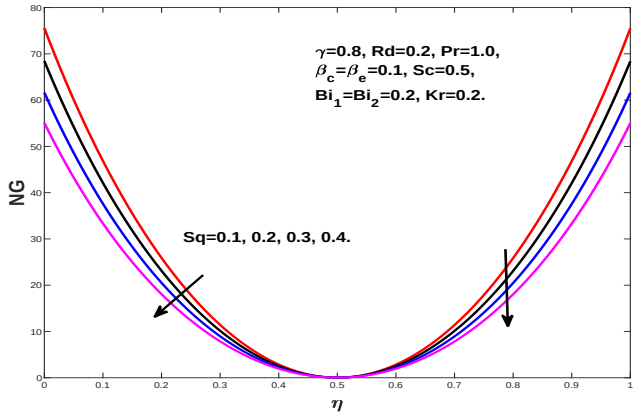

Figure 3.15: Impact of Sq on NG.

figure reveals that with an increment in the squeezing parameter, the entropy generation NG decreases. The entropy is more significant when fluid is closer to the walls of the channel. Variation in entropy profile NG, with the changing Brinkman number β_r, is observed through Figure 3.16. The figure discloses that Brinkman number is directly related to NG.

The irreversibility of the fluid friction produces an escalation in entropy. The influence of Reynolds number Re on NG is demonstrated in Figure. 3.17. It is witnessed that as Re grows, the entropy generation parameter NG also enhances. From figure, it can be visualized that there is more disturbance in the fluid movement. An increment in the entropy due to contribution of fluid friction and heat transfer is observed. Figure 3.18 gives a view of the variation of Casson fluid parameter γ on NG. For an increasing γ, entropy generation NG is found to

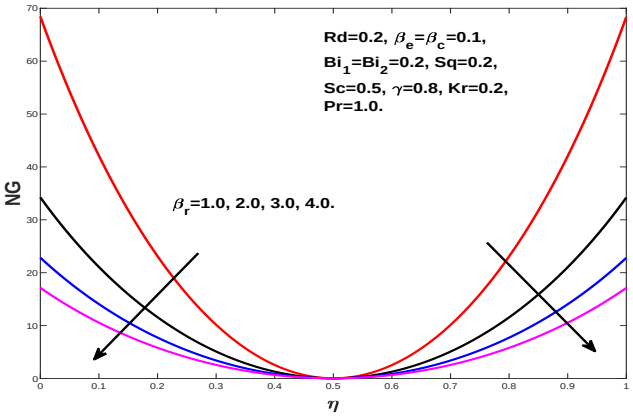

Figure 3.16: Impact of β_r on NG.

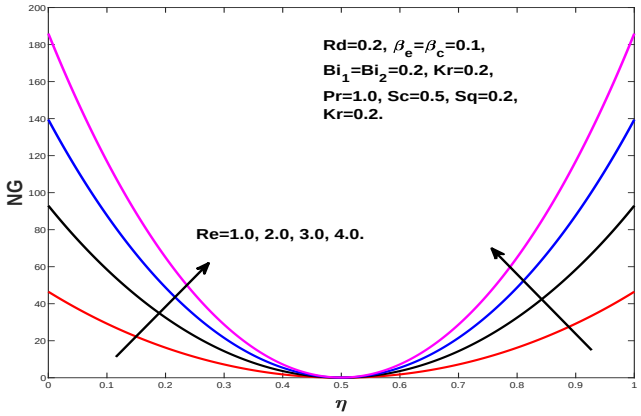

Figure 3.17: Impact of Re on NG.

experience a prominent decay.

Figure 3.19 exhibits the impression of thermal radiation Rd on Bejan number.

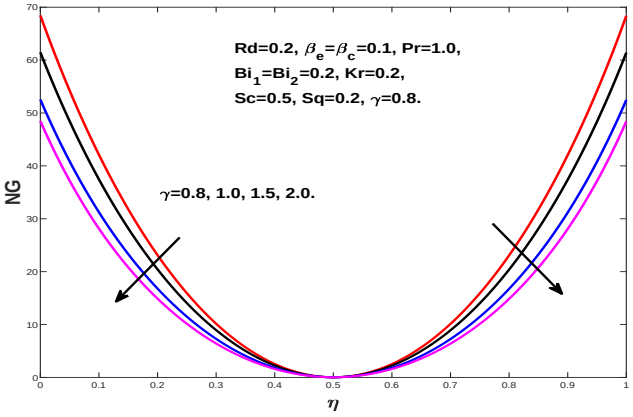

Figure 3.18: Impact of γ on NG.

As the values of Rd escalate Bejan number also increases.

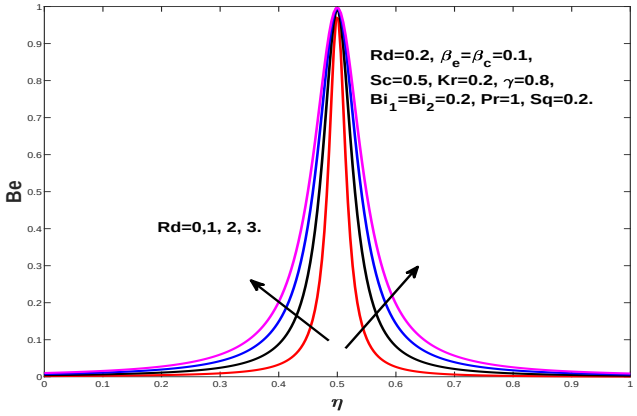

Figure 3.19: Impact of Rd on Be.

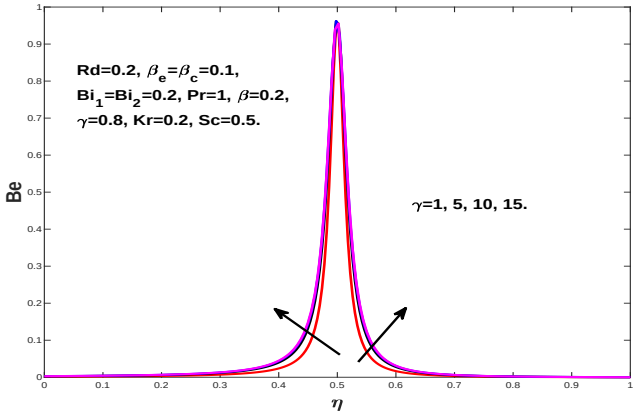

Figure 3.20: Impact of γ on Be.

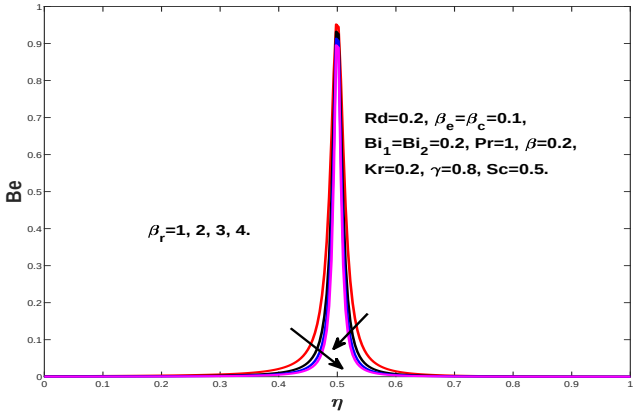

Figure 3.21: Impact of β_r on Be.

Figure 3.20 represents how the Casson fluid parameter γ affects Bejan number. Bejan number and Casson fluid parameter are directly related. Figure 3.21 reveals the impact of the Brinkman number β_r on Bejan number. Increment in Brinkman number is inversely related to Bejan number. Figure 3.22 demonstrates the effect of temperature parameter Ω on Bejan number. The profile of Bejan number decreases when values of Ω increase.

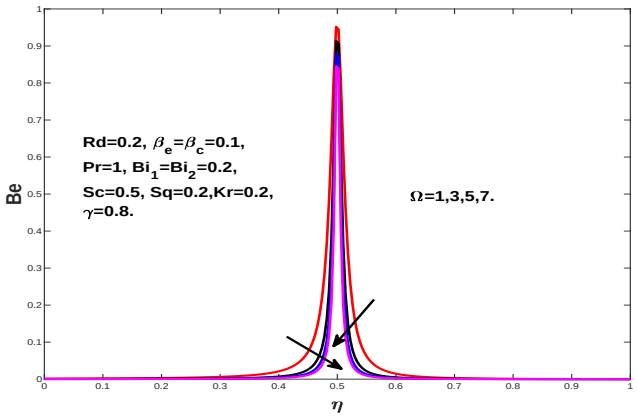

Figure 3.22: Impact of Ω on Be.

3.4.4 Effect of Various Parameters on Nusselt Number

Figures. 3.23-3.27 exhibits the impact of different parameters on Nusselt number. Figure 3.23 is plotted for Nu against squeezing Sq and thermal radiation Rd. The graph shows that thermal radiation and squeezing parameters have an inverse relationship with the Nusselt number. Figure 3.24 examines the impact of squeezing parameter Sq and Prandtl number Pr on Nu. From the figure it is demonstrated that Nusselt number is in direct relation with Prandtl number and squeezing parameter. Impact of squeezing parameter Sq and temperature relaxation parameter β_e on Nu is presented in Figure 3.25. Nusselt number rises as temperature relaxation parameter escalates. Figure 3.26 depicts the effect of squeezing parameter Sq and thermal radiation parameter Rd on Nusselt number. According to this figure, both Prandtl number and thermal radiation parameter yield an increase in the profile. Figure 3.27 is shown to exhibit effect of Biot number Bi_1 and squeezing parameter Sq on Nusselt number. It can be observed that

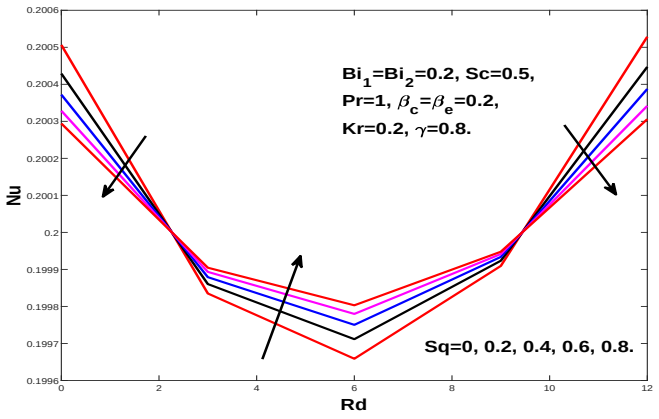

Figure 3.23: Impact of Sq on Nu.

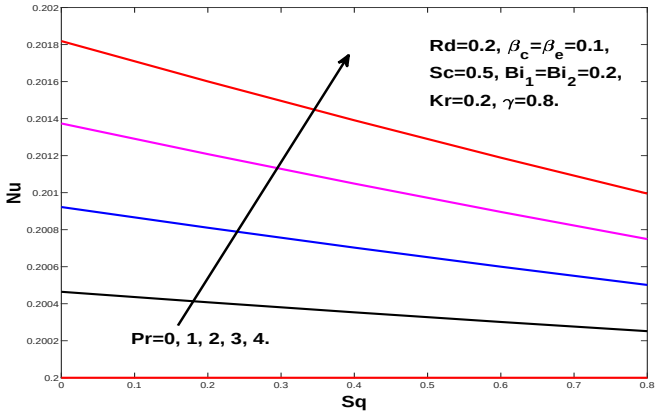

Figure 3.24: Impact of Pr on Nu.

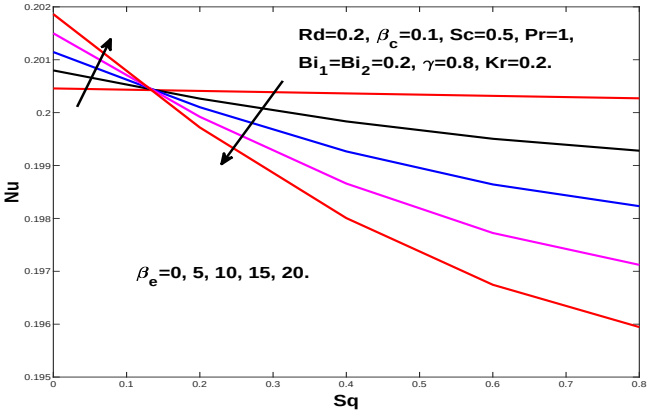

Figure 3.25: Impact of β_e on Nu.

Nusselt number increases for increasing values of squeezing parameter and Biot number.

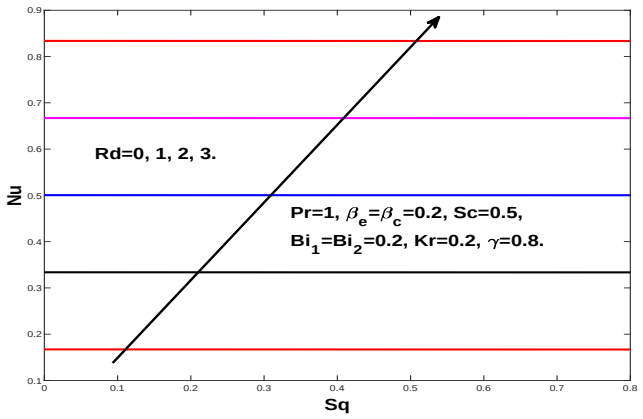

Figure 3.26: Impact of Rd on Nu.

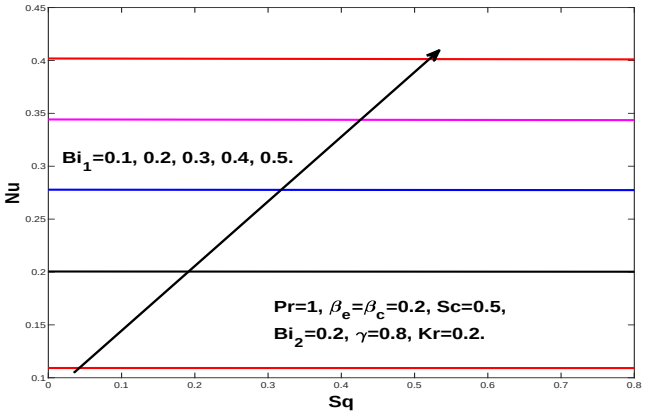

Figure 3.27: Impact of Bi_1 on Nu.

3.5 Conclusion

This chapter investigated the squeezing flow of Casson nanofluid with the effect of Cattaneo-Christov heat and mass flux. Entropy generation is also discussed. Shooting method is used to obtain the solution of the governing equations. Main findings of analysis are given below:

- An increment in velocity field is observed for greater squeezing parameter Sq.
- Temperature field is reduced as Prandtl number Pr increases.
- Temperature profile enhances for temperature relaxation parameter β_e.

- A decline in concentration is noticed for greater chemical reaction Kr.
- By increasing the mass relaxation parameter β_c, the concentration profile is increased.
- An enhancement in Schmidt number Sc exhibits a decay in the concentration.
- Entropy generation NG exhibits decaying behavior as squeezing parameter Sq increases.
- Casson fluid parameter γ demonstrates decreasing behavior for the velocity in the region $0 \leq \eta \leq 0.2$ whereas, velocity enhances in interval $0.2 \leq \eta \leq 0.7$.

Chapter 4

Entropy Generation and Squeezing Flow Past a Riga Plate With Cattaneo-Christov Heat Flux

4.1 Introduction

The study conducted in this chapter focuses on the effect of two-dimensional unsteady squeezing flow past a Riga plate with convective heat transfer. Cattaneo-Christov heat flux model has been considered to examine the heat transfer. Impact of entropy generation on heat transfer has been investigated numerically. The nonlinear PDEs are non-dimensionalized to ODEs by using a suitable similarity transformation. To solve the mathematical model, a numerical scheme known as shooting method is applied. To check the reliability of the obtained results a built in MATLAB function bvp4c has been utilized. The numerical values of mass transfer and skin friction under the influence of emerging parameters are analyzed through tables. Velocity, concentration and temperature graphs are plotted against emerging parameters used in the study. It can be concluded from the study

that as the values of thermal relaxation parameter expand, temperature escalates and concentration decreases.

4.2 Problem Formulation

4.2.1 The Problem Configuration

We examine the squeezing flow of unsteady, viscous and incompressible two dimensional electromagnetohydrodynamic fluid flow between two Riga plates (see Figure 4.1). The bottom plate which is located at $y = 0$ has the stretching velocity $U_w = \frac{ax}{1-\gamma_1 t}$. The top Riga plate is situated at $y = h(t) = \sqrt{\frac{\nu(1-\gamma_1 t)}{a}}$. Fluid is squeezing with the velocity $v_h = \frac{dh}{dt}$. Cattaneo-Christov model [33] has been considered instead of Fourier's law of heat conduction. Here T_f and T_h denote the wall and ambient temperature respectively. Heat flux $\mathbf{q_1}$ is taken as [38]

$$\mathbf{q_1} + \delta_{E_1}\left[\frac{\partial \mathbf{q_1}}{\partial t} + \mathbf{V}.\nabla \mathbf{q_1} + (\nabla.\mathbf{V})\,\mathbf{q_1} - \mathbf{q_1}.\nabla \mathbf{V}\right] = -k_1 \nabla T. \tag{4.1}$$

Putting $\delta_{E_1} = 0$ in Eq. (4.1) reduces it to classical Fourier's law. By using the continuity equation $\nabla.\mathbf{V} = 0$, the Eq. (4.1) reduces to the following form

$$\mathbf{q_1} + \delta_{E_1}\left[\frac{\partial \mathbf{q_1}}{\partial t} + \mathbf{V}.\nabla \mathbf{q_1} - \mathbf{q_1}.\nabla \mathbf{V}\right] = -k_1 \nabla T. \tag{4.2}$$

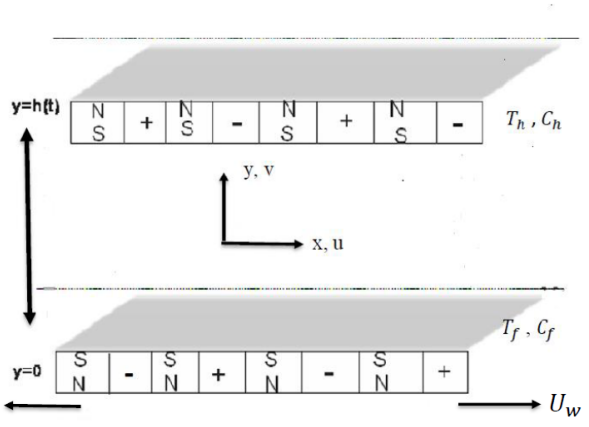

Figure 4.1: Diagram of flow model.

4.2.2 Governing Equations

The governing partial differential equations for continuity, velocity, temperature and concentration are given as follows [99]

$$u_x + u_y = 0, \tag{4.3}$$

$$u_t + uu_x + vu_y = \frac{1}{\rho}P_x + \nu\left(u_{xx} + u_{yy}\right) + \frac{\pi j_0 M_0 Exp\left(\frac{-\pi}{b}y\right)}{8\rho} \tag{4.4}$$

$$v_t + uv_x + vv_y = \frac{1}{\rho}P_y + \nu\left(v_{xx} + v_{yy}\right) \tag{4.5}$$

$$T_t + uT_x + vT_y + \lambda_{E_1}\Omega_{E_1} = \alpha\left(T_{xx} + T_{yy}\right) - \frac{1}{(\rho c_p)}\hat{q}_{ry}, \tag{4.6}$$

$$C_t + uC_x + vC_y = D_B\left(C_{xx} + C_{yy}\right) - K_1\left(C - C_h\right). \tag{4.7}$$

The appropriate boundary conditions subject to the model problem are

$$\left.\begin{aligned} y = 0: \quad & u\left(x,y,t\right) = \frac{ax}{1-\gamma_1 t}, \quad v\left(x,y,t\right) = 0, \\ & -k_1 T_y = h_2(T_f - T), \quad -DC_y = h_3(C_f - C), \\ y = h\left(t\right): \quad & u\left(x,y,t\right) = 0, \quad v\left(x,y,t\right) = v_h = h_t, \\ & T = T_h, \quad C = C_h. \end{aligned}\right\} \tag{4.8}$$

The boundary conditions describe that bottom plate at $y = 0$ is stretched in x-direction with velocity $U_w = \frac{ax}{1-\gamma_1 t}$ and in y-direction with the velocity $V = 0$ [99]. We establish the convective boundary conditions at lower surface for temperature and concentration [100]. The conditions describe energy balance at fluid-solid interface. Velocity in x-direction is zero at top plate and velocity in y-direction is squeezing velocity of fluid.

In the Eq. (4.6) Ω_E is formulated as [38]

$$\begin{aligned} \Omega_{E_1} = {} & T_{tt} + uu_x T_x + vv_y T_y + u^2 T_{xx} + v^2 T_{yy} + u_t T_x + 2uvT_{xy} \\ & + 2uT_{xt} + uv_x T_y + v_t T_y + vu_y T_x + 2vT_{yt}. \end{aligned} \tag{4.9}$$

Thermal radiation heat flux, according to Rosseland approximation [20], is considered

$$\hat{q}_r = \frac{-4\hat{\delta}_e}{3\hat{\beta}_R}\, T_y^4, \tag{4.10}$$

Expanding T^4 about temperature T_h, using Taylor's series and ignoring higher order terms, the following form is obtained

$$T^4 = 4TT_h^3 - 3T_h^4. \tag{4.11}$$

4.2.3 Dimensionless Equations

Similarity transformations [99] introduced to convert the Eqs. (4.3)-(4.7) into nondimensional form are as follows:

$$\left.\begin{aligned} &\Psi = \sqrt{\frac{a\nu}{1-\gamma_1 t}}\, xf(\eta), \quad \theta(\eta) = \frac{T-T_f}{T_h-T_f}, \quad u = \Psi_y = U_w f'(\eta) \\ &v = -\Psi_x = -\sqrt{\frac{a\nu}{1-\gamma_1 t}} f(\eta), \quad \eta = \frac{y}{h(t)}, \quad \phi(\eta) = \frac{C-C_f}{C_h-C_f}. \end{aligned}\right\} \tag{4.12}$$

Eq. (4.3) is identically satisfied and the other Eqs. (4.4)-(4.7) get the following form:

$$f'''' + ff''' - f'f'' - \frac{Sq}{2}(3f'' + \eta f'''') - ZBe^{-B\eta} = 0, \tag{4.13}$$

$$\left.\begin{aligned} &(1+Rd)\,\theta'' + Pr\left(f\theta' - \frac{\eta}{2}Sq\ \theta'\right) - Pr\beta_e\left(ff'\theta' + f^2\theta'' - Sq\ \eta\ f\theta''\right) \\ &- \frac{Pr}{4}\beta_e\ Sq^2\left(3\eta\theta' + \eta^2\theta''\right) + \frac{Pr}{2}Sq\ \beta_e\left(\eta f'\theta' + 3f\theta'\right) = 0, \end{aligned}\right\} \tag{4.14}$$

$$\phi'' + Sc\left(f\phi' - \frac{Sq}{2}\eta\phi' - Kr\ \phi\right) = 0. \tag{4.15}$$

By using the similarity transformation (4.12) into Eq. (4.8), the boundary conditions take the following form:

$$\left.\begin{aligned} &f(0) = 0, \quad f'(0) = 1, \quad \theta'(0) = -Bi_1\left(1-\theta(0)\right), \quad \phi'(\eta) = -Bi_2\left(1-\phi(0)\right), \\ &f(1) = \frac{Sq}{2}, \quad f'(1) = 1, \quad \theta(1) = 0, \quad \phi(1) = 0. \end{aligned}\right\} \tag{4.16}$$

Dimensionless parameters appearing in Eqs. (4.13)-(4.16) are

$$Sq = \frac{\gamma_1}{a}, \quad B = \frac{\pi h(t)}{b}, \quad Z = \frac{\pi_j M_0 x}{8\rho U_w^2}, \quad Rd = \frac{16T_h^3\hat{\sigma}_e}{3\hat{\beta}_R k_1}, \quad Kr = \frac{K_1(1-\gamma_1 t)}{a},$$
$$\Pr = \frac{\nu}{\alpha}, \quad Sc = \frac{\alpha}{D_B}, \quad Bi_1 = \frac{h_2}{k_1}\sqrt{\frac{\nu(1-\gamma_1 t)}{a}}, \quad Bi_3 = \frac{h_3}{k_1}\sqrt{\frac{\nu(1-\gamma_1 t)}{a}}.$$

4.2.4 Physical Quantities

The important parameters skin friction and Sherwood number, are formulated as follows:

$$C_f = \frac{\tau_w}{\rho U_w^2}, \quad Sh_x = \frac{x q_m}{D(C_h - C_f)},$$

where τ_w represents the skin friction and q_m denotes the concentration flux. The above mentioned quantities are stated as

$$\tau_w = \mu \left(u_y\right)_{y=h(t)}, \quad q_m = -D \left(C_y\right)_{y=h(t)}.$$

Skin friction and Sherwood number are formulated into dimensionless form which is given below:

$$C_f Re_x^{1/2} = f''(1), \; Sh_x Re_x^{-1/2} = -\phi'(1).$$

4.2.5 Entropy Generation Analysis

According to [101], entropy generation is given by

$$S'''_{gen} = \frac{k_1}{T_h^2}\left[(T_y)^2 + \frac{16T_h^3\hat{\sigma}_e}{3\hat{\beta}_R k_1}(T_y)^2\right] + \frac{\mu}{T_h}(u_y)^2 + \left[\frac{R_D}{C_h}(C_y)^2 + \frac{R_D}{T_h}(T_y C_y)\right]. \tag{4.17}$$

From above, the first term on right hand side is HTI, second term is FFI and the third term is MTI. The characteristic entropy generation is described as

$$S'''_0 = \frac{k_1 (T_f - T_h)^2}{h^2 T_h^2}. \tag{4.18}$$

By using the similarity transformation, the entropy generation in the dimensionless form, can be written as

$$NG = \frac{S'''_{gen}}{S'''_0} = R_e\left(1+Rd\right)\theta'^2\left(\eta\right) + \frac{R_e B_r}{\Omega} f''^2\left(\eta\right) + R_e\lambda_1\left(\frac{\chi}{\Omega}\right)^2 \phi'^2\left(\eta\right) + R_e\lambda_1\left(\frac{\chi}{\Omega}\right)\theta'\left(\eta\right)\phi'\left(\eta\right). \tag{4.19}$$

where

$$R_e = \frac{\mu h^2}{\nu},\quad B_r = \frac{\mu {U_w}^2}{k_1\left(T_f - T_h\right)},\quad \Omega = \frac{\left(T_f - T_h\right)}{T_h},\quad \chi_1 = \frac{\left(C_f - C_h\right)}{C_h},\quad \lambda_1 = \frac{RDC_h}{k_1}$$

Another dimensionless parameter Bejan number [97] is also considered.

$$Be = \frac{HTI + MTI}{NG}.$$

4.3 Solution Methodology

The numerical scheme, Shooting method [93], is used to obtain the solution of the system. The boundary value problem (4.13)-(4.16) are converted to 8 first order differential equations of the initial value problem.

$$\begin{aligned}
\Lambda_1' &= \Lambda_2,\\
\Lambda_2' &= \Lambda_3,\\
\Lambda_3' &= \Lambda_4,\\
\Lambda_4' &= \Lambda_2\Lambda_3 - \Lambda_1\Lambda_4 + \frac{Sq}{2}\left(3\Lambda_3 + \eta\Lambda_4\right) + ZBe^{-B\eta},\\
\Lambda_5' &= \Lambda_6,\\
\Lambda_6' &= \frac{Pr\begin{bmatrix}\left(\frac{Sq}{2}\eta\Lambda_6 - \Lambda_1\Lambda_6\right)\\ -\beta_e\left(\frac{3}{4}Sq^2\eta\Lambda_6 + \Lambda_1\Lambda_2\Lambda_6 + \frac{Sq}{2}\eta\Lambda_2\Lambda_6 + \frac{3}{2}S\Lambda_1\Lambda_6\right)\end{bmatrix}}{1 + Rd - \frac{1}{4}Pr\beta_e Sq^2\eta^2 - Pr\Lambda_1^2\beta_e + PrSq\beta_e\eta\Lambda_1},\\
\Lambda_7' &= \Lambda_8,\\
\Lambda_8' &= -Sc\left[\Lambda_1\Lambda_8 - \frac{Sq}{2}\eta\Lambda_8 + Kr\Lambda_7\right],
\end{aligned}$$

correspond to the initial conditions

$$\left.\begin{aligned}&\Lambda_1(0)=0,\ \ \Lambda_2(0)=1,\ \ \Lambda_3(0)=\xi_0,\ \ \Lambda_4(0)=\xi_1,\ \ \Lambda_5(0)=\xi_2,\\&\Lambda_6(0)=-Bi_1\left(1-\Lambda_5(0)\right),\ \ \Lambda_7(0)=\xi_3,\ \ \Lambda_8(0)=-Bi_2\left(1-\Lambda_7(0)\right).\end{aligned}\right\}$$

We denote $f \to \Lambda_1$, $\Lambda_1' \to \Lambda_2$, $\Lambda_2' \to \Lambda_3$, $\Lambda_3' \to \Lambda_4$, $\theta \to \Lambda_5$, $\theta' \to \Lambda_6$, $\phi \to \Lambda_7$ and $\phi' \to \Lambda_8$. After choosing the missing initial conditions ξ_0, ξ_1, ξ_2 and ξ_3, the RK4 method is employed to solve the above problem. For refinement of ξ_0, ξ_1, ξ_2 and ξ_3, Newton's method is employed, until we meet the following convergence criterion. Numerical results of the mentioned problem are achieved with $\varepsilon = 10^{-6}$.

$$\max\left\{\left|\Lambda_1(1)-\frac{Sq}{2}\right|,\left|\Lambda_2(1)\right|,\left|\Lambda_5(1)\right|,\left|\Lambda_7(1)\right|\right\}<\varepsilon,$$

4.3.1 Code Validation

To validate our code for the shooting method, we have computed the numerical results by the bvp4c. For further reliability of our results, we reproduce the skin friction coefficient reported by Hayat *et al.* [99]. The comparison is presented in Table 1 indicates a strong agreement between our results and those of Hayat et al. For this comparison, we have chosen $\beta_e = 0$, $K_r = 0.2$, $Sc = 0.5$, $Bi_1 = 0.2 = Bi_2$, $Pr = 1.5$.

		Present results		Hayat *et al.* [99]	
Sq	Z	Shooting	bvp4c	HAM	Numerical
0.1	1.5	1.69643	1.69643	1.69635	1.69634
0.3		1.08549	1.08549	1.08543	1.08543
0.5		0.46756	0.46756	0.46751	0.46751
0.5	0.0	0.42215	0.42215	0.42215	0.42215
	1.0	0.45243	0.45243	0.45239	0.45239
	1.5	0.46756	0.46756	0.46751	0.46751

Table 4.1: Comparison of skin friction cofficient $C_f Re_x^{1/2}$.

4.4 Results and Discussions

Influence of different physical parameters on velocity, temperature and concentration are demonstrated in this section. We first present the numerical results for some parameters of interest in the form of tables, followed by the discussion on the graphical behavior of certain important profiles.

Table 4.2 describes the effect of chemical reaction Kr and Schmidt number Sc on mass transfer rate. The table exhibits that Sherwood number declines for higher chemical reaction Kr and Schmidt number Sc.

		$Sh_x Re_x^{-1/2}$	
Sc	Kr	Shooting	bvp4c
1.0	0.2	0.16598	0.16598
2.0		0.14395	0.14395
3.0		0.12571	0.12571
4.0		0.11044	0.11044
4.0	0.3	0.17513	0.17513
	0.5	0.16825	0.16825
	1.0	0.15288	0.15288
	1.2	0.14737	0.14737

Table 4.2: Numerical values of $Sh_x Re_x^{-1/2}$ when $\beta_e = 0.1, B = 10.0,\ Bi_1 = 0.2 = Bi_2,\ Z = 1.5,\ Sq = 0.2,\ Pr = 1.5$.

4.4.1 Outcome of Different Parameters on Velocity and Temperature

Outcome of velocity and temperature is displayed in Figs. 4.2-4.9 for values of different parameters. Fig. 4.2 is an illustration of the impact of positive values of squeezing parameter Sq on the velocity of the fluid. For higher squeezing parameter, the velocity profile increases. The graph exhibits that as the top plate

moves towards the bottom plate and exerts more pressure on the fluid, the velocity of fluid increases. Fig. 4.3 exhibits the behaviour of velocity profile for negative

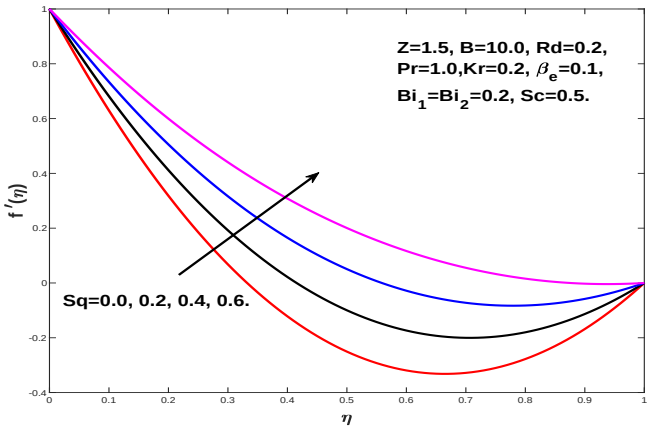

Figure 4.2: Influence of positive Sq on f'.

squeezing parameter Sq. Figure shows that the velocity graph declines for decreasing values of squeezing parameter. Negative values of squeezing parameter are due to motion of top plate away from the bottom plate. Consequently, in the middle of the channel, vacuum is created. As a result, fluid starts moving in the upward direction to fill the gap, which react as the velocity profile declines. The outcome

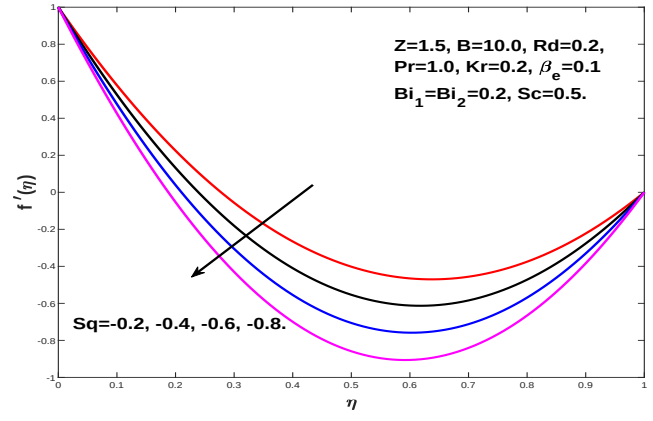

Figure 4.3: Influence of negative Sq on f'.

of modified Hartmann number Z on velocity is discussed in Fig. 4.4. The fluid velocity increases near bottom plate for growing Hartmann number, whereas the velocity near top plate declines. Physically, higher values of modified Hartmann number are responsible for greater intensity of external electric field, which results

in the production of Lorentz force parallel to wall. Variation in the temperature

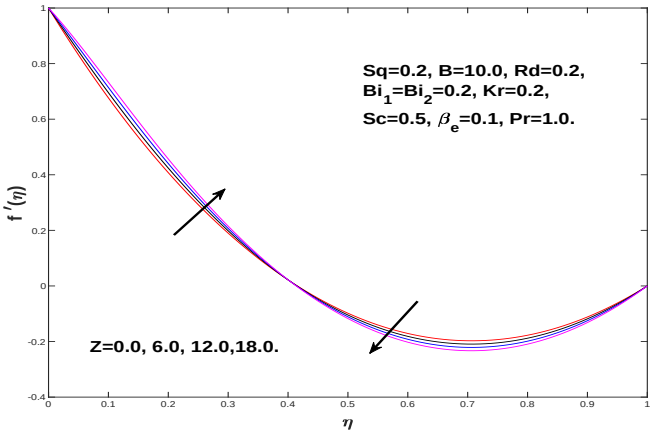

Figure 4.4: Influence of Z on f'.

showed the changing with respect to thermal radiation parameter Rd by the way of Fig. 4.5. By visualization of figure, it is witnessed that higher thermal radiation escalates the temperature. Fig. 4.6 exhibits the decreasing trend in temperature

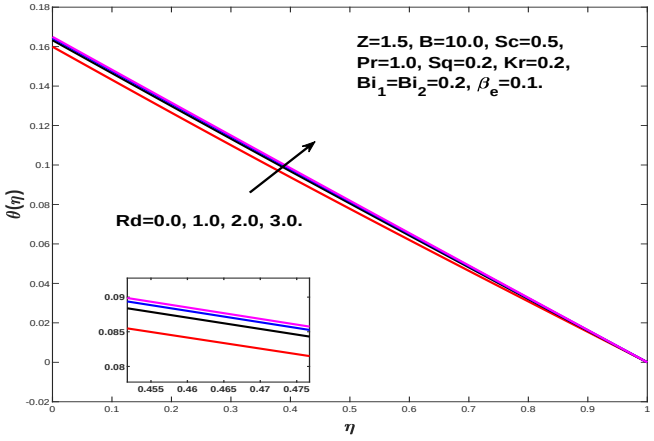

Figure 4.5: Influence of Rd on θ.

for greater Prandtl number Pr. The increasing Prandtl number has less thermal diffusivity. Due to this reason large Prandtl number results in decline in the temperature. Growing tendency of Biot number Bi_1 on temperature is deliberated in Fig. 4.7. Increase in Biot number enhances the temperature profile. For greater Biot number, there is a reduction in the thermal resistance. Due to increase in convection, higher surface temperature is attained. Temperature is plotted in the Fig. 4.8, to exhibit the influence of squeezing parameter Sq. Greater squeezing

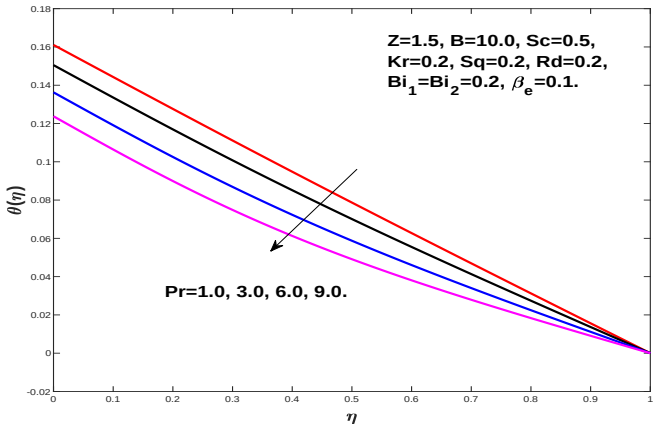

Figure 4.6: Influence of Pr on θ.

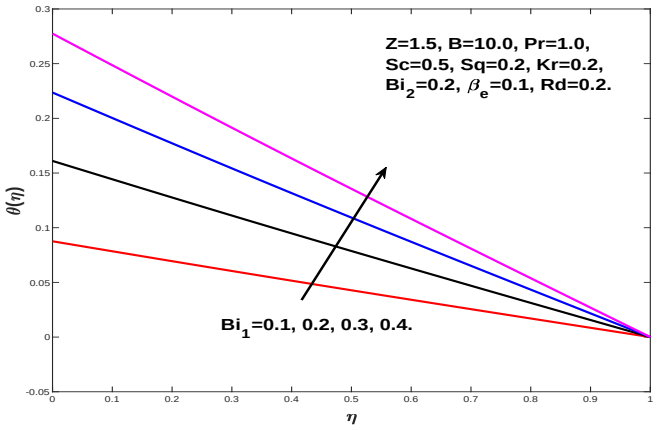

Figure 4.7: Influence of Bi_1 on θ.

parameter exhibits a decline in the temperature. Fig. 4.9 exhibits the impact of

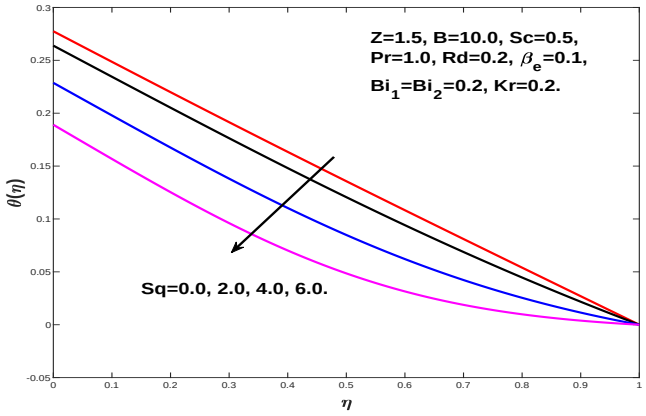

Figure 4.8: Influence of Sq on θ.

temperature relaxation parameter β_e on temperature. Figure exhibits that as thermal relaxation parameter expands, temperature decreases. As thermal relaxation parameter expands, more time is required for the fluid particles to transfer heat to the adjoining particles. Due to this fall in the temperature occurs.

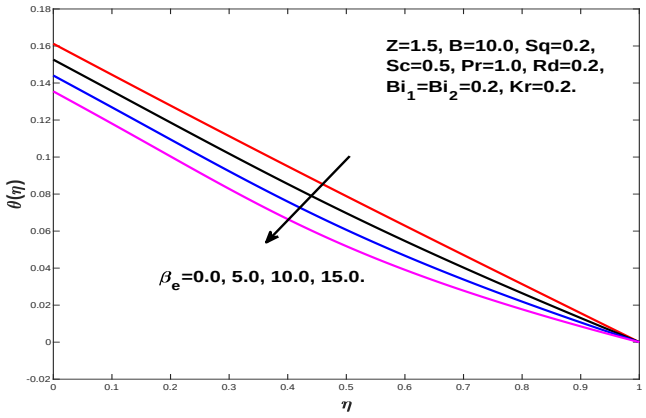

Figure 4.9: Influence of β_e on θ.

4.4.2 Significance of Various Parameters on Concentration

Figs. 4.10-4.14 demonstrate the impact of numerous parameters on concentration. Concentration profile is demonstrated in Fig. 4.10, to exhibit the influence of Schmidt number Sc. A decline in the concentration profile is seen for higher Schmidt number. The greater Schmidt numbers are expected to cause less mass diffusivity. Due to this, concentration decreases. Fig. 4.11 displays the impact of Biot number Bi_2 on concentration. For greater values of Bi_2, concentration increases. This gives a reason that bigger Biot number recommends a deeper penetration of concentration. The impact of relaxation parameter β_e on the concentration is demonstrated in Fig. 4.12. For an increasing thermal relaxation parameter, the concentration increases. Fig. 4.13 is plotted to exhibits the influence of chemical reaction parameter Kr on concentration. Concentration declines for higher chemical reaction. The reason behind this decrease is that for higher chemical reaction, molecular diffusivity reduces. Fig. 4.14 is portrayed to exam-

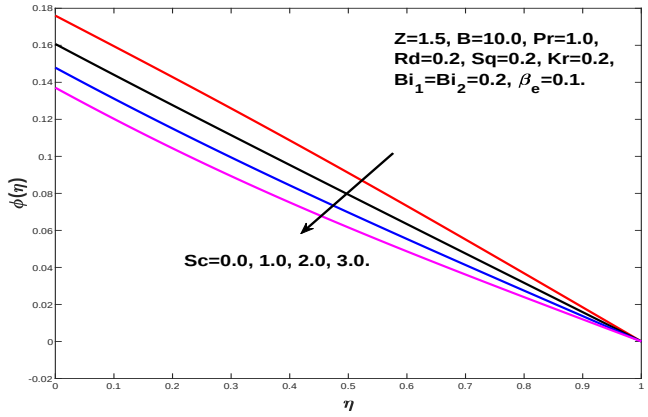

Figure 4.10: Influence of Sc on ϕ.

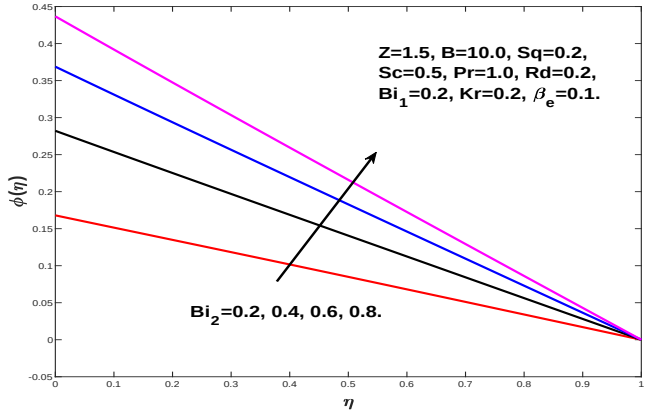

Figure 4.11: Influence of Bi_2 on ϕ.

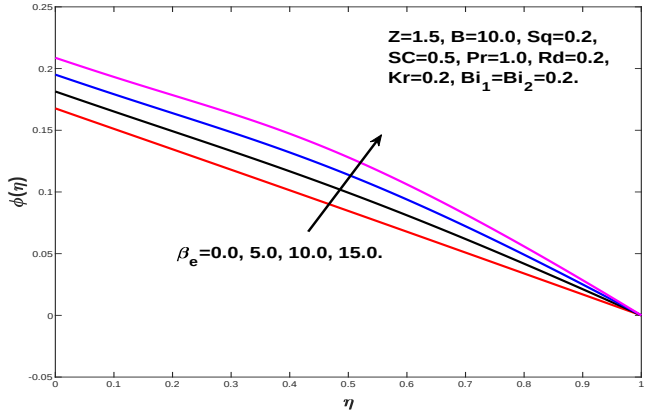

Figure 4.12: Influence of β_e on ϕ.

ine the influence of Prandtl number Pr on concentration. The boundary layer thickness strengthens for growing Prandtl number.

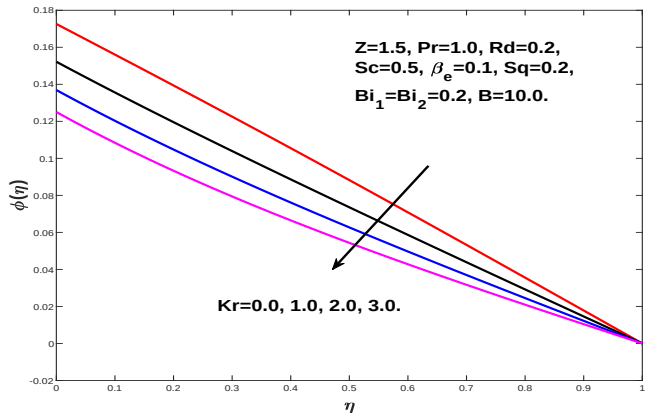

Figure 4.13: Influence of Kr on ϕ.

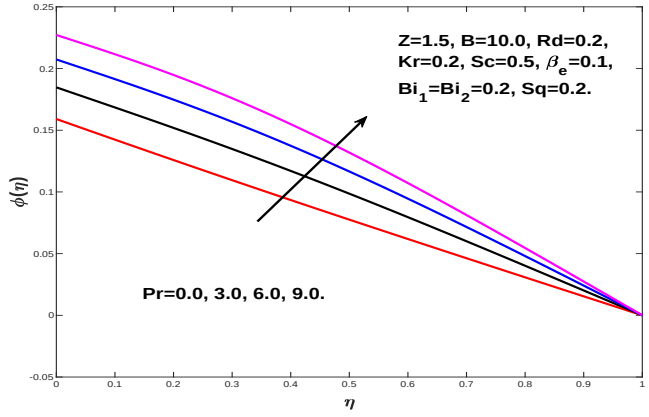

Figure 4.14: Influence of Pr on ϕ.

4.4.3 Consequences of Different Parameters on Entropy Generation

Figs. 4.15-4.21 show the effect of different parameters on entropy generation for $Re = 0.1$, $\Omega = 1.0$, $\chi = 0.2$, $\lambda_1 = 0.2$ and $\beta_r = 1.0$. Fig. 4.15 shows the impact of squeezing parameter Sq on entropy generation NG. The figure exhibits that as squeezing parameter enhances, the entropy generation NG declines. As compared to the center, the entropy is more prominent near the walls. Influence of Brinkman number β_r on entropy profile NG is presented in Fig. 4.16. As Brinkman number escalates, the entropy generation NG enhances. The irreversibility of fluid friction results in escalation of the entropy. Fig. 4.17 shows the impact of Re on entropy

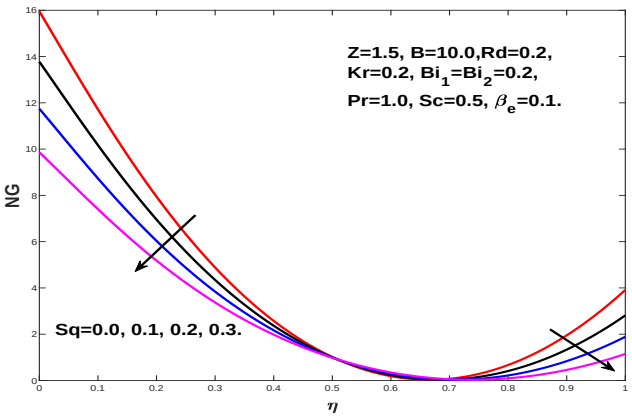

Figure 4.15: Influence of Sq on NG.

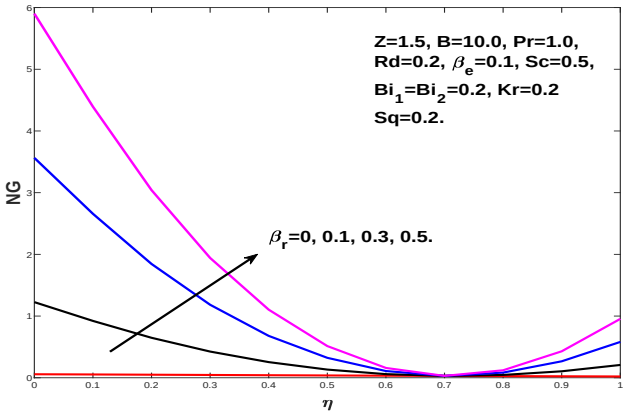

Figure 4.16: Influence of β_r on NG.

generation NG. As Re increases the entropy generation parameter NG increases. From the figure, it can be visualized that there is the more disturbance in the movement of the fluid. The fluid friction and heat transfer contribute to an increase in entropy generation. Variation of Biot number Bi_1 on entropy generation NG is displayed in Fig. 4.18. From the figure, it is concluded that for growing Biot number, the entropy profile increases. The influence of squeezing parameter Sq on Bejan number Be is displayed in Fig. 4.19. For increasing Sq the graph of Be increases. Figure exhibits that near the lower wall of channel the graph is restricted in the region $0 \leq Be < 0.7$ which exhibits that the entropy is dominant. Fig. 4.20 exhibits the impact of Brinkman number β_r on Be. The profile of Be strengthen, as the values of the β_r escalate. Fig. 4.21 exhibits the influence of Biot number Bi_1 on Be. The profile of Be increases as the values of Bi_1 escalates.

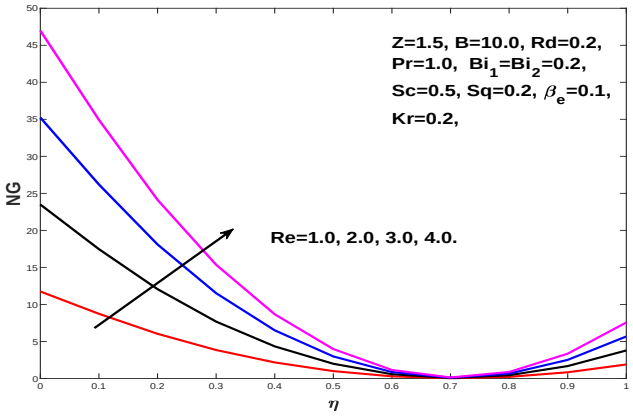

Figure 4.17: Influence of Re on NG.

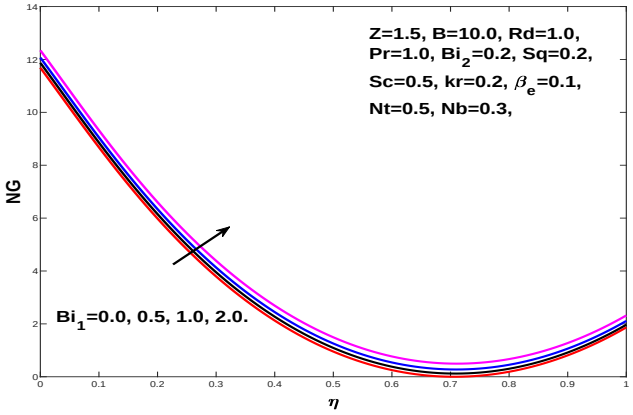

Figure 4.18: Influence of Bi_1 on N_G.

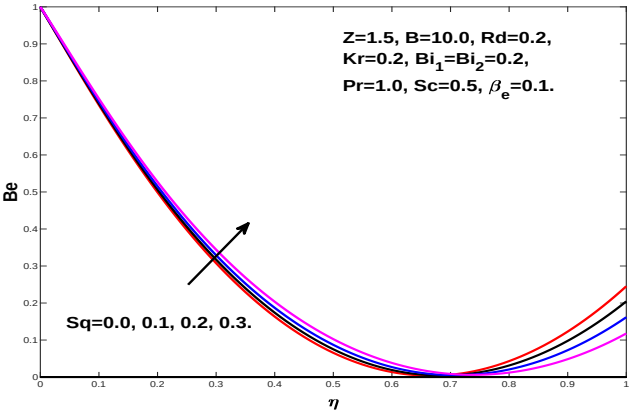

Figure 4.19: Influence of Sq on Be.

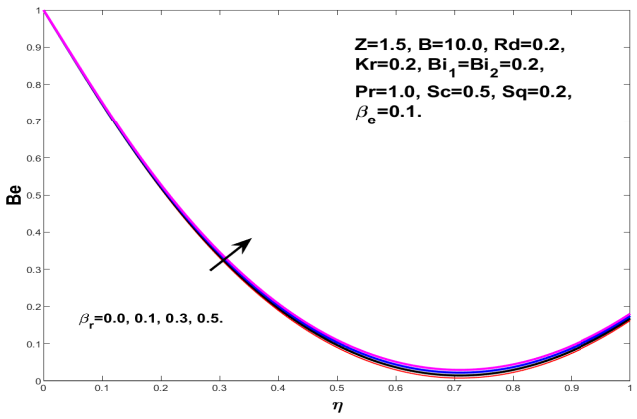

Figure 4.20: Influence of β_r on Be.

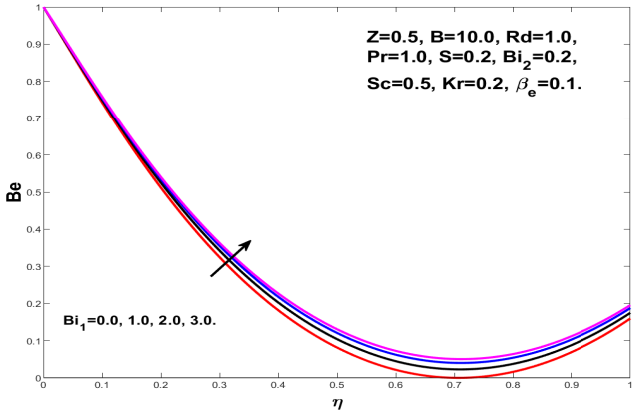

Figure 4.21: Influence of Bi_1 on Be.

4.5 Conclusion

The unsteady squeezing flow is investigated numerically in the existence of magnetic field. Cattaneo-Christov model is incorporated for heat transfer. The system of ODEs was solved numerically with the shooting technique and the comparison is made with bvp4c, a MATLAB built-in function. Main findings of the chapter are listed as:

- Velocity profile grows for positive squeezing parameter Sq and declines for negative squeezing parameter Sq.

- An enhancement in temperature is observed as the thermal radiation Rd escalate and temperature profile has inverse relation with the increasing thermal relaxation parameter β_e.

- Increasing chemical reaction parameter Kr exhibits that the concentration profile declines.

- Entropy generation declines for greater squeezing parameter Sq and increases for growing mean observation constant β_R.

Chapter 5

Squeezing Flow of Upper Convected Maxwell Nanofluid Subject to Entropy Generation and Cattaneo-Christove Double Diffusion

5.1 Introduction

In this chapter, two dimensional squeezing flow is investigate with the effect of upper convected Maxwell fluid. Impact of Cattaneo-Christov model is considered to analyze the heat and mass flux. For modeled problem, entropy generation analysis is also considered. The flow characteristics are explored with temperature and concentration stratification phenomena. The governing partial differential equations are transformed into the ordinary differential equations by using a suitable similarity transformation. The numerical scheme, shooting method, has been applied to solve the mathematical model. The results obtained from the shooting method is compared with those computed by the bvp4c, a built-in MATLAB function.

Impact of emerging parameters on concentration, velocity, and temperature are analyzed and discussed through graphs. To check the reliability of the computed results, a comparison with the previous published results is also included. It is concluded that the squeezing parameter enhances the velocity field and thermal stratified parameter decreases the temperature profile.

5.2 Problem Formulation

5.2.1 Problem Configuration

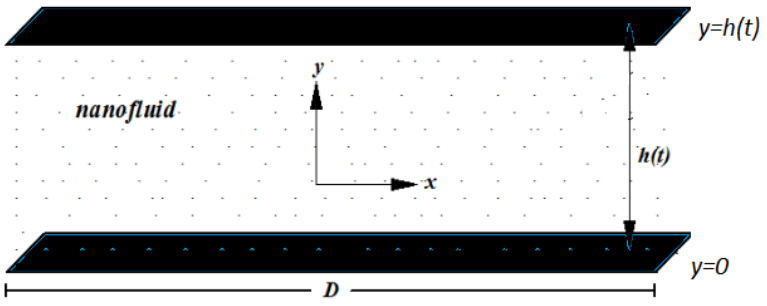

Figure 5.1: Schematic illustration of the squeezing flow.

Two-dimensional unsteady, viscous, incompressible, Maxwell nanofluid flow between two parallel plates (see Figure 5.1) is considered in this section. The lower plate which is positioned at $y = 0$ has the stretching velocity $U_w = \frac{ax}{1-\gamma_1 t}$ along the x-axis. The top plate is situated at $y = h(t) = \sqrt{\frac{\nu(1-\gamma_1 t)}{a}}$. Fluid is squeezing with the velocity $v_h = \frac{dh}{dt}$. Heat and mass flux through the Cattaneo-Christov model [33] have been incorporated instead of Fourier's and Fick's laws. The variable temperature $T_w = T_0 + d_1 x$ at the bottom plate and $T_h = T_0 + d_2 x$ at the top plate, are also under consideration along with the concentration $C_w = C_0 + d_3 x$ at the lower plate and $C_h = C_0 + d_4 x$ at the upper plate. Heat flux $\mathbf{q_1}$ and mass flux $\mathbf{J_1}$ [38], are taken as

$$\mathbf{q_1} + \delta_{E_1}\left[\frac{\partial \mathbf{q_1}}{\partial t} + \mathbf{V}.\nabla \mathbf{q_1} + (\nabla.\mathbf{V})\,\mathbf{q_1} - \mathbf{q_1}.\nabla \mathbf{V}\right] = -k_1 \nabla T, \tag{5.1}$$

$$\mathbf{J_1} + \delta_{C_1}\left[\frac{\partial \mathbf{J_1}}{\partial t} + \mathbf{V}.\nabla\mathbf{J_1} + (\nabla.\mathbf{V})\,\mathbf{J_1} - \mathbf{J_1}.\nabla\mathbf{V}\right] = -D_B\nabla C. \tag{5.2}$$

When $\delta_{E_1} = 0 = \delta_{C_1}$, classical Fourier's and Fick's law are obtained from Eqs. (5.1) and (5.2) respectively. Using the continuity equation $\nabla.\mathbf{V} = 0$, the Eqs. (5.1) and (5.2) are converted into the following form

$$\mathbf{q_1} + \delta_{E_1}\left[\frac{\partial \mathbf{q_1}}{\partial t} + \mathbf{V}.\nabla\mathbf{q_1} - \mathbf{q_1}.\nabla\mathbf{V}\right] = -k_1\nabla T, \tag{5.3}$$

$$\mathbf{J_1} + \delta_{C}\left[\frac{\partial \mathbf{J_1}}{\partial t} + \mathbf{V}.\nabla\mathbf{J_1} - \mathbf{J_1}.\nabla\mathbf{V}\right] = -D_B\nabla T. \tag{5.4}$$

5.2.2 The Governing Equations

The governing partial differential equations for continuity, velocity, temperature and concentration [38], are given as follows

$$u_x + v_y = 0, \tag{5.5}$$

$$u_t + uu_x + vu_y + \lambda_1\left[u^2u_{xx} + v^2u_{yy} + 2uvu_{xy}\right] = -\frac{1}{\rho}P_x + \nu\left(u_{xx} + u_{yy}\right), \tag{5.6}$$

$$v_t + uv_x + vv_y + \lambda_1\left[v^2v_{xx} + v^2v_{yy} + 2uvv_{xy}\right] = -\frac{1}{\rho}P_y + \nu\left(v_{xx} + v_{yy}\right), \tag{5.7}$$

$$T_t + uT_x + vT_y + \lambda_{E_1}\Omega_{E_1} = \alpha\left(T_{xx} + T_{yy}\right) + \tau\left[D_BC_yT_y + \frac{D_T}{T_h}\left(T_y\right)^2\right], \tag{5.8}$$

$$C_t + uC_x + vC_y + \lambda_{C_1}\Omega_{C_1} = D_B\left(C_{xx} + C_{yy}\right) + \frac{D_T}{T_h}\left(T_{xx} + T_{yy}\right). \tag{5.9}$$

For unsteady squeezing flow, the corresponding boundary conditions are

$$\left.\begin{aligned} y=0: \quad u\left(x,y,t\right)&=\frac{ax}{1-\gamma_1 t}, \quad v\left(x,y,t\right)=0,\\ T\left(x,y,t\right)=T_w=T_0+d_1x,\ & C\left(x,y,t\right)=C_w=C_0+d_3x,\\ y=h\left(t\right): \quad u\left(x,y,t\right)&=0, \quad v\left(x,y,t\right)=v_h=h_t,\\ T=T_h=T_0+d_2x,\quad & C=C_h=C_0+d_4x. \end{aligned}\right\} \tag{5.10}$$

In Eqs. (5.8)-(5.9), Ω_{E_1} and Ω_{C_1} [38] are formulated as

$$\begin{aligned}\Omega_{E_1}&=T_{tt}+uu_xT_x+vv_yT_y+U^2T_{xx}+V^2T_{yy}+u_tT_x+2uvT_{xy}\\&\quad+2uT_{xt}+uv_xT_y+v_tT_y+vu_yT_x+2vT_{yt}.\end{aligned} \tag{5.11}$$

$$\begin{aligned}\Omega_{C_1}&=C_{tt}+uu_xC_x+vv_yC_y+u^2C_{xx}+v^2C_{yy}+u_tC_x+2uvC_{xy}\\&\quad+2uC_{xt}+uv_xC_y+v_tC_y+vu_yC_x+2vC_{yt}.\end{aligned} \tag{5.12}$$

5.2.3 Dimensionless Governing Equations

Following transformations [38] have been introduced to convert Eqs. (5.5)-(5.9) into the nondimensional form:

$$\left.\begin{aligned} \Psi=\sqrt{\frac{a\nu}{1-\gamma_1 t}}xf\left(\eta\right), \quad \theta(\eta)&=\frac{T-T_h}{T_w-T_0}, \quad u=\frac{ax}{1-\gamma_1 t}f'(\eta),\\ v=-\sqrt{\frac{a\nu}{1-\gamma_1 t}}f(\eta), \quad \eta=\sqrt{\frac{a}{\nu(1-\gamma_1 t)}}y, \quad \phi(\eta)&=\frac{C-C_h}{C_w-C_0}. \end{aligned}\right\} \tag{5.13}$$

Eq. (5.5) is verified and the other Eqs. (5.6)-(5.9), get the following form

$$f''''+ff'''-f'f''-\frac{Sq}{2}\left(3f''+\eta f'''\right)-De\left(2f'^2f''+2ff''^2-f^2f''''\right)=0, \tag{5.14}$$

$$\left.\begin{aligned}&\theta'' + Pr\left(f\theta' - \frac{\eta}{2}Sq\ \theta'\right) - Pr\beta_e\left(ff'\theta' + f^2\theta'' - Sq\eta f\theta''\right)\\&-\frac{Pr}{4}\beta_e Sq^2\left(3\eta\theta' + \eta^2\theta''\right) + \frac{Pr}{2}Sq\beta_e\left(\eta f'\theta' + 3f\theta'\right) + Pr\left(Nb\theta'\phi' + Nt\theta'^2\right) = 0,\end{aligned}\right\} \tag{5.15}$$

$$\left.\begin{aligned}&\phi'' + PrSc\left(f\phi' - \frac{Sq}{2}\eta\phi'\right) + \frac{Nt}{Nb}\theta'' - PrSc\beta_c\left(ff'\phi' + f^2\phi'' - Sq\eta f\phi''\right)\\&-\frac{\eta}{4}ScPr\beta_c Sq^2\left(3\phi' + \eta\phi''\right) + \frac{Pr}{2}Sc\beta_c Sq\left(3f\phi' + f'\phi'\eta\right) = 0.\end{aligned}\right\} \tag{5.16}$$

By using the similarity transformation (5.13) the boundary conditions (5.10) reduced as:

$$\left.\begin{aligned}&f(0) = 0,\quad f'(0) = 1,\quad \theta(0) = 1 - S_1,\quad \phi(0) = 1 - S_2,\\&f(1) = \frac{Sq}{2},\quad f'(1) = 0,\quad \theta(1) = 0,\quad \phi(1) = 0.\end{aligned}\right\} \tag{5.17}$$

Some emerging parameters in equations (5.14)-(5.17), are defined as follows

$$\begin{aligned}&Sq = \frac{\gamma_1}{a},\quad Pr = \frac{\nu}{\alpha},\quad Nb = \frac{\tau D_B}{\nu}\left(C_h - C_f\right),\\&Nt = \frac{D_T}{T_f}\frac{\tau}{\nu}\left(T_h - T_f\right),\quad Sc = \frac{\nu}{D_B},\quad S_1 = \frac{d_2}{d_1},\\&S_2 = \frac{d_4}{d_3},\quad De = \frac{\lambda_1 Sq^2}{\rho}, \beta_e = \frac{a\delta_{E_1}}{1-\gamma_1 t}, \beta_c = \frac{a\delta_{C_1}}{1-\gamma_1 t}.\end{aligned}$$

5.2.4 Physical Quantities of Interest

The important physical parameters of interest, the skin friction coefficient and the Sherwood number, are formulated as:

$$C_f = \frac{\tau_w}{\rho U_w^2},\quad Sh_x = \frac{xq_m}{D(C_f - C_h)},$$

The above quantities are listed as

$$\tau_w = \mu\left(u_y\right)_{y=0},\quad q_m = -D\left(C_y\right)_{y=0}.$$

After using the similarity transformation, the skin friction and the Sherwood number take the following form

$$C_f Re_x^{1/2} = f''(0), \quad Sh_x Re_x^{-1/2} = -\phi'(0).$$

5.2.5 Entropy Generation Analysis

According to [101], the entropy is given by

$$\left.\begin{aligned} S'''_{gen} = \frac{k_1}{T_h^2}\left[(T_x + T_y)^2\right] + \frac{\mu}{T_h}\left[2\left((U_x)^2 + (V_y)^2\right) + (U_y + V_x)\right] \\ + \frac{R_D}{C_h}\left[(C_x)^2 + (C_y)^2\right] + \frac{R_D}{T_h}\left[(T_x C_x) + (T_y C_y)\right]. \end{aligned}\right\} \tag{5.18}$$

The characteristic entropy generation is defined as

$$S'''_0 = \frac{k\left(T_f - T_h\right)^2}{h^2 T_h^2}. \tag{5.19}$$

In dimensionless form, the entropy generation can be written as

$$\begin{aligned} NG = \frac{S'''_{gen}}{S'''_0} = Re\theta'^2(\eta) + \frac{ReBr}{\Omega} f'^2(\eta) + \frac{ReBr}{\Omega} f''^2(\eta) + Re\lambda_1 \left(\frac{\chi}{\Omega}\right)^2 \phi'^2(\eta) \\ + Re\lambda_1 \left(\frac{\chi}{\Omega}\right) \theta'(\eta)\phi'(\eta), \end{aligned} \tag{5.20}$$

where

$$Re = \frac{\mu h^2}{\nu}, Br = \frac{\mu {U_w}^2}{k\left(T_f - T_h\right)}, \Omega = \frac{\left(T_f - T_h\right)}{T_h}, \chi = \frac{\left(C_f - C_h\right)}{C_h}, \lambda_1 = \frac{RDC_h}{k_1}.$$

5.3 Solution Methodology

The shooting method [93] is adopted to solve the system of ordinary differential Eqs. (5.14)-(5.16) with the boundary conditions (5.17). We denote $f \to \Gamma_1$, $\Gamma_1' \to \Gamma_2$, $\Gamma_2' \to \Gamma_3$, $\Gamma_3' \to \Gamma_4$, $\theta \to \Gamma_5$, $\theta' \to \Gamma_6$, $\phi \to \Gamma_7$ and $\phi' \to \Gamma_8$. The system of nonlinear ordinary differential Eqs.(5.14)-(5.16) is converted to eight first order

differential equations. The initial value problem can be written as

$$
\begin{aligned}
\Gamma_1' &= \Gamma_2,\\
\Gamma_2' &= \Gamma_3,\\
\Gamma_3' &= \Gamma_4,\\
\Gamma_4' &= \frac{\left[\Gamma_2\Gamma_3 - \Gamma_1\Gamma_4 + \frac{Sq}{2}\left(3\Gamma_3 + \eta\Gamma_4\right) + De\left(2\Gamma_3\Gamma_2^2 + 2\Gamma_1\Gamma_3^2\right)\right]}{1 + De\Gamma_1^2},\\
\Gamma_5' &= \Gamma_6,\\
\Gamma_6' &= \frac{Pr\left[\begin{array}{c}\left(\frac{Sq}{2}\eta\Gamma_6 - \Gamma_1\Gamma_6\right) - \left(Nb\Gamma_6\Gamma_8 + Nt\Gamma_6^2\right)\\ +\beta_e\left(\frac{3}{4}Sq^2\eta\Gamma_6 + \Gamma_1\Gamma_2\Gamma_6 - \frac{Sq}{2}\eta\Gamma_2\Gamma_6 - \frac{3}{2}Sq\Gamma_1\Gamma_6\right)\end{array}\right]}{1 - \frac{1}{4}Pr\beta_e Sq^2\eta^2 - Pr\Gamma_1^2\beta_e + PrSq\beta_e\eta\Gamma_1},\\
\Gamma_7' &= \Gamma_8,\\
\Gamma_8' &= \frac{PrSc\left[\begin{array}{c}\left(-\Gamma_1\Gamma_8 + \frac{Sq}{2}\eta\Gamma_8\right)\\ +\beta_c\left(\frac{3}{4}\eta Sq^2\Gamma_8 + \Gamma_1\Gamma_2\Gamma_8 - \frac{Sq}{2}\eta\Gamma_2\Gamma_8 - \frac{3}{2}Sq\Gamma_1\Gamma_8\right)\end{array}\right] - \frac{Nt}{Nb}\Gamma_6{}'}{1 - \frac{1}{4}PrSc\beta_c Sq^2\eta^2 - PrSc\Gamma_1^2\beta_c + PrSc\eta Sq\beta_c\Gamma_1}.
\end{aligned}
$$

subject to the initial conditions

$$
\left.\begin{array}{l}\Gamma_1(0) = 0,\ \ \Gamma_2(0) = 1,\ \ \Gamma_3(0) = \xi_0,\ \ \Gamma_4(0) = \xi_1,\ \ \Gamma_5(0) = 1 - S_1,\\ \Gamma_6(0) = \xi_2,\ \ \Gamma_7(0) = 1 - S_2,\ \ \Gamma_8(0) = \xi_3.\end{array}\right\}
$$

After choosing the missing conditions, the above initial value problem has been solved by the RK4 method by choosing some appropriate values for ξ_0, ξ_1, ξ_2 and ξ_3. For the refinement of ξ_0, ξ_1, ξ_2 and ξ_3, the Newton's method has been used until we meet the following convergence criteria:

$$
\max\left\{\left|\Gamma_1(1) - \frac{Sq}{2}\right|, \left|\Gamma_2(1)\right|, \left|\Gamma_5(1)\right|, \left|\Gamma_7(1)\right|\right\} < \varepsilon,
$$

$\varepsilon > 0$ represents the small positive real number. Numerical results of the above mention problem is achieved with $\varepsilon = 10^{-6}$.

To validate the MATLAB code for the shooting method, the numerical results have also been computed by the bvp4c, a built-in MATLAB function. For further reliability of numerical results, the skin friction coefficient reported by Noor *et al.* [38] has been reproduced. The comparison presented in Table 5.1 indicates a strong agreement between the present results and those of Noor *et al.*. For this comparison, different parameters are given the following values $\beta_e = 0.1$, $\beta_c = 0.1$, $De = 0$, $S_1 = 0.1$, $S_2 = 0.1$, $Nt = 0.5$, $Nb = 0.3$.

			Present results		Noor *et al.* [38]	
Sq	Sc	Pr	Shooting	bvp4c	HAM	BVPh2
1.0	1.1	2.0	1.17039	1.17039	1.17039	1.170381
1.1			0.86900	0.86900	0.86900	0.869032
1.2			0.56585	0.56585	0.56585	0.565647
1.0	1.1	2.0	1.17039	1.17039	1.17039	1.170381

Table 5.1: Comparison of the skin friction cofficient $C_f Re_x^{1/2}$.

5.4 Results and Discussions

Impact of the different important physical parameters is illustrated in this section. Numerical results for emerging parameters are displayed in the form of tables followed by the discussion on the graphical behavior of certain important profiles.

Table 5.2 exhibits the effect of squeezing parameter Sq, thermophoresis parameter Nt and Brownian motion parameter Nb on mass transfer rate. As squeezing parameter Sq escalates, there is a less increasing effect on the Sherwood number. For higher thermophoretic Nt, the Sherwood number shows a prominent increasing behavior whereas for the greater Brownian motion parameter Nb, the

Sherwood number decreases.

$Sh_x Re_x^{-1/2}$				
Sq	Nt	Nb	Shooting	bvp4c
0.5	0.5	0.3	1.78936	1.78936
1.0			1.79018	1.79018
1.1			1.79069	1.79069
1.2			1.79131	1.79131
1.2	0.5	0.3	1.58396	1.58396
	1.0		3.27724	3.27724
	1.5		5.08039	5.08039
	2.0		6.96800	6.96800
1.2	0.5	0.3	1.58396	1.58396
		1.0	1.39393	1.39393
		1.5	1.30641	1.30641
		2.0	1.25110	1.25110

Table 5.2: Numerical values of $Sh_x Re_x^{-1/2}$ when $\beta_e = \beta_c = 0.1, De = 0.0, S_1 = 0.1, Sc = 1.1, S_2 = 0.1, Pr = 2.0$.

5.4.1 Outcome of Velocity and Temperature for Different Values

Figure 5.2 exhibits the influence of squeezing parameter $Sq > 0$ on the velocity. Positive values of the Sq denote that the top plate shifts towards the bottom plate. As the plate shifts towards bottom plate, there is a force which produces higher velocity of fluid. It is noticeable that the higher squeezing parameter Sq increase the velocity. The impact of squeezing parameter $Sq < 0$ on the velocity profile is plotted in Fig. 5.3. When the top plate shifts far away from the bottom plate. It leaves a gap and to fill up this gap, the fluid starts moving towards the upper plate. Consequently, the velocity of fluid is decreased. Fig. 5.4 exhibits the behviour of

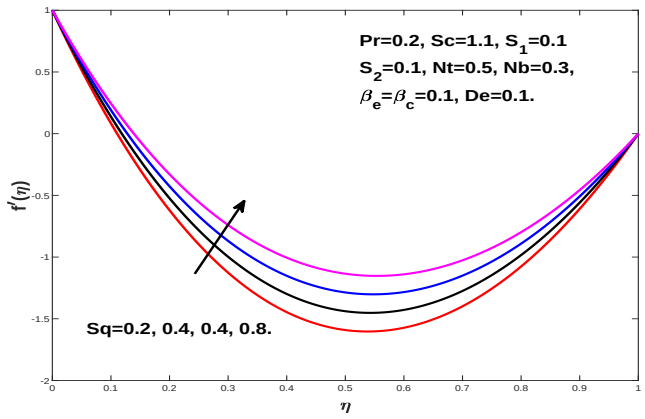

Figure 5.2: Impact of positive Sq on f'.

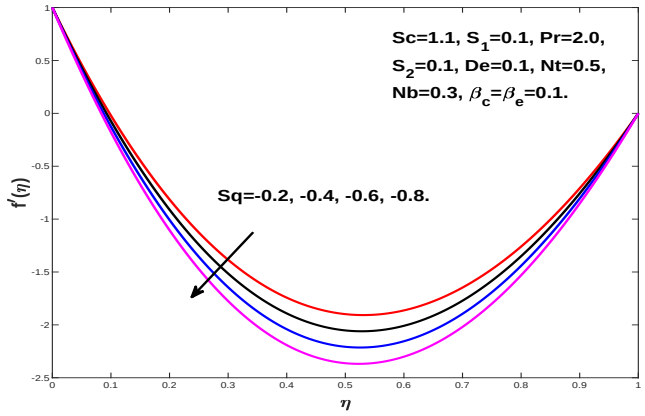

Figure 5.3: Impact of negative Sq on f'.

velocity under the impact of the Deborah number De. The velocity increases in the region $0 \leq \eta \leq 0.5$ near the bottom plate for greater Deborah number, whereas the velocity in the region $0.5 \leq \eta \leq 1$ declines. The influence of thermal relaxation parameter β_e on temperature is displayed in Fig. 5.5. The figure demonstrates a decay in temperature as thermal relaxation parameter β_e escalates. Physically, as β_e increases, the molecules attain more time to move the heat to neighboring particles. This exhibits decrease in the temperature. When $\beta_e = 0$, reduces the given model to the model of the classical Fourier's law. Feature of Brownian motion parameter Nb against temperature is discussed in Fig. 5.6. Figure exhibits that as Nb escalates, temperature is enhanced. Large Brownian motion parameter have higher diffusion and less viscous force which enhanced the temperature profile. Fig. 5.7 is portrayed for temperature profile versus thermophoresis

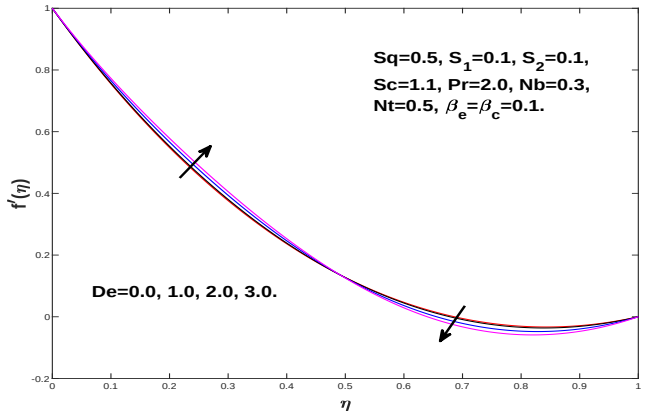

Figure 5.4: Impact of De on f'.

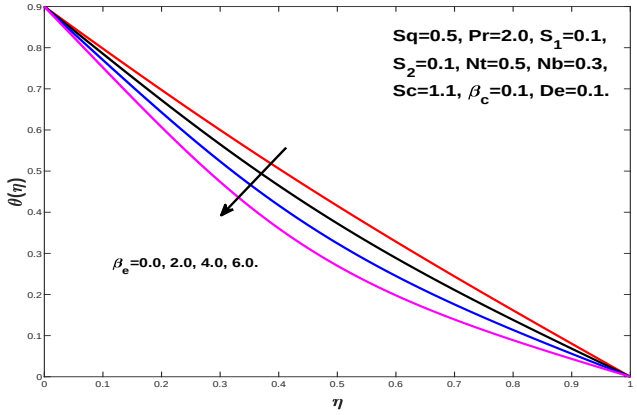

Figure 5.5: Impact of β_e on θ.

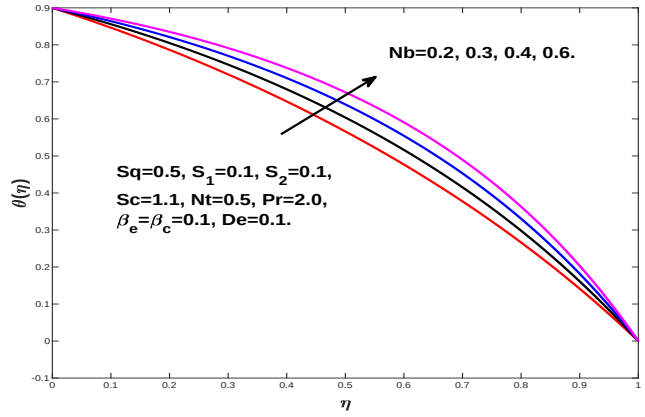

Figure 5.6: Impact of Nb on θ.

parameter Nt. The graph exhibits that as Nt increases, temperature field also increases. Physically, as a consequence of the increasing values of Nt, there is a powerful thermophoretic force. This force permits an extensive movement of

those nanoparticles in fluid, which are away from the surface. This delivers an

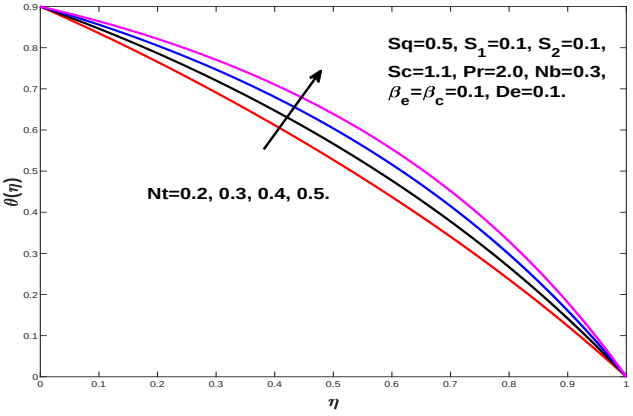

Figure 5.7: Impact of Nt on θ.

increased in temperature and stratification of thermal layer. Fig. 5.8 exhibits that for greater Pr, the temperature profile declines. Physically, the Prandtl number Pr is natural part of thermal diffusivity. Higher Pr creates lower thermal diffusivity which relates to lower temperature field and less thickness in boundary layer. Fig. 5.9 demonstrates the impact of thermal stratification S_1 on the temperature.

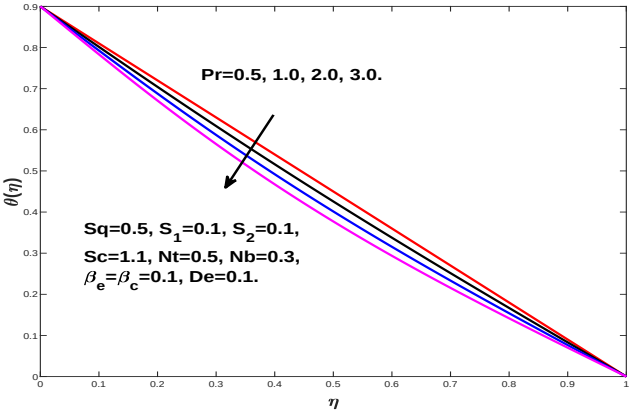

Figure 5.8: Impact of Pr on θ.

A decrease of the temperature profile is seen for higher S_1. The reduction in temperature field is responsible for temperature difference.

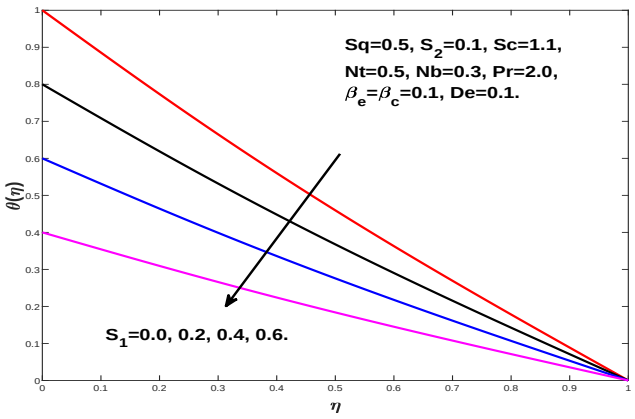

Figure 5.9: Impact of S_1 on θ.

5.4.2 Effect of Various Parameters on Concentration

Fig. 5.10 illustrates the impact of concentration relaxation parameter β_c on concentration. It is witnessed from the figure that for greater β_c, the thickness of concentration profile declines. For $\beta_c = 0$, given model reduces to the Fick's law. Impact of Brownian motion Nb on concentration profile is displayed in Fig. 5.11. It

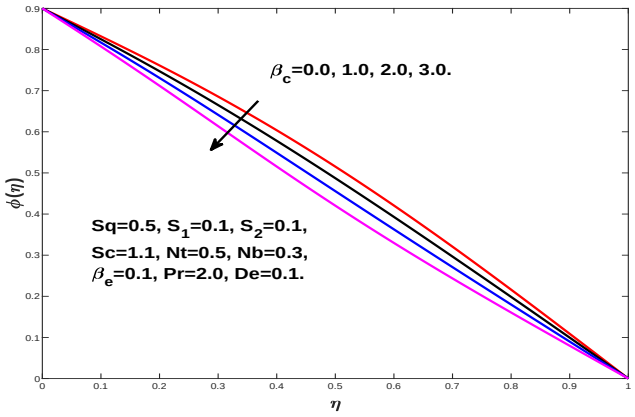

Figure 5.10: Impact of β_c on ϕ.

is remarked that concentration declines for higher Nb. Greater Brownian motion produces a weaker concentration. Fig. 5.12 depicts the impact of thermophoretic parameter Nt on concentration profile. For enlarging Nt the concentration profile declines. The figure exhibits that greater values of Nt generate a stronger concentration. Fig. 5.13 highlights the impact of the Prandtl number Pr on concentration. Greater Pr exhibits the increase in concentration profile. It is noted

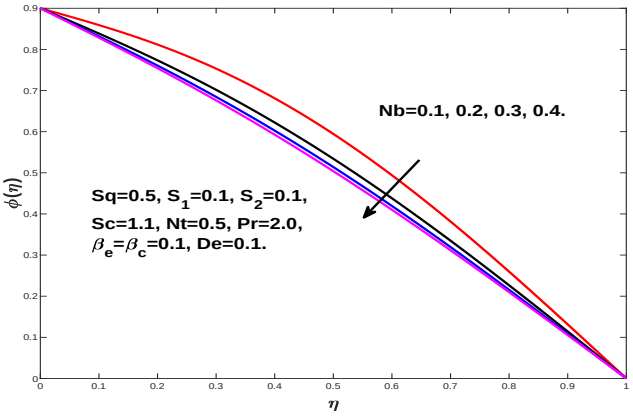

Figure 5.11: Impact of Nb on ϕ.

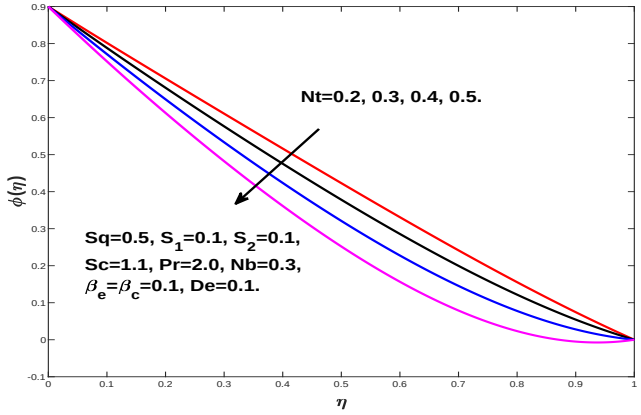

Figure 5.12: Impact of Nt on ϕ.

that concentration profile increases for higher Pr. Fig. 5.14 demonstrates the

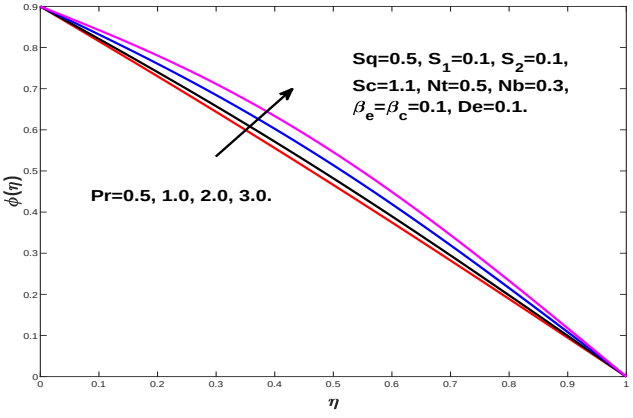

Figure 5.13: Impact of Pr on ϕ.

effect of solutal stratification S_2 on concentration profile. Concentration profile

declines for higher S_2. Fig. 5.15 exhibits the impact of Schmidt number Sc on the

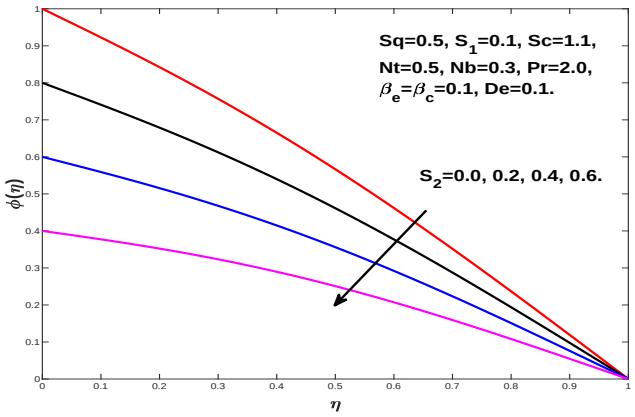

Figure 5.14: Impact of S_2 on ϕ.

concentration profile. For higher Sc, the concentration profile grows.

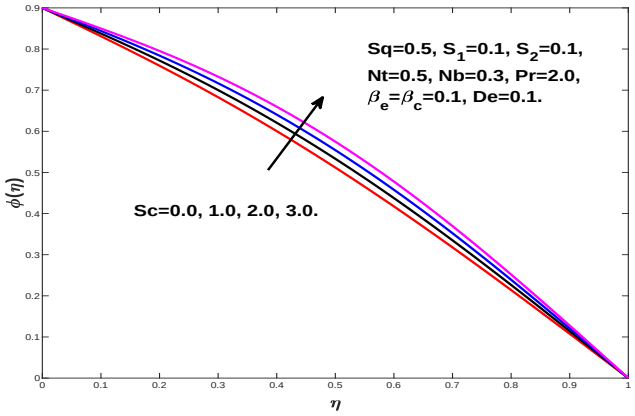

Figure 5.15: Impact of Sc on ϕ.

5.4.3 Consequence of Different Parameters on Entropy Generation

Figs. 5.16-5.19 show the effects of Brinkman number Br, thermal stratification parameter S_1 and squeezing parameter S on entropy generation for $Re = 0.1$, $\Omega = 1.0$, $\chi = 0.2$, $\lambda_1 = 0.2$ and $\beta_r = 1.0$. Fig. 5.16 shows the influence of Brinkman number Br on entropy NG. For higher Brinkman number, entropy generation NG increases. An increment in entropy is produced by the irreversibility of fluid

friction. Fig. 5.17 exhibits the impact of the thermal stratification S_1 on entropy

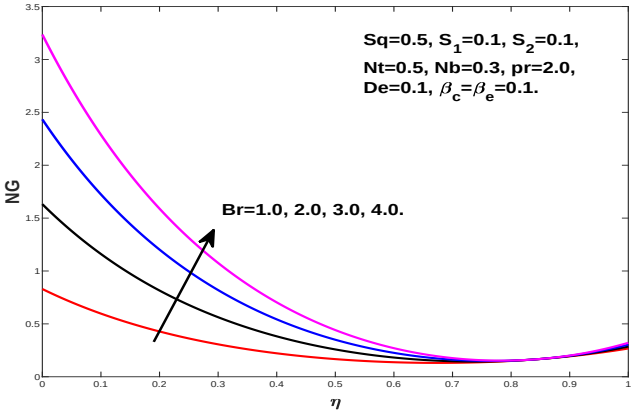

Figure 5.16: Impact of Br on N_G.

NG. The figure shows that the entropy NG decreases, as the stratification parameter for temperature increases. The entropy is more distinguished near the walls of the channel as compared to the center. Fig. 5.18 explains the influence of

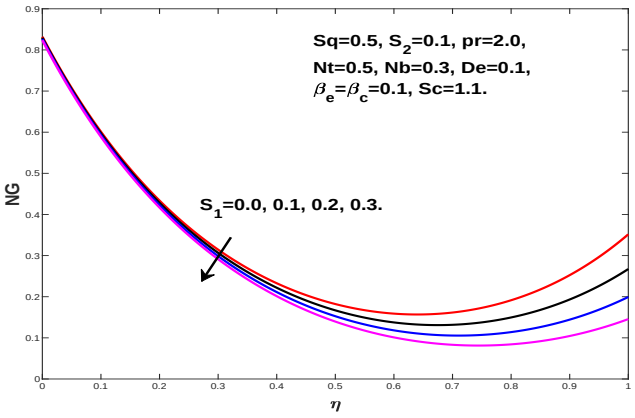

Figure 5.17: Impact of S_1 on N_G.

the squeezing parameter Sq on the entropy generation NG. It can be visualized from the figure that due to an increment in the squeezing parameter, the entropy generation NG declines. The entropy is more prominent near the walls of the channel than at the center. Fig. 5.19 exhibits the impact of Reynolds number Re on entropy generation NG. The figure exhibits that as Reynolds number escalates, the entropy NG also increases.

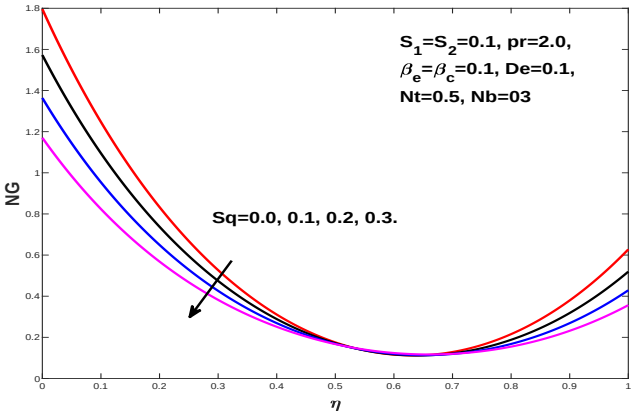

Figure 5.18: Impact of Sq on N_G.

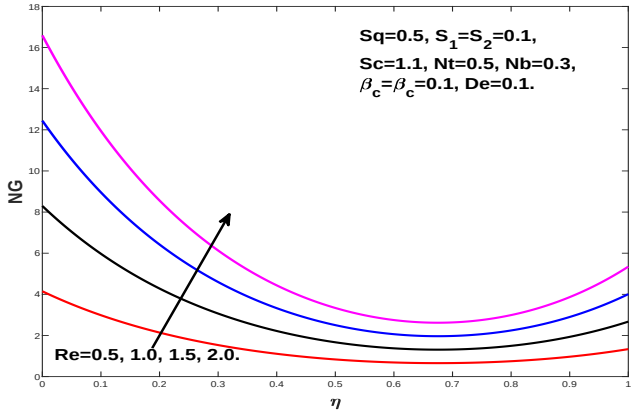

Figure 5.19: Impact of Re on N_G.

5.5 Conclusion

In this chapter, a two dimensional squeezing flow along with Cattaneo-Christov double diffusion is examined. The main findings of the present analysis are summarized as follows:

- Increasing values of Deborah number De, cause an increasing behaviour in the region $0 \leq \eta \leq 0.5$, whereas the velocity in the region $0.5 \leq \eta \leq 1$ decreases.
- Temperature decreases for higher Brownian motion parameter Nb.
- As thermophoresis parameter arises, an enhancement is observed in temperature profile whereas a decline is seen in concentration profile.

- Increasing values of thermal relaxation β_e cause decreasing behavior in temperature profile.
- As Prandtl number Pr grows, decreasing trend is observed in the temperature.
- The increasing concentration relaxation parameter β_c, causes a decrease in concentration profile.
- The entropy generation has a decreasing behaviour for increasing values of the squeezing parameter Sq.

Chapter 6

Squeezing Flow of Micropolar Nanofluid between Two Parallel Plates

6.1 Introduction

Present study deals with the unsteady micropolar nanofluid squeezing between two parallel plates. Impact of viscous dissipation and thermal radiation is also considered. The modeled nonlinear differential equations are solved numerically. The governing partial differential equations are transformed into ordinary differential equations by using a similarity transformation. Further, numerical solution is obtained by using the shooting method. The reduced ordinary differential equations with the boundary conditions are solved by the shooting method. For verification of numerical results, bvp4c a MATLAB built in function, has been invoked. The presently computed results are validated with already published results. The influence of different parameters on velocity, temperature, concentration and entropy generation is presented in the form of graphs.

6.2 Problem Formulation

6.2.1 The Physical Configuration

Let us consider the unsteady, viscous, two dimensional, incompressible, micropolar nanofluid squeezed flow between two parallel plates. The plates are placed in such a way that the bottom plate is fixed at $y = 0$ and the top plate is moving with the velocity $y = h(t)$. The distance between the two plates is $h(t) = l(1 - \gamma_1 t)^{\frac{1}{2}}$. The two plates are squeezed until they touch each other at $t = \frac{1}{\gamma_1}$, when $\gamma_1 > 0$. The two plates are separated for $\gamma_1 < 0$. Thermal radiation and viscous dissipation impacts are included. Thermophoresis diffusion and Brownian motion impact are also considered. The temperature of the bottom plate is T_1 while the temperature of the top plate is T_2. C_1 and C_2 are the concentration of the lower and upper plate respectively.

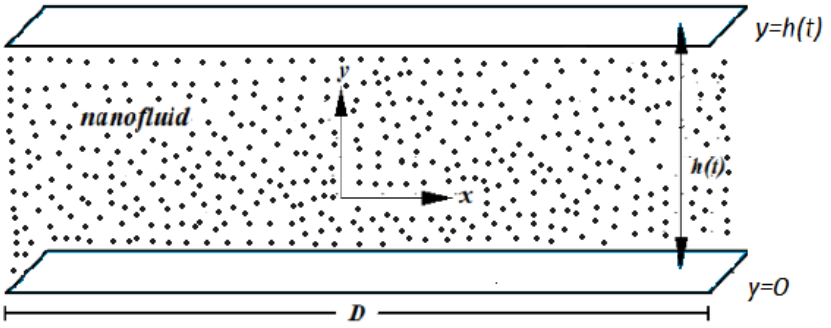

Figure 6.1: Schematic illustration of squeezing flow.

6.2.2 The Governing Equations

Equations reflecting the physical aspects of the problem in the sense of [102, 103], are as follows

$$u_x + v_y = 0, \tag{6.1}$$

$$u_t + uu_x + vu_y = -\frac{1}{\rho}P_x + (\nu + \frac{k_f}{\rho})(u_{xx} + u_{yy}) + \frac{k_f}{\rho}N_y, \tag{6.2}$$

$$v_t + uv_x + vu_y = -\frac{1}{\rho}P_y + (\nu + \frac{k_f}{\rho})(v_{xx} + v_{yy}) - \frac{k_f}{\rho}N_x, \tag{6.3}$$

$$\rho_j (N_t + UN_x + VN_y) = \gamma_n (N_{xx} + N_{yy}) - k_f (2N + U_y - V_x), \tag{6.4}$$

$$\left.\begin{aligned} T_t + uT_x + vT_y = \alpha (T_{xx} + T_{yy}) - \frac{1}{(\rho c_p)_f}\hat{q}_{ry} + \frac{\mu + \frac{k_f}{2}}{(\rho c_p)_f}(u_y)^2 \\ + \frac{(\rho c_p)_p}{(\rho c_p)_f}\left[D_B (C_y T_y + C_x T_x) + \left(\frac{D_T}{T_2}\right)\left((T_x)^2 + (T_y)^2\right)\right], \end{aligned}\right\} \tag{6.5}$$

$$C_t + uC_x + vC_y = D_B (C_{xx} + C_{yy}) + \frac{D_T}{T_2}(T_{xx} + T_{yy}). \tag{6.6}$$

Here the formulation of γ_n [104] has been taken as

$$\gamma_n = \left(\mu + \frac{k_f}{2}\right) j. \tag{6.7}$$

According to the Rosseland approximation, the radiation heat flux [20] is defined as

$$\hat{q}_r = \frac{-4\hat{\delta}_e}{3\hat{\beta}_R} T_y^4. \tag{6.8}$$

Using the Taylor's series, T^4 is expanded about the temperature T_2 and omitting higher order terms, one obtains

$$T^4 = 4TT_2^3 - 3T_2^4. \tag{6.9}$$

The appropriate boundary conditions are

$$\left.\begin{aligned} y = 0: \quad u(x,y,t) = 0, \quad v(x,y,t) = 0, \\ N = -nU_y, \quad T(x,y,t) = T_2, \quad C(x,y,t) = C_2, \\ y = h(t): \quad u(x,y,t) = 0, \quad v(x,y,t) = h_t, \\ N = -nU_y, \quad T(x,y,t) = T_1, \quad C(x,y,t) = C_1. \end{aligned}\right\} \tag{6.10}$$

6.2.3 The Dimensionless Governing Equations

The following similarity transformation [20] is used to convert the Eqs. (6.1)-(6.6) along with the boundary conditions (6.10) into dimensionless form:

$$\left.\begin{aligned} \eta = \frac{y}{l\sqrt{1-\gamma_1 t}}, \quad \theta(\eta) = \frac{T-T_2}{T_1-T_2}, \quad u = \frac{\gamma_1 x}{2\left(1-\gamma_1 t\right)} f'(\eta), \\ v = -\frac{\gamma_1 l}{2\sqrt{1-\gamma_1 t}} f(\eta), \; N = \frac{\gamma_1 x}{2l\left(1-\gamma_1 t\right)^{\frac{3}{2}}} g\left(\eta\right), \quad \phi(\eta) = \frac{C-C_2}{C_1-C_2}. \end{aligned}\right\} \tag{6.11}$$

By making use of (6.11) in Eqs. (6.1)-(6.6), the continuity equation is identically satisfied, whereas Eqs. (6.2)-(6.6) take the following form

$$\left(1+K\right) f'''' - Sq\left(3f'' + \eta f''' + f'f'' - ff'''\right) + Kg'' = 0, \tag{6.12}$$

$$\left(1+\frac{K}{2}\right) g'' - Sq\left(3g + \eta g' + f'g - fg'\right) - N1\left(2g + f''\right) = 0, \tag{6.13}$$

$$\left(1+\frac{4}{3}Rd\right)\theta'' + SqPr\left(\eta\theta' - f\theta'\right) + PrNb\theta'\phi' + PrNt\left(\theta'\right)^2 + \left(1+\frac{K}{2}\right) PrEcf'' = 0, \tag{6.14}$$

$$\phi'' + \frac{Nt}{Nb}\theta'' + SqSc\left(f\phi' - \eta\phi'\right) = 0. \tag{6.15}$$

The boundary conditions (6.10) in the dimensionless form are

$$\left.\begin{aligned} f(0) = 0, \quad f'(0) = 0, \quad \theta(0) = 0, \quad \phi(0) = 0, \quad g(0) = -nf''(0), \\ f(1) = 1, \quad f'(1) = 0, \quad \theta(1) = 1, \quad \phi(1) = 1, \quad g(1) = -nf''(1). \end{aligned}\right\} \tag{6.16}$$

6.2.4 Physical Quantities of Interest

The parameters appearing in equations (6.12)-(6.16), are defined as follows

$$\begin{aligned} &Sq = \frac{\alpha l^2 \rho}{2\mu}, \quad Pr = \frac{\nu}{\alpha}, \quad Nb = \frac{(\rho c_p)_p D_B\left(C_1 - C_2\right)}{(\rho c_p)_f}, \\ &Nt = \frac{(\rho c_p)_p D_B\left(T_1 - T_2\right)}{(\rho c_p)_f}, \quad Sc = \frac{\nu}{D_B}, \quad Rd = \frac{4T_h^3 \hat{\sigma}_e}{3\hat{\beta}_R k_f}, \\ &Ec = \frac{1}{cp}\left(\frac{\gamma_1 x}{2(1-\gamma_1 t)}\right)^2, \quad K = \frac{k_f}{\mu}, \quad N_1 = k_f l^2 (1-\gamma_1 t). \end{aligned}$$

The important physical parameters of interest, Nusselt and Sherwood number, are formulated as follows.

$$Nu = \frac{-l(T_y)_{y=0}}{k_1(T_1 - T_2)}\left(k_1 + \frac{16T_h^3\hat{\sigma}_e}{3\hat{\beta}_R}\right), \quad Sh_x = \frac{-l(C_y)_{y=0}}{(C_1 - C_2)}.$$

The heat and mass transfer take the following dimensionless form after using the similarity transformation (6.11)

$$\sqrt{1-\gamma_1 t}\; Nu = -\left(1 + \frac{4}{3}Rd\right)\theta'(0), \;\; \sqrt{1-\gamma_1 t}\; Sh = -\phi'(0).$$

6.2.5 Entropy Generation Analysis

Entropy generation is given by [105, 106]

$$S'''_{gen} = \frac{k_1}{T_\infty^2}\left[(T_x + T_y)^2\right] + \frac{4T_h^3\hat{\sigma}_e}{3\hat{\beta}_R k_1}\left[T_y\right]^2 + \frac{RD}{C_\infty}\left[(C_x)^2 + (C_y)^2\right] + \frac{k_f}{T_\infty}\left[u_y + 2N\right]^2$$
$$+ \frac{\mu + k_f}{T_\infty}\left[2\left((u_x)^2 + (v_y)^2\right) + (u_y + v_x)^2\right] + \frac{RD}{T_\infty}\left[(T_x C_x) + (T_y C_y)\right] + \frac{\gamma_1}{T_\infty}\left[N_y\right]^2. \tag{6.17}$$

The characteristics entropy generation is written as

$$S'''_0 = \frac{k_1\left(T_1 - T_2\right)^2}{h^2 T_\infty^2}. \tag{6.18}$$

The dimensionless form of the entropy generation can be written as

$$NG = Re(1 + \frac{4}{3}Rd)\theta'^2 + \left(1 + \frac{1}{K}\right)\frac{ReBr}{\Omega}\left(f'^2 + f''^2\right) + Re\lambda_1\left(\frac{\chi}{\Omega}\right)^2\phi'^2(\eta)$$
$$+ Re\lambda_1\left(\frac{\chi}{\Omega}\right)\theta'(\eta)\,\phi'(\eta) + \frac{ReBr}{\Omega}\left(f'' + g\right)^2 + \frac{ReBr}{\Omega}\delta^2 g'^2,$$

where

$$Re = \frac{\mu h^2}{\nu}, \;\; Br = \frac{\mu h^2}{k_f\left(T_1^* - T_2^*\right)}, \;\; \Omega = \frac{(T_1 - T_2)}{T_\infty}, \;\; \chi = \frac{(C_1 - C_2)}{C_\infty}, \;\; \lambda_1 = \frac{RDC_\infty}{k_f}.$$

6.3 Solution Methodology

The system of equations (6.12)-(6.15) and boundary conditions (6.16) have been solved numerically by using the shooting technique [93]. We denote $f \rightarrow \Gamma_1$, $\Gamma_1' \rightarrow \Gamma_2$, $\Gamma_2' \rightarrow \Gamma_3$, $\Gamma_3' \rightarrow \Gamma_4$, $g \rightarrow \Gamma_5$, $g' \rightarrow \Gamma_6$, $\theta \rightarrow \Gamma_7$,$\theta' \rightarrow \Gamma_8$, $\phi \rightarrow \Gamma_9 \rightarrow$ and $\phi' \rightarrow \Gamma_{10}$. The system of nonlinear ODEs (6.12)-(6.15) is converted to ten first order differential equations. The initial value problem can be written as

$$\left.\begin{aligned}
\Gamma_1' &= \Gamma_2, \\
\Gamma_2' &= \Gamma_3, \\
\Gamma_3' &= \Gamma_4, \\
\Gamma_4' &= \frac{Sq}{1+K}\left[3\Gamma_3 + \eta\Gamma_4 + \Gamma_2\Gamma_3 - \Gamma_1\Gamma_4\right] - \frac{K}{1+K}(\Gamma_6'), \\
\Gamma_5' &= \Gamma_6, \\
\Gamma_6' &= \frac{2Sq}{2+K}\left[3\Gamma_5 + \eta\Gamma_6 + \Gamma_2\Gamma_5 - \Gamma_1\Gamma_6\right] + \frac{2N_1}{2+K}\left[2\Gamma_5 + \Gamma_3\right], \\
\Gamma_7' &= \Gamma_8, \\
\Gamma_8' &= \frac{3Pr}{3+4Rd}\left[\begin{array}{c} Sq\left(\Gamma_1\Gamma_8 - \eta\Gamma_8\right) - Nb\Gamma_8\Gamma_{10} \\ -Nt(\Gamma_8')^2 - \frac{1}{2}\left(2+K\right)PrEc{\Gamma_3}^2 \end{array}\right], \\
\Gamma_9' &= \Gamma_{10}, \\
\Gamma_{10}' &= SqSc\left(\eta\Gamma_{10} - \Gamma_1\Gamma_{10}\right) - \frac{Nt}{Nb}\left(\Gamma_8'\right).
\end{aligned}\right\} \tag{6.19}$$

subject to the initial conditions

$$\left.\begin{aligned}
&\Gamma_1(0) = 0, \;\; \Gamma_2(0) = 0, \;\; \Gamma_3(0) = \xi_0, \;\; \Gamma_4(0) = \xi_1, \;\; \Gamma_5(0) = -n\Gamma_3(0), \\
&\Gamma_6(0) = \xi_2, \;\; \Gamma_7(0) = 0, \;\; \Gamma_8(0) = \xi_3, \;\; \Gamma_9(0) = 0, \;\; \Gamma_{10}(0) = \xi_4.
\end{aligned}\right\}$$

After chosen the missing condition, the above system of initial value problem is solved by using the RK4 method. To refine the above missing conditions $\xi_0, \xi_1, \xi_2, \xi_3$ and ξ_4, we employ the Newton's method. The procedure is repeated as far as we meet the specified convergence criteria:

$$\max\left\{\left|\Gamma_1(1) - 1\right|, \left|\Gamma_2(1)\right|, \left|\Gamma_5(1) + n\Gamma_3(1)\right|, \left|\Gamma_7(1) - 1\right|, \left|\Gamma_9(1) - 1\right|\right\} < \varepsilon.$$

From above ε is a small positive real number. Numerical results of above mention problem are achieved with $\varepsilon = 10^{-6}$.

The MATLAB code for the shooting method is validated, by the bvp4c, a MATLAB built-in function. For further reliability of numerical results, the numerical values of Nusselt number reported by [107] and [20] have been reproduced. The comparison presented in Table 6.1 indicates a strong agreement between the present results and those reported by Sheikholeslami and Ganji [107], and Atlas *et al.* [20].

		Ref. [107]	Ref. [20]	Present	
Rd	*Sc*			Shooting	bvp4c
0	0.5	0.270410	0.270420	0.270420	0.270420
	1	0.270421	0.270420	0.270420	0.270420
	10	0.270507	0.270521	0.270521	0.270521
	20	0.270602	0.270612	0.270612	0.270612
3	0.5	0.296127	0.296131	0.296131	0.296131
	1	0.296127	0.296130	0.296130	0.296130
	10	0.296130	0.296131	0.296131	0.296131
	20	0.296133	0.296132	0.296132	0.296132
6	0.5	0.298606	0.298610	0.298610	0.298610
	1	0.298607	0.298612	0.298612	0.298612
	10	0.298607	0.298677	0.298677	0.298677
	20	0.298608	0.298654	0.298654	0.298654
12	0.5	0.299542	0.299548	0.299548	0.299548
	1	0.299543	0.299548	0.299548	0.299548
	10	0.299543	0.299512	0.299512	0.299512
	20	0.299544	0.299538	0.299538	0.299538

Table 6.1: Comparison of the Nusselt number in the absence of the micropolar fluid with those of [107] and [20] by taking $Nb = 0.1$, $Nt = 0.2$, Pr, $Sq = 0.5$, and $Ec = 0.01$ and in the absence of micropolar fluid.

6.4 Results and Discussion

								Shooting method		bvp4c	
Nb	Nt	Rd	Sq	Ec	Pr	Sc	K	Nu	Sh	Nu	Sh
0.3	0.3	1	0.5	0.02	2	0.5	0.2	3.28375	0.58982	3.28376	0.58982
0.6								3.65605	0.71334	3.65604	0.71334
0.9								4.05245	0.75106	4.05245	0.75106
1								4.18975	0.75794	4.18976	0.75794
	0.5							3.52940	0.14425	3.52940	0.14424
	0.7							3.78601	0.45219	3.78602	0.452204
	0.9							4.05331	1.20857	4.05332	1.20858
		2						4.59172	0.74440	4.59172	0.74440
		3						5.91318	0.81383	5.91318	0.81383
		4						7.23964	0.85324	7.23964	0.85324
			1					3.30517	0.57787	3.30517	0.57787
			1.5					3.32632	0.56610	3.32632	0.56610
			2.0					3.34722	0.55451	3.34721	0.55451
				0.05				3.70097	0.41130	3.70098	0.41130
				0.1				4.39635	0.11377	4.39636	0.113770
				0.2				5.78715	0.48131	5.78717	0.48131
					0.72			2.65939	0.85659	2.65939	0.85659
					1			2.79109	0.83003	279109	0.8003
					1.5			3.03307	0.69694	3.03307	0.69694
						1		3.28383	0.58694	3.28383	0.58694
						1.5		3.28391	0.58407	3.28391	0.58120
						2		3.28399	0.58120	3.28399	0.58120
							0.1	3.27107	0.59525	3.27107	0.59525
							0.3	3.29643	0.58440	3.29643	0.58439
							0.5	3.32177	0.57355	3.32178	0.57355

Table 6.2: Nusselt number Nu and Sherwood number Sh.

This section is illustrated to the numerical solutions of the mathematical model (6.12)-(6.16). We first present the numerical results for some parameters of interest in the form of tables followed by the discussion on the graphical behaviour of certain important profiles.

Table 6.2 exhibits the effect of Brownian motion parameter Nb, thermophoresis parameter Nt, radiation parameter Rd, squeezing parameter Sq, Eckert number Ec, Prandtl number Pr, Schmidt number Sc and micropolar prameter K on the Nusselt and Sherwood numbers. It can be visualized from the table that the Nusselt number increases for increasing all the parameters and the Sherwood number increases for Nt, Nb and Rd and decreases on Sq, Ec, Sc, K and Pr.

6.4.1 Influence of Various Parameters on Velocity and Temperatures

Fig. 6.2 exhibits increasing impact of squeezing parameter Sq on velocity profile. The figure exhibits that as squeezing parameter enhances, an increase in $f'(\eta)$ is observed in the section $0 \leq \eta \leq 0.3$. The velocity profile declines in the region $0.3 \leq \eta \leq 0.7$ and an opposite behavior is seen in region $0.7 \leq \eta \leq 1$. Fig. 6.3 is

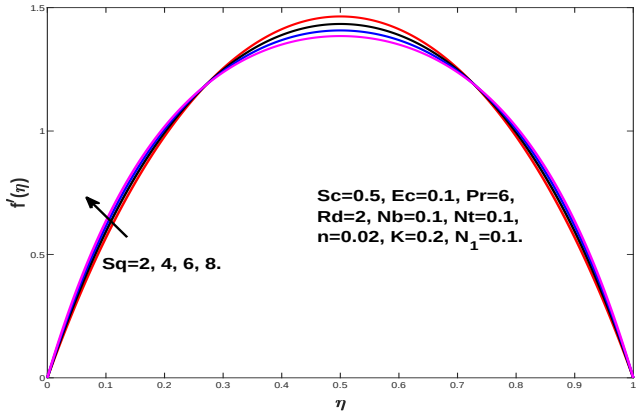

Figure 6.2: Influence of Sq on $f'(\eta)$.

sketched to exhibit the impact of micropolar parameter K on the velocity profile. The velocity enhances as micropolar parameter arises. Influence of the squeezing parameter Sq on the temperature profile is sketched in Fig. 6.4. Physically, as

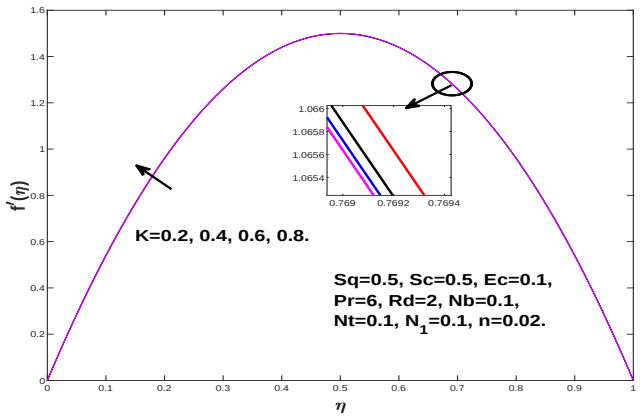

Figure 6.3: Influence of K on $f'(\eta)$.

the plates move away from each other, particles of nanofluid mixture disperse. This dispersion causes a reduction in the collision of nanoparticles. As a result, the influence of the inertial forces is declined. Fig. 6.5 exhibits the effect of mi-

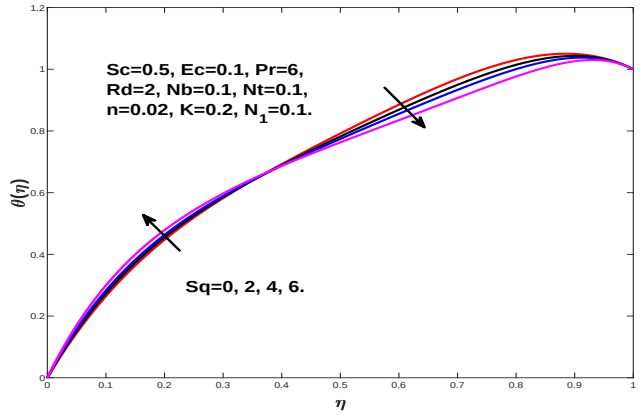

Figure 6.4: Influence of Sq on $\theta(\eta)$.

cropolar parameter K on the temperature. For higher micropolar parameter, the temperature increases. Fig. 6.6 depicts the impact of Prandtl number Pr on temperature profile. Momentum diffusitivity is greater than the thermal diffusitivity when $Pr > 1$. As a result higher Prandtl number results in higher fluid viscosity. In Fig. 6.7, the behaviour of temperature profile is examined for increased Eckert number Ec. As Eckert number escalates the temperature profile also increases. The temperature profile significantly increases due to viscous dissipation effects between two plates. Fig. 6.8 presents the impact of Brownian motion parameter Nb on temperature. For growing Brownian motion parameter, an enhancement in

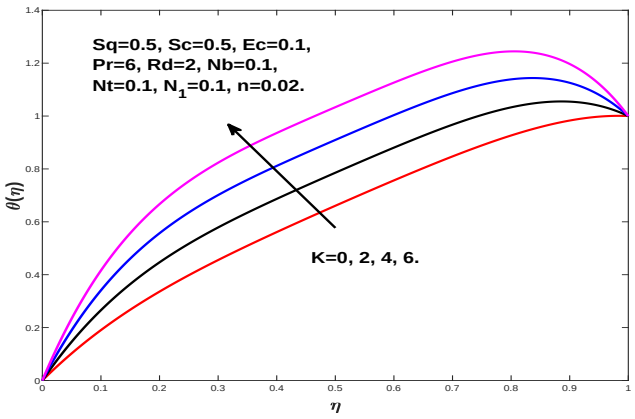

Figure 6.5: Influence of K on $\theta(\eta)$.

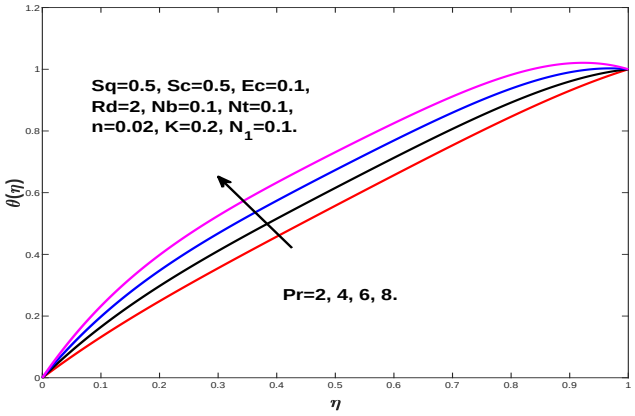

Figure 6.6: Influence of Pr on $\theta(\eta)$.

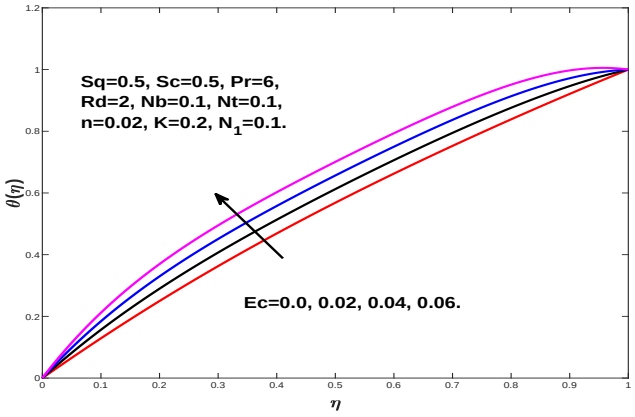

Figure 6.7: Influence of Ec on $\theta(\eta)$.

temperature is observed. Random motion of particles within base fluid is known as the Brownian motion. Brownian motion creates collion of nanoparticles within the base fluid. This phenomenon increases the temperature profile. Fig. 6.9 illus-

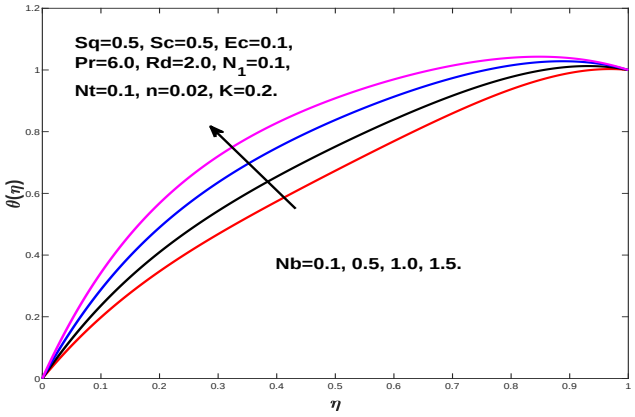

Figure 6.8: Influence of Nb on $f\theta(\eta)$.

trates the influence of thermophoretic parameter Nt on temperature. Temperature profile increases for higher thermophoretic parameter. The influence of radiation

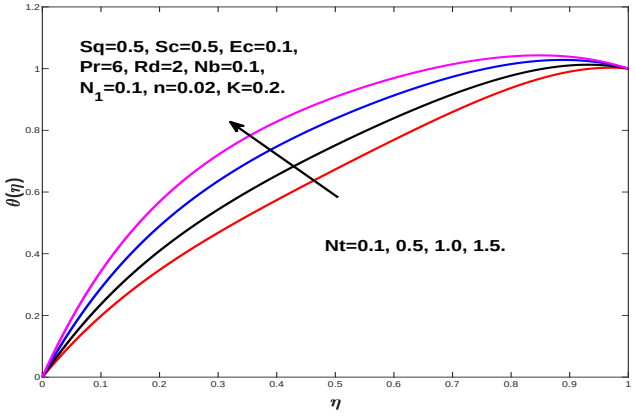

Figure 6.9: Influence of Nt on $\theta(\eta)$.

parameter Rd on temperature is visualized in Fig. 6.10. However, figure demonstrates that higher thermal radiation parameter causes a decrease in temperature. Physically, an enhancement in the thermal radiation leads to a decay in absorption coefficient. As a results an enhancement of the radiative heat flux occurs. When the rate of radiative heat transfer increases, the fluid temperature decreases.

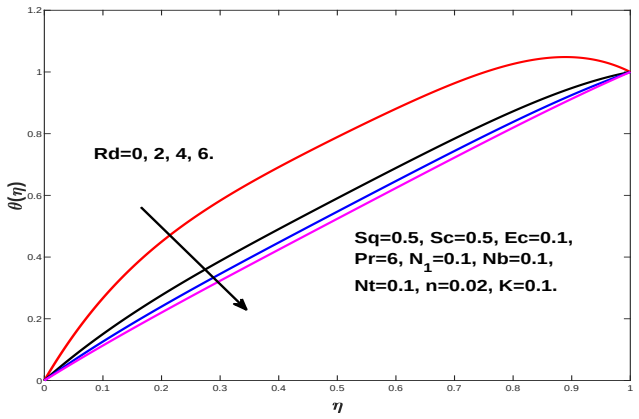

Figure 6.10: Influence of Rd on $\theta(\eta)$.

6.4.2 Outcome of Concentration for Numerous Parameters

Fig. 6.11 exhibits the effect of Sq on concentration. Enhancement in the thickness of concentration is examined for higher squeezing parameter. Fig. 6.12 visualizes

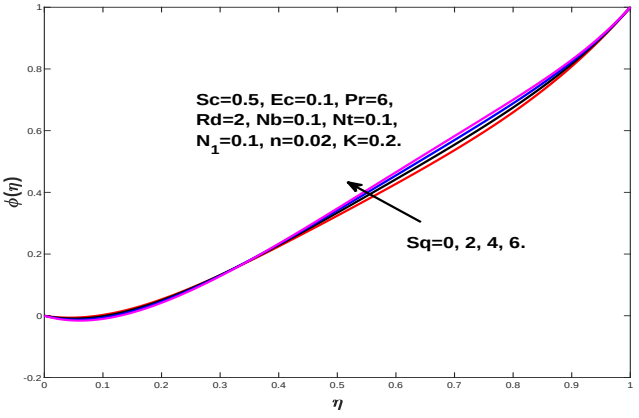

Figure 6.11: Influence of Sq on $\phi(\eta)$.

the impact of the Prandtl number Pr on concentration. The concentration profile declines for growing Prandtl number. Impact of thermal radiation Rd on concentration profile is plotted in Fig. 6.13. As thermal radiation enhances, concentration profile also increases. In Fig. 6.14, concentration is plotted to seen the influence of thermophoretic parameter Nt. Here, for the greater thermophoretic parameter, the concentration profile is found to decrease. Thermophoretic force tries to move the nanoparticles from warmer to the colder temperature gradient. As a result, the

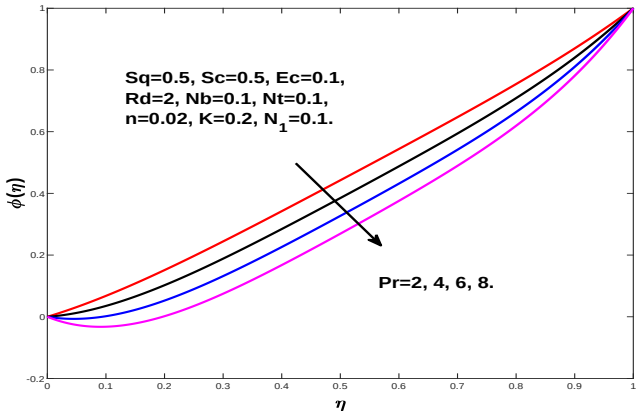

Figure 6.12: Influence of Pr on $\phi(\eta)$.

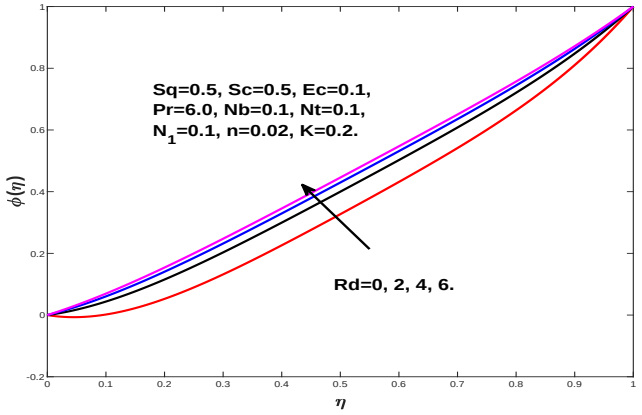

Figure 6.13: Influence of Rd on $\phi(\eta)$.

concentration distribution of the non uniform nanoparticles alters. Thus greater the thermophoretic force is, lower is the concentration. In Fig. 6.15 influence of

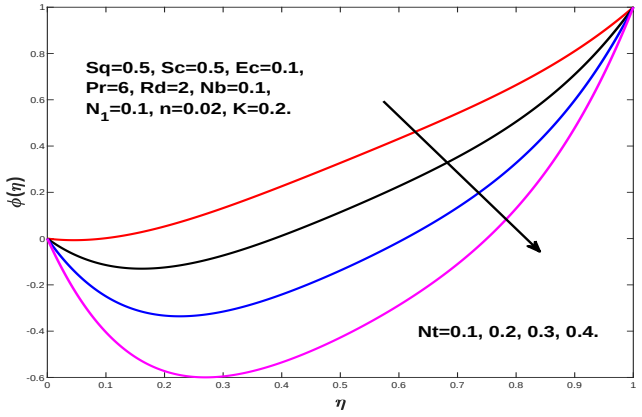

Figure 6.14: Influence of Nt on $\phi(\eta)$.

the Brownian motion parameter Nb on concentration is demonstrated. Higher values of Nb exhibits the greater concentration. Physically, the Brownian motion makes the nanofluid more homogeneous and pushes the particles across from each others. Hence concentration is attained for higher Brownian motion. Impact of

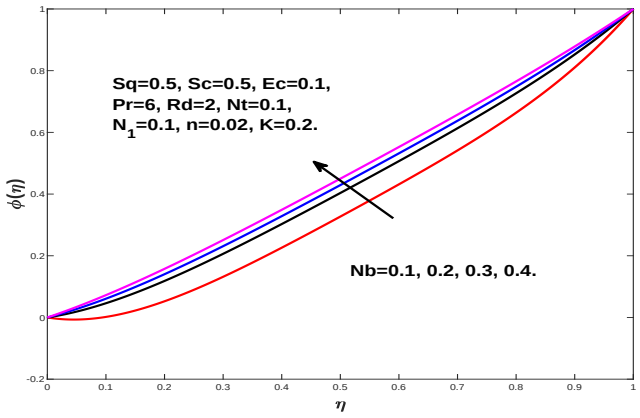

Figure 6.15: Influence of Nb on $\phi(\eta)$.

micropolar parameter K on concentration is seen in Fig. 6.16. Increasing values of micropolar parameter correspond to the decreasing behaviour of concentration. Fig. 6.17 displayed the effect of Eckert number Ec on the concentration. The

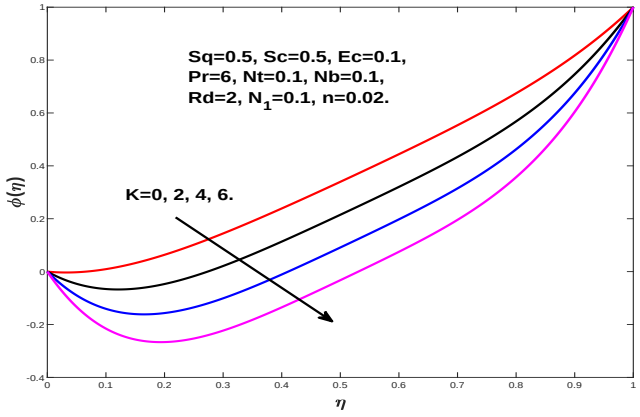

Figure 6.16: Influence of K on $\phi(\eta)$.

graph exhibits that decreasing behavior for greater Eckert number. The influence of Schmidt number Sc on concentration is evident in Fig. 6.18. Higher Schmidt number exhibits, decay in concentration profile.

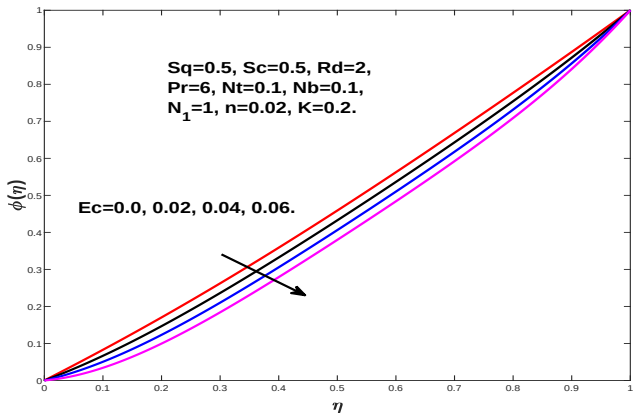

Figure 6.17: Influence of Ec on $\phi(\eta)$.

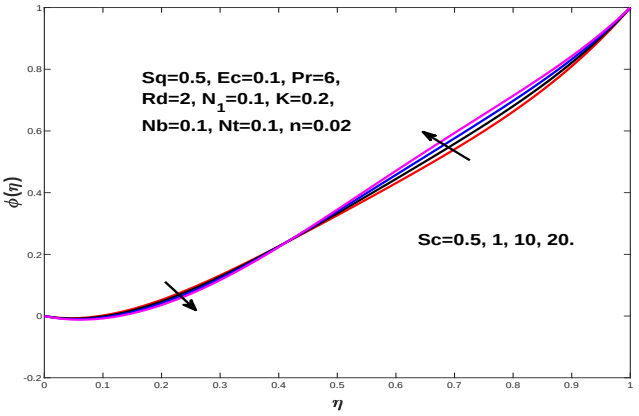

Figure 6.18: Influence of Sc on $\phi(\eta)$.

6.4.3 Impact of Various Parameters on Microrotation Profile

The impact of micropolar parameter K on microrotation profile $g(\eta)$ is displayed in Fig. 6.19. Higher values of micropolar parameter exhibit increasing behaviour on the lower surface and decreasing on the upper surface. Fig. 6.20 is depicted to exhibit the influence of the boundary parameter n on the microrotation. Figure exhibits that the microrotation profile increases in $0 \leq \eta \leq 0.5$ and decreases in the region $0.5 \leq \eta \leq 1$. The value $n = 0$ means that micro elements near the wall do not rotate. The value $n \neq 0$ exhibits that the micro elements rotate near the wall. At the lower wall, the microrotation profile increases, which means that there is a strong rotation as the parameter n increases. The value of the microrotation

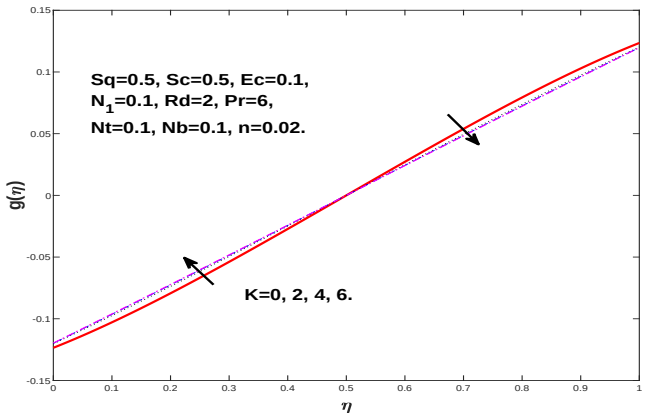

Figure 6.19: Influence of K on $\phi(\eta)$.

at the center of the channel is zero. Fig. 6.21 displays the impact of coupling

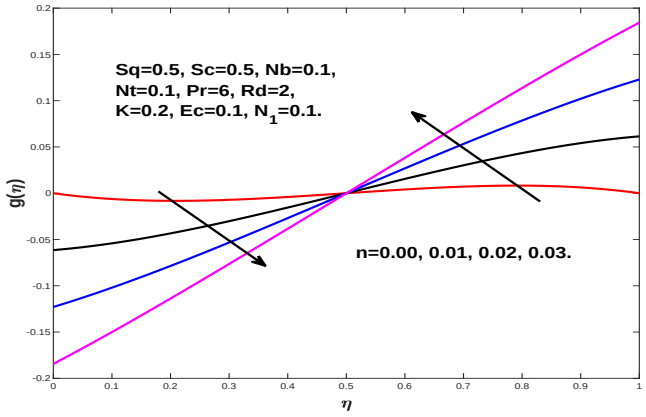

Figure 6.20: Influence of n on $g(\eta)$.

parameter N_1 on the microrotation profile. For higher coupling parameter, the microrotation profile increases at the lower channel whereas at the upper channel it decreases. The influence of squeezing parameter Sq on the microrotation profile is displayed in Fig. 6.22. The grapg decreases in $0 \leq \eta \leq 0.1$ and increases in the region $0.1 \leq \eta \leq 0.5$.

6.4.4 Outcome of Concentration for Varied Parameters

Figs. 6.23-6.27 show the effect of Brinkman number β_r, Reynolds number Re and squeezing parameter Sq and micropolar parameter K on the entropy generation

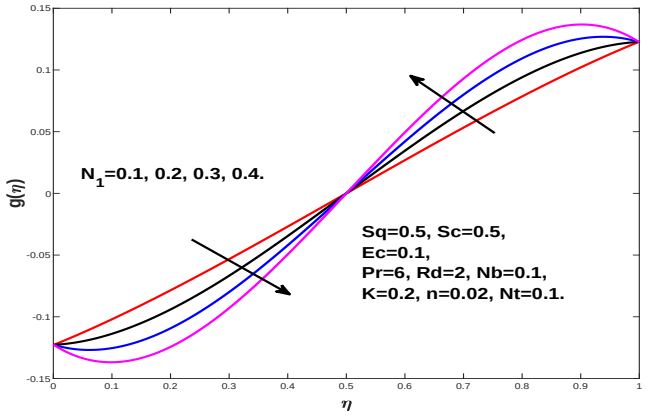

Figure 6.21: Influence of N_1 on $g(\eta)$.

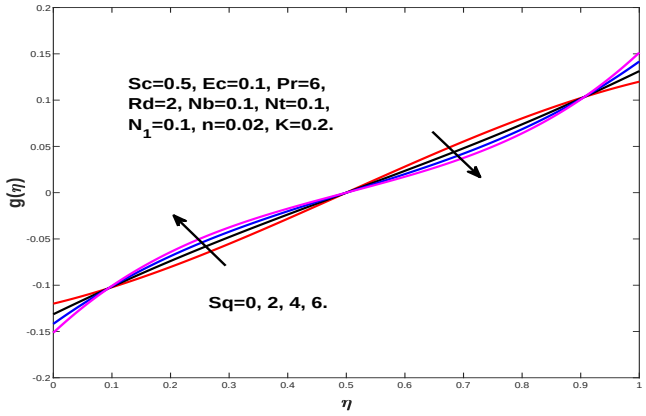

Figure 6.22: Influence of Sq on $g(\eta)$.

for $Re = 0.1$,$\Omega = 1.0$, $\chi = 0.2$, $\lambda_1 = 0.2$ and $\beta_r = 1.0$. The impact of Brinkman number β_r on entropy NG is plotted in Fig. 6.23. As Brinkman number increases, entropy profile increases. The enhancement in entropy is produced by the irreversibility of fluid friction. Fig. 6.24 exhibits the impact of Reynolds number Re on NG. The figure shows that NG increases as Reynolds number increases. Fig. 6.25 explains the impact of squeezing parameter Sq on NG. It can be visualized from the figure that in the region $0 \leq \eta \leq 0.1$, NG decreases whereas the entropy generation enhances in the region $0.1 \leq \eta \leq 0.5$. Fig. 6.26 displays the impact of the micropolar parameter K on NG. The figure exhibits that for increasing micropolar parameter, the entropy generation NG decreases. Fig. 6.27 exhibits the influence of the boundary parameter n on NG. Increasing values of boundary parameter exhibits that the entropy generation NG increases.

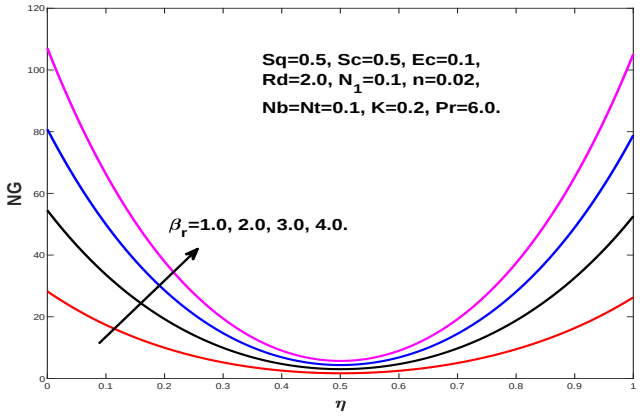

Figure 6.23: Influence of β_r on NG.

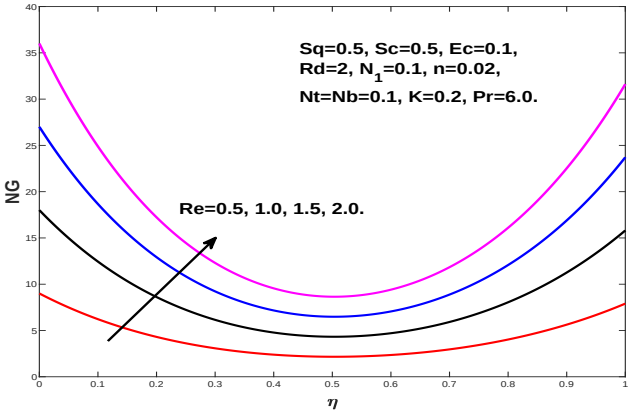

Figure 6.24: Influence of Re on NG.

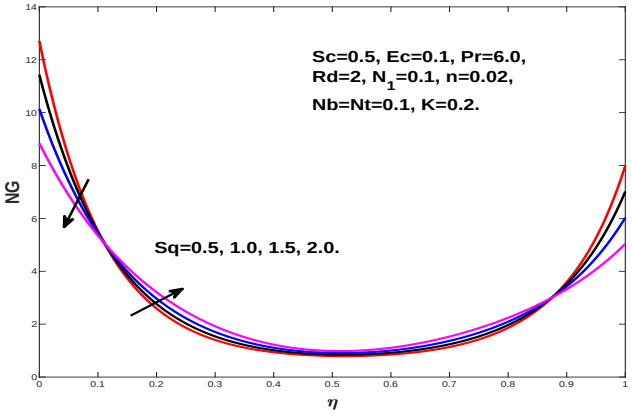

Figure 6.25: Influence of Sq on NG.

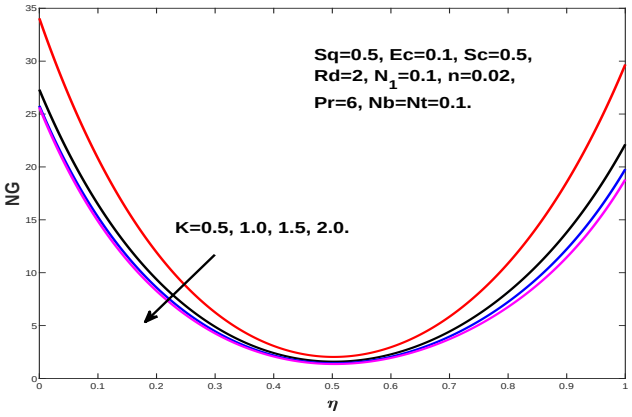

Figure 6.26: Influence of K on NG.

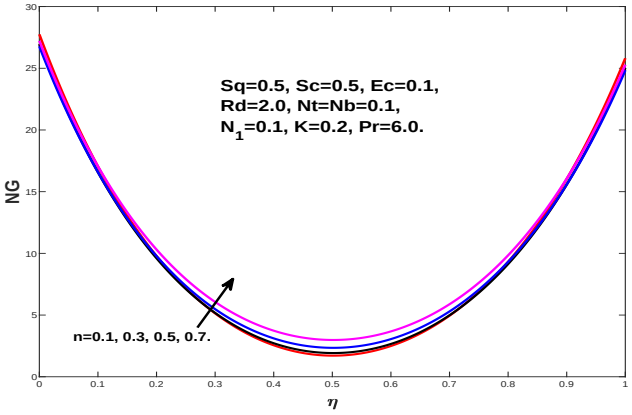

Figure 6.27: Influence of n on NG.

6.5 Concluding remarks

In this chapter, a two dimensional unsteady micropolar nanofluid squeezing flow with thermal radiation and viscous dissipation is considered. The numerical method named as shooting technique is employed. The results are graphically analyzed for different governing parameters. Concluding remarks of present analysis are summarized as follows:

- The velocity, thermal and concentration profiles increase with an increase in the squeezing parameter Sq.
- For the increasing values of the radiation parameter Rd, the temperature profile decreases and the concentration profile increases.

- The thermal profile increases for increasing values of thermophoresis parameter Nt.
- For higher Brownian motion parameter Nb, a direct relation for temperature and concentration is exhibited.
- An increment in micropolar parameter K exhibits the increasing behavior of velocity and temperature profiles.
- An enhancement in the coupling parameter N, microrotation profile has an increasing behaviour at bottom channel and decreasing at the top of channel.
- Entropy generation increases for increasing values of the Brinkman number β_r and Reynolds number Re.

Chapter 7

Conclusion and The Future Work

In this thesis, mathematical modeling for the squeezing flow problem in channel is considered and numerical results are obtained. Initially, we consider the impact of entropy generation on unsteady Casson fluid. Cattaneo-Christove heat flux model is also employed. The entropy generation along with the aforementioned flux passing through a Riga plate is then examined. Furthermore, squeezing flow of upper convected Maxwell nanofluid subject to entropy generation and Cattaneo-Christov double diffusion are analyzed. At the end, this flow for the case of micropolar nanofluid between two parallel plates is investigated. For all the cases, shooting method, through the RK4 scheme, is applied to get numerical results. Moreover, the graphs are plotted to exhibit the impact of skin friction, heat and mass transfer rates. Influence of different parameters like entropy generation, squeezing flow, Casson fluid parameter, thermal radiation, relaxation time of heat and mass fluxes, Prandtl and Schmidt numbers, thermal stratification, solutal stratification, Brownian motion and thermophoretic parameters, Deborah number, microrotation velocity, boundary parameter, modified Hartman number, Biot number on velocity, temperature and concentration are displayed through graphs. The final remarks on the whole study are mentioned here.

7.1 Concluding Remarks

- An augmentation in the positive values of the squeezing flow parameter causes an increase in the velocity for all the models which are discussed in this thesis.
- It has been noticed that an increase in Prandtl number causes a decrease in the temperature profile as discussed in Chapter 3 and 5.
- It is also observed that with the rise in temperature relaxation parameter, the temperature profile declines in Chapter 4 and 5.
- As the chemical reaction parameter increases, the concentration is reduced for the Maxwell and Newtonian fluid.
- A decline in concentration is perceived with an increment in mass relaxation parameter in an upper convected Maxwell fluid in Chapter 5.
- The entropy generation exhibits a decreasing pattern in the case of Newtonian, Maxwell and Casson fluids for higher values of squeezing parameter.
- A reduction in the concentration is observed in presence of Schmidt number in the Casson fluid flow.
- Temperature distribution depends directly on the radiation parameter in the Casson and micropolar fluid flow.
- Bejan number demonstrates that fluid friction impact is stronger near lower stretching wall while heat and mass transfer effects are prominent near the upper wall in the case of Casson fluid.
- For Maxwell and micropolr fluid, when the thermophoresis parameter is increased, the temperature is also increased and reverse behavior is observed for concentration.
- The temperature profile reduces for higher Brownian motion.
- The temperature and velocity both increase as micropolar parameter increases.

7.1.1 Future Outlook

We have considered the squeezing flow problems with different types of fluids. The impact of Cattaneo-Christov heat and mass fluxes with thermal radiation is considered and analyzed. Non-Newtonian fluid flow models such as Maxwell fluid and Casson fluid flow are taken into account. Thermal and solutal stratification are also studied. For the problems given below further analysis can be conducted.

- Different types of Newtonian and non-Newtonian fluid models can be explored for the similar configurations.
- Impact of different boundary conditions can be studied for similar fluid flow problems.
- Further attempt can be made to model the fluid flow problem in the case of flow between two parallel disks or flow between two orthogonal moving plates.
- Different numerical technique can be utilized to solve the fluid flow problems.

Bibliography

[1] C. Xu, L. Yuan, Y. Xu, and W. Hang, "Squeeze flow of interstitial Herschel-Bulkley fluid between two rigid spheres," *Particuology*, vol. 8, pp. 360–364, 2010.

[2] M. J. Stefan, "Versuche über die scheinbare Adhäsion," *Sitzungsber sächs. Akad. wien. Math-Nat Wiss Kl*, vol. 69, pp. 713–721, 1874.

[3] O. Reynolds, "On the theory of lubrication," *Trans. R. Soc. Lond.*, vol. 177, pp. 157–234, 1886.

[4] F. R. Archibald, "Load capacity and time relations in squeezing films," *Trans. ASME. J. Lub. Tech.*, vol. 78, pp. 29–35, 1956.

[5] C. Y. Wang, "The squeezing of a fluid between two plates," *J. Appl. Mech.*, vol. 43, no. 4, pp. 579–583, 1976.

[6] S. Bhattacharyya and A. Pal, "Unsteady MHD squeezing flow between two parallel rotating discs," *Mech. Research Commun.*, vol. 24, no. 6, pp. 615–623, 1997.

[7] R. L. Verma, "A numerical solution for squeezing flow between parallel channels," *Wear*, vol. 72, no. 1, pp. 89–95, 1981.

[8] H. M. Duwairi, B. T. Shtoush, and R. A. Domesh, "On heat transfer effects of viscous fluid squeezed and extruded between two parallel plates," *Heat Mass Trans.*, vol. 14, pp. 112–117, 2004.

[9] J. Engmann, C. Servais, and A. S. Burbidge, "Squeeze flow theory and applications to rheometry: A review," *J. non-newton. fluid mech.*, vol. 132, no. 1-3, pp. 1–27, 2005.

[10] Q. K. Ghori, M. M. Ahmed, and A. M. Siddiqui, "Application of homotopy perturbation method to squeezing flow of a Newtonian fluid," *Int. J. Nonlinear Sci. Num. Simulation*, vol. 8, no. 2, pp. 179–184, 2007.

[11] A. S. A. Saif and A. Harfash, "Perturbation-iteration algorithm for solving heat and mass transfer in the unsteady squeezing flow between parallel plates," *J. Appl. Comput. Mechanics*, vol. 5, no. 4, pp. 804–815, 2019.

[12] M. S. Khan, R. A. Shah, and A. Khan, "Effect of variable magnetic field on the flow between two squeezing plates," *The Eur. Phys. J. Plus*, vol. 134, no. 5, p. 219, 2019.

[13] S. U. S. Choi and J. A. Eastman, "Enhancing thermal conductivity of fluids with nanoparticles," *Int. Mech. Eng. Congr. Expo.*, vol. 66, pp. 99–105, 1995.

[14] T. Hayat, R. Sajjad, A. Alsaedi, T. Muhammad, and R. Ellahi, "On squeezed flow of couple stress nanofluid between two parallel plates," *Res. phys.*, vol. 7, pp. 553–561, 2017.

[15] J. Buongiorno, "Convective transport in nanofluids," *Int. J. Heat Transf.*, vol. 128, pp. 240–250, 2006.

[16] M. M. Rashidi, S. Abelman, and N. F. Mehar, "Entropy generation in steady MHD flow due to a rotating porous disk in nanofluid," *Int. J. Heat Mass Trans.*, vol. 62, pp. 515–525, 2013.

[17] M. Sheikholeslami, D. D. Ganji, and H. R. Ashorynejad, "Investigation of squeezing unsteady nanofluid flow using ADM," *Powder Technol.*, vol. 239, pp. 259–265, 2013.

[18] G. Domairry and H. Hatami, "Squeezing Cu-water nanofluid flow analysis between parallel plates by DTM-Pade method," *J. Mol. Liq.*, vol. 193, pp. 37–44, 2014.

[19] K. Singh, S. K. Rawat, and M. Kumar, "Heat and mass transfer on squeezing unsteady MHD nanofluid flow between parallel plates with slip velocity effects," *J. Nanosci.*, vol. 2016, p. 11, 2016.

[20] M. Atlas, R. U. Haq, and M. Mekkaoui, "Active and zero flux of nanoparticles between a squeezing channel with thermal radiation effects," *J. Mol. Liq.*, vol. 223, pp. 289–298, 2016.

[21] M. Sheikholeslami, D. D. Ganji, and M. M. Rashidi, "Magnetic field effect on unsteady nanofluid flow and heat transfer using Buongiorno model," *J. Magn Magn. Mater.*, vol. 416, pp. 164–173, 2016.

[22] G. H. R. Kafayati, "Mixed convection of non-Newtonian nanofluid in an enclosure using Buongiorno's mathematical model," *Int. J. Heat Mass Trans.*, vol. 108, pp. 1481–1500, 2017.

[23] S. Ahmad, M. I. Khan, T. Hayat, M. I. Khan, and A. Alsaedi, "Entropy generation optimization and unsteady squeezing flow of viscous fluid with five different shapes of nanoparticles," *Colloids Surf. A*, vol. 554, pp. 197–210, 2018.

[24] K. H. Hosseinzadeh, M. Alizadeh, and D. D. Ganji, "Hydrothermal analysis on MHD squeezing nanofluid flow in parallel plates by analytical method," *Int. J. Mech. Mater. Eng.*, vol. 13, no. 1, p. 4, 2018.

[25] I. Ullah, M. Waqas, T. Hayat, A. Alsaedi, and M. I. Khan, "Thermally radiated squeezed flow of magneto-nanofluid between two parallel disks with chemical reaction," *J. Therm. Anal. Calorim.*, vol. 135, no. 2, pp. 1021–1030, 2019.

[26] M. Farooq, S. Ahmad, M. Javed, and A. Anjum, "Melting heat transfer in squeezed nanofluid flow through Darcy Forchheimer medium," *J. Heat Tran.*, vol. 141, no. 1, pp. 12–402, 2019.

[27] S. E. Ahmed and Z. Z. Rashed, "MHD natural convection in a heat generating porous medium-filled wavy enclosures using Buongiorno's nanofluid model," *Case Stud. Therm. Eng.*, vol. 14, pp. 100–430, 2019.

[28] R. Derakhshan, A. Shojaei, K. H. Hosseinzadeh, M. Nimafar, and D. D. Ganji, "Hydrothermal analysis of magneto hydrodynamic nanofluid flow between two parallel by AGM," *Case Stud. Therm. Eng.*, vol. 14, pp. 100–439, 2019.

[29] M. V. Krishna and A. J. Chamkha, "Hall effects on MHD squeezing flow of a water-based nanofluid between two parallel disks," *J. Porous Media*, vol. 22, no. 2, pp. 209–223, 2019.

[30] M. Imtiaz, A. Alsaedi, A. Shafiq, and T. Hayat, "Impact of chemical reaction on third grade fluid flow with cattaneo-christov heat flux," *J. Mol. Liq.*, vol. 229, pp. 501–507, 2017.

[31] J. B. J. Fourier, "Theorie Analytique De La Chaleur," *Chez Firmin Didot, Paris*, 1822.

[32] C. Cattaneo, "Sulla conduzione del calore atti semin," *Mat. Fis.Univ. Modena Reggio Emilia*, vol. 5, pp. 83–101, 2009.

[33] C. I. Christov, "On frame indifferent formulation of the Maxwell-Cattaneo model for finite speed heat conduction," *Mech. Res. Commun.*, vol. 36, pp. 481–486, 2009.

[34] M. E. Ali and N. Sandeep, "Cattaneo-Christov model for radiative heat transfer of magnetohydrodynamic Casson-Ferrofluid: A numerical study," *Res. Phys.*, vol. 7, pp. 21–30, 2016.

[35] S. Shah, S. Hussain, and M. Sagheer, "MHD effects and heat transfer for the UCM fluid along with Joule heating and thermal radiation using Cattaneo-Christov heat flux model," *AIP Adv.*, vol. 6, pp. 85–103, 2016.

[36] J. Sui, J. Zheng, and X. Zhang, "Boundary layer heat and mass transfer with Cattaneo-Christov double diffusion in upper convected Maxwell nanofluid

past a stretching sheet with slip velocity," *Int. J. Therm. Sci.*, vol. 104, pp. 161–168, 2016.

[37] T. Hayat, T. Muhammad, A. Alsaedi, and B. Ahmad, "Three dimensional flow of nanofluid with Cattaneo-Christov double diffusion," *Res. Phys.*, vol. 6, pp. 897–903, 2016.

[38] N. Muhammad, S. Nadeem, and T. Mustafa, "Squeezed flow of a nanofluid with Cattaneo- Christov heat and mass fluxes," *Res. Phys.*, vol. 7, pp. 862–869, 2017.

[39] A. D. Dogonchi and D. D. Ganji, "Impact of cattaneo–christov heat flux on mhd nanofluid flow and heat transfer between parallel plates considering thermal radiation effect," *J. Taiwan Inst. Chem. Eng.*, vol. 80, pp. 52–63, 2017.

[40] N. Akmal, M. Sagheer, and S. Hussain, "Numerical study focusing on the entropy analysis of MHD squeezing flow of a nanofluid model using Cattaneo–Christov theory," *AIP Adv.*, vol. 8, no. 5, pp. 55–201, 2018.

[41] A. S. Dogonchi, A. J. Chamkha, S. M. Seyyedi, and D. D. Ganji, "Radiative nanofluid flow and heat transfer between parallel disks with penetrable and stretchable walls considering Cattaneo–Christov heat flux model," *Heat Transfer Asian Res.*, vol. 47, no. 5, pp. 735–753, 2018.

[42] L. U. Dianchen, Z. L. I, M. Ramzan, A. Shafee, and J. D. Chung, "Unsteady squeezing carbon nanotubes based nano-liquid flow with Cattaneo–Christov heat flux and homogeneous–heterogeneous reactions," *Appl. Nanoscience*, vol. 9, no. 2, pp. 169–178, 2019.

[43] M. Zubair, Z. Shah, S. Islam, W. Khan, and A. Dawar, "Study of three dimensional Darcy–Forchheimer squeezing nanofluid flow with Cattaneo–Christov heat flux based on four different types of nanoparticles through entropy generation analysis," *Adv. Mech. Eng.*, vol. 11, no. 5, pp. 1–17, 2019.

[44] B. Ramadevi, V. Sugunamma, K. A. Kumar, and J. V. R. Reddy, "MHD flow of Carreau fluid over a variable thickness melting surface subject to Cattaneo-Christov heat flux," *Multidiscip. Model. Mater. Strutures*, 2019.

[45] U. Shankar and N. B. Naduvinamani, "Magnetized impacts of Cattaneo-Christov double-diffusion models on the time-dependent squeezing flow of Casson fluid: A generalized perspective of Fourier and Fick's laws," *The Eur. Phys. J. Plus*, vol. 134, no. 7, p. 344, 2019.

[46] S. Mukhopadhyay and R. S. R. Gorla, "Unsteady MHD boundary layer flow of an upper convected Maxwell fluid past a stretching sheet with first order constructive/destructive chemical reaction," *J. Naval Arch. Marine Eng.*, vol. 9, no. 2, pp. 123–133, 2012.

[47] M. Jamil and C. Fetecau, "Helical flows of Maxwell fluid between coaxial cylinders with given shear stresses on the boundary," *Nonlinear Anal. Real world Appl.*, vol. 11, pp. 4302–4311, 2010.

[48] M. Awais, T. Hayat, A. Alsaedi, and S. Asghar, "Time-dependent three-dimensional boundary layer flow of a Maxwell fluid," *Comput. Fluids*, vol. 91, pp. 21–27, 2016.

[49] W. Ibrahim, "Magnetohydrodynamic (MHD) stagnation point flow and heat transfer of upper-convected Maxwell fluid past a stretching sheet in the presence of nanoparticles with convective heating," *Frontiers Heat Mass Tran.*, vol. 7, no. 1, 2016.

[50] P. B. Reddy, S. S. Suneetha, and N. B. Reddy, "Numerical study of magneto-hydrodynamics MHD boundary layer slip flow of a Maxwell nanofluid over an exponentially stretching surface with convective boundary condition," *Prop. Power Research*, vol. 6, no. 4, pp. 259–268, 2017.

[51] M. Farooq, S. Ahmad, M. Javed, and A. Anjum, "Magnetohydrodynamic flow of squeezed Maxwell nano-fluid with double stratification and convective conditions," *Adv. Mech. Eng.*, vol. 10, no. 9, pp. 1–13, 2018.

[52] N. N. Kumar, P. K. Kambhatla, and O. Ojjela, "Double dispersion effects on MHD squeezing flow of ucm fluid through a porous medium," *Defect Diffus. Forum*, vol. 392, pp. 10–28, 2019.

[53] S. S. Rashid, M. I. Khan, T. Hayat, M. Ayub, and A. A. Alsaedi, "Darcy–Forchheimer flow of Maxwell fluid with activation energy and thermal radiation over an exponential surface," *Appl. Nanoscience*, pp. 1–11, 2019.

[54] D. A. McDonald, *Blood flow in arteries.* Williams & Wilkins, 1974.

[55] E. W. Merrill, A. M. Benis, E. R. Gilliland, T. K. Sherwood, and E. W. Salzman, "Pressure-flow relations of human blood in hollow fibers at low flow rates," *J. Appl. Physiol.*, vol. 20, no. 5, pp. 954–967, 1965.

[56] N. S. Shashikumar, M. Archana, B. C. Prasannakumara, B. J. Gireesha, and O. D. Makinde, "Effects of nonlinear thermal radiation and second order slip on Casson nanofluid flow between parallel plates," *Defect Diffus. Forum*, vol. 377, pp. 84–94, 2017.

[57] M. S. Kumar, N. Sandeep, B. R. Kumar, and S. Saleem, "Effect of aligned magnetic field on MHD squeezing flow of Casson fluid between parallel plates," *Defect Diffus. Forum*, vol. 384, pp. 1–11, 2018.

[58] R. H. Patel, "Effects of heat generation, thermal radiation, and hall current on MHD casson fluid flow past an oscillating plate in porous medium," *Multiphase Science Tech.*, vol. 31, no. 1, pp. 87–107, 2019.

[59] A. Saif, J. A. Sattar, and A. M. Jasim, "A novel algorithm for studying the effects of squeezing flow of a casson fluid between parallel plates on magnetic field," *J. Appl. Mathematics*, vol. 2019, 2019.

[60] A. Ahmadpour, M. Nasiri, M. Khazayinejad, and N. Asgharian, "Flow and convective heat transfer of casson fluid between squeezing porous disks in the presence of thermal radiation, viscous dissipation, and variable heat source/sink," *J. Brazilian Society Mech. Sciences Eng.*, vol. 40, no. 3, p. 135, 2018.

[61] A. Mirzaaghaian and D. D. Ganji, "Application of differential transformation method in micropolar fluid flow and heat transfer through permeable walls," *Alex. Eng. J.*, vol. 55, no. 3, pp. 2183–2191, 2016.

[62] A. C. Eringen, "Theory of micropolar fluids," *J. Math. Mech*, vol. 16, pp. 1–18, 1966.

[63] P. S. Ramachandran, M. N. Mathur, and S. K. Ojha, "Heat transfer in boundary layer flow of a micropolar fluid past a curved surface with suction and injection," *Int. J. Eng. sci.*, vol. 17, no. 5, pp. 625–639, 1979.

[64] A. N. Kelson and T. W. Farrell, "Micropolar flow over a porous stretching sheet with strong suction or injection," *Int. Commun. Heat Mass Tran.*, vol. 28, no. 4, pp. 479–488, 2001.

[65] M. Ashraf, M. A. Kamal, and K. S. Syed, "Numerical study of asymmetric laminar flow of micropolar fluids in a porous channel," *Comput. Fluids*, vol. 38, no. 10, pp. 1895–1902, 2009.

[66] A. A. Joneidi, D. D. Ganji, and M. M. Babaelahi, "Micropolar flow in a porous channel with high mass transfer," *Int. Commun. Heat Mass Trans.*, vol. 36, no. 10, pp. 1082–1088, 2009.

[67] N. S. Gibanov, M. A. Sheremet, and I. Pop, "Free convection in a trapezoidal cavity filled with a micropolar fluid," *Int. J. Heat Mass Trans.*, vol. 99, pp. 831–838, 2016.

[68] M. Bilal, S. Hussain, and M. Sagheer, "Boundary layer flow of magneto-micropolar nanofluid flow with Hall and ion-slip effects using variable thermal diffusivity," *Bull. Pol. Acad. Sci., Techn. Sci.*, vol. 65(3), pp. 383–390, 2017.

[69] M. Alizadeh, A. S. Dogonchi, and D. D. Ganji, "Micropolar nanofluid flow and heat transfer between penetrable walls in the presence of thermal radiation and magnetic field," *Case Stud. Ther. Eng.*, vol. 12, pp. 319–332, 2018.

[70] A. M. Rashad, S. Abbasbanday, and A. J. Chamkha, "Non-darcy natural convection from a vertical cylinder embedded in a thermally stratified and nanofluid saturated porous medium," *J. Heat Trans.*, vol. 136, pp. 022–503, 2013.

[71] W. Ibrahim and O. D. Makinde, "The effect of double stratification on boundary layer flow and heat transfer of nanofluid over a vertical plate," *J. Heat Trans.*, vol. 86, pp. 433–441, 2013.

[72] D. Srinivasacharya and O. Surender, "Effect of double stratification on mixed convection boundary layer flow of a nanofluid past a vertical plate in a porous medium," *Appl. Nanoscience*, vol. 28, pp. 433–441, 2014.

[73] A. Bejan, "Entropy generation minimization: The new thermodynamic of finite size devices and finite time process," *J. Appl. Physics*, vol. 79, pp. 1191–1218, 1996.

[74] M. Sheikholeslami and D. D. Ganji, "Entropy generation of nanofluid in presence of magnetic field using Lattic Boltzman method," *Physica A*, vol. 417, pp. 515–525, 2015.

[75] A. S. Butt and A. Ali, "Analysis of entropy generation effects in unsteady squeezing flow in a rotating channel with lower stretching permeable wall," *J. Taiwan Inst. Chem. Eng.*, vol. 48, pp. 8–17, 2015.

[76] M. H. Abolbashari, N. Freidoonimehr, F. F. Nazari, and M. M. Rashidi, "Analytical modeling of entropy generation for Casson nano-fluid flow induced by a stretching surface," *Adv. Powder Tech.*, vol. 26, no. 2, pp. 542–552, 2015.

[77] D. Srinivasacharya and K. H. Bindu, "Entropy generation in a micropolar fluid flow through an inclined channel," *Alex. Eng. J.*, vol. 55, no. 2, pp. 973–982, 2016.

[78] S. Hussain, K. Mehmood, and M. Sagheer, "MHD mixed convection and entropy generation of water-alumina nanofluid flow in a doubled lid driven

cavity with discrete heating," *J. Magn. Magn. Mater*, vol. 419, pp. 140–155, 2016.

[79] A. Zeeshan, M. Hassan, R. Ellahi, and M. Nawaz, "Shape effects of nano-size particles in unsteady mixed convection flow of nanofluid over disk with entropy generation," *J. Proc. Mech. Eng.*, pp. 1–9, 2016.

[80] M. I. Khan, S. Ahmad, T. Hayat, and A. Alsaedi, "Entropy generation and activation energy impact on radiative flow of viscous fluid in presence of binary chemical reaction," *Int. J. Chem. Reactor Eng.*, vol. 16, no. 9, 2018.

[81] O. Ojjela, K. Ramesh, and K. S. Das, "Second law analysis of MHD squeezing flow of Casson fluid between two parallel disks," *Int. J. Chem. Reactor Eng.*, vol. 16, no. 6, 2018.

[82] M. I. Khan, A. Kumar, T. Hayat, M. Waqas, and R. Singh, "Entropy generation in flow of Carreau nanofluid," *J. Mol. Liq.*, vol. 278, pp. 677–687, 2019.

[83] M. Siavashi, R. Yousofvand, and S. Rezanejad, "Nanofluid and porous fins effect on natural convection and entropy generation of flow inside a cavity," *Adv. Powder Tech.*, vol. 29, no. 1, pp. 142–156, 2018.

[84] A. Dawar, Z. Shah, W. Khan, M. Idrees, and S. Islam, "Unsteady squeezing flow of magnetohydrodynamic carbon nanotube nanofluid in rotating channels with entropy generation and viscous dissipation," *Adv. Mech. Eng.*, vol. 11, no. 1, pp. 1–18, 2019.

[85] T. Papanastasiou, G. Georgiou, and A. N. Alexandrou, *Viscous fluid flow*. CRC press, 1999.

[86] K. S. Raju, *Fluid mechanics, heat transfer, and mass transfer: chemical engineering practice*. John Wiley & Sons, 2011.

[87] M. Thirumaleshwar, *Fundamentals of heat and mass transfer*. Pearson Education India, 2006.

[88] C. I. Christov, "On frame indifferent formulation of the Maxwell-Cattaneo model of finite-speed heat conduction," *Mech. Res. Commun.*, vol. 36, pp. 481–486, 2009.

[89] E. Brujan, *Cavitation in Non-Newtonian fluids: with biomedical and bio-engineering applications*. Springer Science & Business Media, 2010.

[90] M. Sajid, Z. Abbas, N. Ali, and T. Javed, "Note on effect of joule heating and mhd in the presence of convective boundary condition for upper-convected maxwell fluid through wall jet," *J. Mol. Liq.*, vol. 230, pp. 235–236, 2017.

[91] K. Tanishita and K. Yamamoto, *Vascular Engineering: New Prospects of Vascular Medicine and Biology with a Multidiscipline Approach*. Springer, 2016.

[92] A. Bejan, *Entropy generation minimization: the method of thermodynamic optimization of finite-size systems and finite-time processes*. CRC press, 2013.

[93] T. Y. Na, "Computational methods in engineering boundary value problem," *Academic Press*, pp. 71–76, 1979.

[94] R. L. Burden and J. D. Faires, *Numerical analysis*. Cengage Learning, 1997, vol. 8.

[95] J. Li, L. Zheng, and L. Liu, "MHD viscoelastic flow and heat transfer over a vertical stretching sheet with Cattaneo-Christov heat flux effects," *J. Mol. Liq.*, vol. 221, pp. 19–25, 2016.

[96] B. Mahanthesh, B. Gireesha, S. R. Gorla, and O. D. Makinde, "Magnetohydrodynamic three-dimensional flow of nanofluids with slip and thermal radiation over a nonlinear stretching sheet: a numerical study," *Neural Comput. Appl.*, vol. 30, no. 5, pp. 1557–1567, 2018.

[97] G. H. R. Kefayati, "Simulation of double diffusive convection and entroy generation of power-law fluids in an inclined porous cavity with Soret and Dufour effects," *Int. J. Heat Mass Transfer*, vol. 94, pp. 582–624, 2016.

[98] O. Pourmehran, M. R. Gorji, M. G. Bandpy, and D. D. Ganji, "Analytical investigation of squeezing unsteady nanofluid flow between parallel plates by LSM and CM," *Alax. Eng. J.*, vol. 54, no. 1, pp. 17–26, 2015.

[99] T. Hayat, M. khan, M. Imtiaz, and A. Alsaedi, "Squeezing flow past a Riga plate with chemical reaction and convective conditions," *J. Mol. Liq.*, vol. 225, pp. 569–576, 2016.

[100] T. Hayat, K. K. Muhammad, M. Farooq, and A. Alsaedi, "Unsteady squeezing flow of carbon nanotubes with convective boundary conditions," *PloS one*, vol. 11, no. 5, pp. 152–923, 2016.

[101] T. Abbas, M. Ayub, M. M. Bhatti, M. M. Rashidi, and M. E. S. Ali, "Entropy generation on nananofluid flow through a horizontal Riga plate," *Entropy*, vol. 18, p. 223, 2016.

[102] X. H. Si, L. C. Zheng, X. X. Zhang, and Y. Chao, "The flow of micropolar flow through a porous channel with expanding and contracting walls." *Cent. Eur. J. Phys.*, vol. 9, pp. 825–834, 2011.

[103] X. Si, M. Pan, L. Zheng, J. Zhoo, and L. Li, "The solutions for the flow of micropolar fluid through an expanding or contracting channel with porous walls," *Bound. Val. Probl.*, vol. 176, 2016.

[104] T. Y. Na and I. Pop, "Boundary-layer flow of a micropolar fluid due to a stretching wall," *Arch. Appl. Mech.*, vol. 64, 1997.

[105] D. Srinivas and K. H. Bindu, "Entropy generation in a micropolar fluid flow through an inclined channel," *Alexan. Eng. J.*, vol. 55, pp. 972–982, 2016.

[106] S. Jangili, S. O. Adesanya, J. A. Falade, and N. Gajjela, "Entropy generation analysis for a radiative micropolar fluid flow through a vertical channel satureted with non-Darcian porous media," *Int. J. Appl. Comput. Math.*, pp. 1–24, 2017.

[107] M. Sheikholeslami and D. D. Ganji, "Unsteady nanofluid flow and heat transfer in presence of magnetic field considering thermal radiation." *J. Braz. Soc. Mech. Sci. Eng.*, vol. 37, pp. 895–902, 2015.

Appendix A

The bvp4c Function

"The bvp4c, a MATLAB built-in function, which can be used to solve the system of non linear boundary value problems. Lobatto IIIa, three-stage formula embedded with a finite difference scheme, plays a vital role in the construction of built-in coding process of bvp4c. Basically it is a collocation formula, C-1 continuous solution is provided by the collocation polynomial and it is a fourth order accurate in $[a, b]$. The residual of the continuous solution depends on the error control and the mesh selection. The following MATLAB syntax is used for it: $sol = bvp4c\,(@odefun, @bcfun, solinit, options)$".